INAUGURAL – DISSERTATION

ZUR

ERLANGUNG DER DOKTORWÜRDE

DER NATURWISSENSCHAFTLICH-MATHEMATISCHEN

GESAMTFAKULTÄT

DER

RUPRECHT-KARLS-UNIVERSITÄT

HEIDELBERG

Vorgelegt von

Diplom-Geoökologe Benjamin Kopp

Aus: Schönhofen / Nittendorf

Tag der mündlichen Prüfung: 29. April 2016

THEMA

RUNOFF GENERATING PROCESSES IN A MOUNTAINOUS HEADWATER IN THE TRANSITION ZONE BETWEEN STEPPE AND TAIGA IN NORTHERN MONGOLIA

Gutachter: Prof. Dr. Lucas Menzel

Prof. Dr. Kurt Roth

KURZZUSAMMENFASSUNG

Die nördliche Mongolei weist eine Vielzahl von wasserbezogenen Problemen auf. Diese sind zum einen Folge der harschen naturräumlichen Gegebenheiten, und zum anderen in fehlenden Strukturen hinsichtlich einheitlicher Verteilung und Schutz der wertvollen Ressource Wasser begründet. Das Kharaa Einzugsgebiet (KRB), nördlich der mongolischen Hauptstadt Ulaanbaatar, wurde als Modellgebiet im Rahmen eines Integrierten Wasserressourcen Management (IWRM) Projektes (MoMo, Modellregion Mongolei) ausgewählt. Das Ziel des IWRM ist es, gesellschaftliche Rahmenbedingungen sowie das Ökosystem jeweils als Ganzes zu erfassen. Neben einer Verbesserung der urbanen Strukturen werden alle wasserrelevanten Prozesse im Einzugsgebiet identifiziert. Hierzu zählt insbesondere die Erfassung der Quellgebiete und der abflussgenerierenden Prozesse. Das KRB erstreckt sich über ein breites Spektrum an landestypischen Naturräumen von der Steppe bis in das westliche Khentii Gebirge, und ist repräsentativ für weite Bereiche der Mongolei.

Der Sugnugr Gol im westlichen Khentii Gebirge ist einer der wichtigsten Zuflüsse des Kharaa. Das vorherrschende Klima ist hochkontinental und semi-arid, mit jährlichen Niederschlagsmengen von bis zu 400 mm im Mittellauf. Etwa 90 % der jährlichen Niederschläge fallen im hydrologischen Sommerhalbjahr (Mai – Oktober). In 2011 und 2012 betrugen die jährlichen Lufttemperaturen -2°C und -3°C, mit monatlichen Temperaturen zwischen -28°C im Januar und 16°C im Juli. Das Sugnugr Einzugsgebiet liegt in der Übergangszone zwischen Steppe und Taiga und ist Teil der diskontinuierlichen Permafrostzone. Es wird durch ein mosaikartiges Vegetationsmuster, mit artenreicher Steppenvegetation an südexponierten Hängen und mit Taiga bewachsenen, von Permafrost unterlagerten, nordexponierten Hängen charakterisiert. Oberhalb der Baumgrenze von etwa 2300 m erstrecken sich weitläufige Blockschutthalden. Große Waldflächen, insbesondere in den Oberläufen, wurden 2004 und 2007 durch Waldbrände zerstört. Die Regeneration der Bestände in diesen naturräumlichen Gegebenheiten erfolgt sehr langsam, über einen Zeitraum von mindestens 200 Jahren. Die im Folgenden vorgestellten abflussgenerierenden Prozesse basieren auf umfangreichen und detaillierten Feldmessungen in einem, von menschlichen Aktivitäten nahezu unbeeinflussten, Einzugsgebiet im Oberlauf des Sugnugr.

Die Ergebnisse zeigen einen deutlichen Zusammenhang zwischen den dominanten hydrologischen Prozessen und dem vorherrschenden Vegetationstyp. So werden die mit

Steppenvegetation bewachsenen südexponierten Hänge nur während starker Niederschlagsereignisse über Oberflächenabfluss abflusswirksam. Die Infiltration in den Boden ist gering und erfolgt gleichmäßig in die Bodenmatrix, und nicht über präferentielle Fließwege entlang von Makroporen. Generell weisen diese Standorte trockene Bedingungen auf, wobei der Bodenwassergehalt während der Sommermonate vereinzelt den permanenten Welkepunkt erreicht. Ein Großteil der Abflussbildung wird demnach in den von Taiga bewachsenen nordexponierten Hängen generiert. Insbesondere die mächtige organische Auflage sowie die sommerlich auftauende Bodenschicht oberhalb des Permafrosts wirken sich hier abflussregulierend auf. So zeigen auf Einzugsgebietsebene Abflussganglinienanalysen einen schnellen Transfer von Niederschlagswasser in den Vorfluter während des Frühsommers auf. Mit zunehmender Mächtigkeit der Auftauschicht im Laufe des Sommers erhöht sich die Speicherkapazität, die Rezessionsperiode verlängert sich und Niedrigwasserabflüsse steigen. Gleichzeitig konnte gezeigt werden, dass Niederschläge erst abflusswirksam werden, wenn eine relative Zunahme des volumetrischen Wassergehaltes der oberen Bodenzone und der organischen Auflage von 5 % erfolgt. Waldbrände können dieses System nachhaltig verändern. Der Verlust der isolierenden organischen Auflage führt zu signifikant steigenden Bodentemperaturen während der Permafrost degradiert. Dadurch entsteht ein Netzwerk aus präferentiellen Fließwegen auf der Oberfläche des Permafrosts, welches Niederschlagswasser effektiv dem Vorfluter zuführt, ohne dass ein messbarer Anteil zurückgehalten wird. Die Modellierung von großräumigen Waldbrandflächen mit dem konzeptionellen hydrologischen Modell HBV-D weist auf ein Absinken der monatlichen Abflüsse während des hydrologischen Winterhalbjahres hin, während diese im hydrologischen Sommerhalbjahr zunehmen. Die Ergebnisse der Feldmessungen zeigen aber, dass der simulierte Anstieg der sommerlichen Abflüsse nicht die allgemeine Wasserverfügbarkeit erhöht. Als Folge der Waldbrände nehmen die Hochwasserabflüsse zu, während sich Niedrigwasserabflüsse verringern.

Die Ergebnisse verdeutlichen die Schutzwürdigkeit der alpinen Quellgebiete vor allem vor Abholzung und Waldbränden. Insbesondere im Hinblick auf das anhaltend hohe Wirtschaftswachstum und dem steigenden Wasserbedarf in der Mongolei gilt es, die gegenwärtigen Bedingungen in den Oberläufen zu bewahren.

SHORT SUMMARY

Northern Mongolia faces a variety of water-related problems that are related to both, the harsh natural conditions and the lack of structures to control the distribution and protection of water. The Kharaa River Basin (KRB), which is located north of Mongolia's capital Ulaanbaatar, was chosen as a model region for the development and implementation of an integrated water resources management (IWRM) project called MoMo (Model Region Mongolia). The aim of IWRM is to provide insight into both, societal structural and eco-systematic conditions as a whole. Besides an improvement of the structures, especially in the urban sector, all relevant water related processes are captured. This includes the identification of "water towers" and the underlying runoff generating processes. The KRB stretches from the steppe towards the western Khentii Mountains. Thus, it covers a wide range of environmental conditions and can be considered to be representative for many regions within Mongolia.

The Sugnugr Basin situated within the western Khentii Mountain ranges is one of the most important tributaries of the Kharaa. The climate is highly continental and semi-arid; average annual precipitation in the mid-reaches remains below 400 mm. With a fraction of 90 %, precipitation is predominantly falling during the summer half year (May to October). Air temperature in 2011 and 2012 was -2°C and -3°C, with monthly air temperatures ranging between -28°C in January and 16°C in July. The Sugnugr Basin is situated in the transition zone between steppe and taiga, and is part of the discontinuous permafrost zone. Thus, it is characterized by a heterogeneous mosaic of herbaceous steppe vegetated south-exposed slopes and taiga vegetated north-exposed slopes that exhibit permafrost. Above the tree line of approximately 2300 m a.s.l. alpine scree prevails. In 2004 and 2007 widespread forest fires destroyed considerable amounts of the taiga, especially in the headwaters. Forest regrowth under the prevailing natural conditions can last 200 years and more. The following presented runoff generating processes are based on comprehensive and detailed field studies in an anthropogenic unaffected headwater of the Sugnugr.

The results indicate hydrological processes in the study area to be controlled by the dominant vegetation cover. It has been shown that steppe vegetated south-exposed hillslopes only sporadically contribute to river runoff during intense precipitation events. Infiltration rates into the soil matrix are small and evenly distributed and no signs of preferential flow were found. In general, these sites were characterized by dry conditions and soil moisture content occasionally reached the permanent wilting point during the summer months. A majority of

river runoff must hence be generated by taiga vegetated north-exposed hillslopes. Especially the thick organic surface layer and the depth of the active layer have been shown to control runoff response. On the catchment scale, hydrograph recession analysis revealed a quick transfer of event water on top of a thin active layer towards the rivers in early summer. In the course of summer, active layer depth and thus storage capacity is increasing, resulting in enhanced recession periods and increased low-flow runoff. Simultaneously, it could be shown that hillslope runoff only occurs after a threshold of 5 % increase of the relative volumetric water content of the upper soil zone, including the organic surface, is reached. Wildfires alter this system sustainably. As the insulating organic surface cover is removed, soil temperatures have been shown to increase, while permafrost subsided to deeper depth. This resulted in a network of preferential flow paths on top of the frost table, which effectively transfers event water towards the adjacent river without substantial retention. Land-cover change scenarios were simulated with the conceptual hydrological model HBV-D. As a consequence of a wildfire, with all taiga stands being burned, monthly runoff was simulated to decrease during the winter half year, while it increased during the summer half year. However, results of the field studies suggest that the simulated increase in summer runoff following wildfire does not lead to greater water availability, as stormflow runoff increased while low-flow runoff decreased.

The results support the conservation of the alpine headwaters, especially from deforestation and wildfire in order to safeguard the current amount of surface water quantity. This gains further importance regarding the flourishing Mongolian economy and the related increasing water demands.

ACKNOWLEDGMENT

First of all, I would like to thank Prof. Dr. Lucas Menzel for giving me the opportunity to write this dissertation, to work in the beautiful country of Mongolia and for scientific support.

I would also like to thank a variety of German and Mongolian colleagues and friends, without their guidance and support this work could not have been successfully completed. Special thanks to Steffen Füssel, Matthias Bents and Hans Kopp for help during field work, Henning Götz for support of the land-cover classification, Dr. Jens Lange for scientific support, Gerd Schuhkraft for advice in the laboratory, Chimegsaikhan Altangerel for logistic support, Nasanbayar Narantsogt as a friend and reliable driver, Khuhuu Gunsenbat and his wife for warm welcomes and Nugonhayaar Gansukh and his horses for the transport of the equipment to the study site.

Special thanks to Stefanie Kopp, formerly Minderlein, who accompanied and supported this work from the beginning. Thank you for help purchasing the scientific equipment and the handling of the logistics, the wonderful and intensive field stays with all ups and downs, rewarding scientific discussions and patience allowing me to finish this dissertation. Special thanks to Isabell for love, laughter's and patience exercises. Finally, I would like to thank my parents, my brother and sisters and all of my friends.

This study was conducted within the German Federal Ministry of Education and Research (BMBF) financed MoMo II Project (Integrated Water Resources Management in Central Asia – Model Region Mongolia, Phase II, contract number: 033L003C).

TABLE OF CONTENTS

CHAPTER 6

CHAPTER 7

LIST OF FIGURES

LIST OF TABLES

LIST OF ABBREVIATIONS

°C	Degree Celsius
$\%_v$	Percent by Volume
^2H	Hydrogen-2; Stable Isotope of Hydrogen
^{18}O	Oxygen-18; Stable Isotope of Oxygen
α	Recession Coefficient (d^{-1})
a.s.l.	Above Sea Level
AE	Actual Evapotranspiration
ANOVA	Analysis of Variance
c	Tracer Concentration
C	Sub-Catchment
$c_e^{t_i}$	Event Water (Precipitation) Tracer Concentration
$c_p^{t_i}$	Pre-Event Water (Baseflow) Tracer Concentration
cm	Centimeter
cm^3	Cubic Centimeter
CUZ	Upper Soil Zone Reservoir
CVSNOW	Coefficient of Variation of Snow Distribution
CXREL	Correction Factor on Temperature Index
$\delta^{18}O$	Ratio of Stable Isotopes Oxygen-18 and Oxygen-16
d	Day
DEM	Digital Elevation Model
DF_p	Measure for the Importance of Delayed Flow (%)
DOC	Dissolved Organic Carbon
DRAW	Capillary Rise (mm d^{-1})
DS	Downslope
E	East
EC	Electric Conductivity (µS cm^{-1})
EPVAR	Correction Factor for Potential Evapotranspiration
ET	Evapotranspiration (mm d^{-1})
f	Mixing Fraction of Event and Pre-Event Water
F	Floodplain
FC	Field Capacity
FCREL	Adjustment of Maximum Soil Moisture Content
FDR	Frequency Domain Reflectometry
g	Gramm
GMWL	Global Meteoric Water Line
GST	Ground Surface Temperature (°C)
h	Hour
HB	Heavily Burned Forest
HBV	Conceptual Hydrological Model HBV (Hydrologiska Byråns Vattenbalanssektionsmodell)
HRU	Hydrological Response Unit
I	Infiltration Rate (m d^{-1})
ICMAX	Interception Storage (mm)

INSOIL	Precipitation and Melt Water Input (mm)
IPCC	Intergovernmental Panel on Climate Change
IRWM	Integrated Water Resources Management
$K_{f(unsat)}$	Unsaturated Soil Hydraulic Conductivity
KLZ	Constant Controlling Very Slow Runoff (Q_2)
km²	Square Kilometer
KRB	Kharaa River Basin
KUZ1	Constant Controlling Slow Runoff (Q_1)
KUZ2	Constant Controlling Fast Runoff (Q_0)
l	Liter
LB	Lightly Burned Forest
Log	Logarithmic
LPDEL	Specific Soil Water Content Regulating the Fraction of Actual to Potential Evapotranspiration
Lst	Lower Zone Storage
m	Meter
m^2	Square Meter
m^3	Cubic Meter
MAAT	Mean Annual Air Temperature
MAARC	Mongolian Assessment Report on Climate Change
mg	Milligramm
ml	Milliliter
mm	Millimeter
min	Minute
MoMo	Model Region Mongolia
MP	Macropore
N	North
NDVI	Normal Difference Vegetation Index
Nf	North Exposed
no	Number
NS	Nash-Sutcliffe Coefficient
p	Significance Value
P	Piezometer
PE	Potential Evapotranspiration (mm d^{-1})
PERC	Percolation Parameter (mm d^{-1})
PIK	Potsdam Institute for Climate Change Research
PP	Catchment Precipitation
PWP	Permanent Wilting Point
Q	Runoff (Discharge) (m^3 s^{-1})
Q_0	Fast Runoff Component
Q_1	Slow Runoff Component
Q_2	Very Slow Runoff Component
Q_e	Event Water Component
Q_F	Quick Flow Volume (m^3)
Q_{obs}	Observed Specific Runoff (mm d^{-1})
Q_p	Pre-Event Water Component
Q_{sim}	Simulated Specific Runoff (mm d^{-1})

Q_T	Total Runoff
Q_{tot}	Total Event Runoff (m^3)
R^2	Correlation Coefficient
RMSE	Root Mean Square Error
R_p	Volume of Quick Flow Q_F as a fraction of Catchment PP (%)
R_y	Volume of Quick Flow Q_F as a fraction of Total Event Runoff Q_{tot} (%)
s	Second
S	Steppe
Sf	South Exposed
SFF	Subsurface Stormflow
SM	Soil Moisture Content
SMHI	Swedish Meteorological and Hydrological Institute, Stockholm
T	Temperature (°C)
T_{2d}	Antecedent Wetness Sum Two Days Prior to the Event
TSDIFF	Adjustment on Zero Melt Temperature Threshold (°C)
θ_r	Residual Water Content ($m^3\ m^{-3}$)
θ_s	Saturated Water Content ($m^3\ m^{-3}$)
US	Upslope
Ust	Upper Zone Storage
UZ1	Threshold for Fast Runoff (Q_0)
V-SMOW	Vienna Standard Ocean Water
VWC	Volumetric Soil Water Content ($m^3\ m^{-3}$)
VWC_i	Relative Increase in Volumetric Soil Water Content ($m^3\ m^{-3}$) (Specific Water Retardation Capacity)
$\overline{VWC_0}$	Mean Pre-Event Volumetric Soil Water Content ($m^3\ m^{-3}$)
$\overline{VWC_t}$	Mean Increase of Volumetric Soil Water Content during stormflow ($m^3\ m^{-3}$)
W	Watt
W	Uncertainty of the Hydrograph Separation (%)

CHAPTER 1

Introduction

The Selenge River Basin in northern Mongolia is part of the Arctic Ocean Basin. It drains an area of approximately 459 000 km^2 northwards and is the major inflow into Lake Baikal. The basin is characterized by a cold, continental and semi-arid climate, where mean annual precipitation is below 300 mm and constitutes only 15 % of mean annual potential evapotranspiration (Ma *et al*., 2003). It is populated by approximately 70 % of the entire Mongolian inhabitants. The Kharaa River is an important tributary positioned north of the Mongolian capital Ulaanbaatar at the south-eastern border of the Selenge River Basin between latitudes 47°53'N and 49°38'N and longitudes 105°19'E and 107°22'E. It drains into the Orkhon River that in turn drains into the Selenge River close to the Mongolian-Russian border. The Kharaa River Basin stretches over an area of 14 534 km² including the dry steppe and the western range of the Khentii Mountains, thus representing environmental conditions typical for large parts of Central Asia. The population is approximately 147 000 (data from 2005), which corresponds to a mean population density of 8 to 10 inhabitants per km^2 (Hofmann *et al*., 2015). About half of the population lives in Darkhan, which is close to the river outlet. The Kharaa River Basin is covered by approximately 59 % grassland, 26 % forest and 11 % arable land (Priess *et al*., 2011).

The Khentii Mountain range is an alpine-type massif characterized by mid- to high mountain ranges that peak at about 2800 m a.s.l. Climate is highly continental and semi-arid with mean annual precipitation of approximately 400 mm, of which at least 70 % fall during summer months (Menzel *et al*., 2011). Especially in arid and semi-arid regions, water availability of the lowlands has been identified to be controlled by mountainous regions (Viviroli *et al*., 2007). Thus, Menzel *et al*. (2011) found the western regions of the Khentii Mountains, especially the Sugnugr Basin and the Bayan Basin, to be the main tributaries ("water towers") of the Kharaa River. Due to their remote location these basins hardly exhibit anthropogenic influence and can be considered to represent pristine and natural conditions. They are partly covered by the Khan-Khentii Strictly Protected Area and have been classified as being in a natural reference state regarding benthic invertebrates (Hofmann *et al*., 2015)

The Sugnugr River is mainly east-west directed, thus subdividing the catchment of approximately 100 km² in size into southerly (Sf) and northerly exposed slopes (Nf). It is

defined as a small siliceous highland river dominated by coarse substrate, characterized by an ice cover from October until April/May and high fluctuations in discharge over the year with pronounced peaks in spring after snow melt and in late summer (Hofmann *et al.*, 2015). Soils in the catchment are generally shallow with underlying crystalline rocks, mainly gneiss and granite. River valleys are covered by alluvial deposits and permafrost is found under Nf-slopes and at higher elevation, but is absent beneath Sf-slopes. The warm, dry and silty soils of the Sf-slopes are vegetated with herb-rich grasslands. On the Nf-slopes, cool, moist and stone-rich silt loam soils are covered by a thick organic surface layer dominated by *Ledum palustre*, *Vaccinium vitis-idaea* and mosses. Here, widespread taiga forests, consisting of *Pinus Sibirica, Larix Sibirica* and *Betula Platyphylla* have developed. All slopes are frequently intermitted by bedrock outcrops and ridges are round-topped. Above the tree line of approximately 2200-2300 m, slopes and summits are dominated by alpine scree.

Mountainous regions in northern Mongolia, including the Khentii Mountains, are part of the discontinuous permafrost zone. The distribution of permafrost in the transition belt between the boreal and dry mid-latitude climates of the Northern Hemisphere is strongly influenced by exposition and vegetation cover, which directly and indirectly influence the surface energy balance (Dulamsuren *et al*., 2005; Dulamsuren and Hauck, 2008). According to the classification of Shur and Jorgenson (2007), this region can be characterized as a climate-driven, ecosystem-protected permafrost area, where permafrost persists at undisturbed late-successional ecosystems. Thus, a forest-steppe mosaic is prevalent, with Sf steppe slopes that are permafrost free and experience seasonal frost. Here, vertical water percolation is assumed to dominate (Ishikawa *et al*., 2005) and soil moisture has been found to be generally low (Li *et al*., 2007a; Dulamsuren and Hauck, 2008; Liancourt *et al*., 2012). In contrast, Nf-slopes are covered with taiga forest and hydrological conditions are influenced by the presence of permafrost. It acts as an impermeable layer that restricts vertical water infiltration and permits lateral downward water movement beneath the surface (Ishikawa *et al*., 2005). The discontinuous permafrost zone is one of the most sensitive areas to climate warming in the world (Gunin *et al*., 1999; Yoshikawa *et al*., 2003; Shur and Jorgenson, 2007).

In Mongolia, an ongoing warming trend of 1.8°C since the second half of the 20th century has been reported by Batima *et al*. (2005). Substantial increases in air temperature and in the frequency of extreme precipitation events have been observed in the Hövsgöl area in northern Mongolia over the last 40 years (Namkhaijanstan, 2006; Nandintsetseg *et al*., 2007). A further significant increase in mean annual air temperature (MAAT) between 1.8 and 4.0°C is predicted

to occur at the end of the 21st century at high latitudes as well as in major parts of Central Asia, including Mongolia (IPCC, 2007; MARCC, 2009). Sato *et al*. (2007) predicts an increase in air temperature by 2°C in summer and 1°C in winter for the near future. However, the authors report high uncertainties regarding future precipitation input.

These warming conditions will increase the evaporative demand and lead to prolonged drought periods during summer. Hence, the frequency and duration of low-flow periods will most likely extend. Already under the current climatic conditions more than 85 % of the annual precipitation is lost due to evapotranspiration (Menzel *et al*., 2011). Minderlein and Menzel (2015) found summer evapotranspiration to exceed precipitation in steppe areas. The authors argue that the majority of stream discharge must be generated by old successional forests. However, the taiga stands are under increasing pressure: besides intensifying logging activities, the frequency and severity of wildfires has been hypothesized to increase as a consequence of climate warming (Flannigan and Van Wagner, 1991). Also the presence of lifestock breeders and wild food gatherers in remote natural systems has increased since the 1990s (Priess *et al*., 2011), further aggravating the risk of forest fires (Hessl *et al*., 2012). As a consequence, the fire regime is expected to shift towards a higher frequency of extreme fire years (Beck *et al*., 2011). Liu *et al.* (2013) found wildfire occurrence to have increased during the last decade in Inner Asia and Nyamjav *et al*. (2007) report the recent fire pattern to affect 14 percent of the total forest land in Mongolia. Especially under natural conditions in remote areas, where fuel is not removed, forest fires can destroy considerable amounts of the widespread taiga forests. The moisture condition of the fire fuels is among the regulating factors of wildfires (Rowe and Scotter, 1973). Wildfires have been shown to significantly affect the hydrological regime in the northern boreal hemisphere (e.g. Brown, 1983; Hinzman *et al*., 2003; Valeo *et al*., 2003; Burke *et al*., 2005).

The abundance of droughts since the end of the 20th century has increased (Davi *et al*., 2010). Although meteorological data are spatially and temporally rare, tree-ring-based reconstructions have shown a high variability of hydroclimatic conditions over the last centuries in north-eastern Mongolia, with alternating drought and wet conditions (Hessl *et al*., 2012; Davi *et al*., 2013; Pederson *et al*., 2013). The authors found evidence that most of the 20th century must be characterized as a relatively wet era and that the severe droughts since the end of the 20th century were not unprecedented. The recent drought periods might rather indicate a backward shift to earlier climatic conditions. However, the observed ongoing changes are of particular importance regarding todays flourishing economy (Karthe *et al*., 2013; Hofmann *et al*., 2015).

Water demands frequently exceeded the water availability after the transition from a socialist to a market-oriented economy since the early 1990s in the Kharaa catchment (Priess *et al*., 2011). Although water availability is today's most important limiting factor for agricultural production (Karthe *et al*., 2015), the Mongolian agricultural sector is currently propagating to a high degree (Pederson *et al*., 2013). Future increase in agricultural lands between 50 % and 100 % are expected (Priess *et al*., 2011), while irrigation is considered to fulfill the related growing water demands. Considering the current and expected rapid growth of the mining, agricultural and urban sectors, each accompanied by rising water demands (Hofmann *et al*., 2015; Karthe *et al*., 2015), it becomes evident that a thorough understanding of runoff generating processes in the mountainous headwaters of the transition zone between steppe and taiga is essential. Still little is known about the factors governing freshwater generation in this data scarce region, and how they are affected by wildfires. This dissertation is primarily based on the results of comprehensive field work that are supplemented by the simulation of land-cover change effects on runoff generation applying a conceptual hydrological model. The results serve as a scientific basis for stakeholders and political decision-makers in order to identify, localize and prioritize protection and rehabilitation measures.

Aims and Objectives

This dissertation aims at an improved understanding of ecohydrological processes in a heterogeneous headwater of the Kharaa River, situated at the western slope of the Khentii Mountains, northern Mongolia. This major aim can be sub-divided into five more specific ones:

1. To examine soil moisture and soil temperature distribution and dynamics as well as physical soil variables at a steppe, pristine and burned taiga site.

2. To examine dominant freshwater generating processes at a steppe and pristine taiga site.

3. To examine changes of dominant freshwater generating processes as a result of wildfires.

4. To simulate the natural runoff from a variety of headwater watersheds.

5. To simulate the hydrological response under land-cover change scenarios in a variety of headwater watersheds.

Just as this chapter acts as an introduction to the dissertation, Chapter 2 gives background information about the identified important ecohydrological conditions in the study region. Chapter 3 and 4 present the dominant freshwater generating processes as a result of a variety of field measurements. Chapter 5 introduces the conceptual hydrological model HBV-D. In Chapter 6, runoff in 2011 and 2012 is simulated applying the HBV-D model, supplemented by the simulation of two different land-cover scenarios in the study region. Chapter 7 gives final comments on the most important outcomes of this dissertation. As the Chapters 2, 3, 4 and 6 cover all relevant informations of the treated subject, they can be excluded from the dissertation as stand-alone articles.

CHAPTER 2

Soil moisture dynamics in a mountainous headwater area in the discontinuous permafrost zone of northern Mongolia

2.1. Introduction

A significant increase in mean annual air temperature (MAAT) between 1.8 and 4.0°C at the end of the 21st century is predicted to occur at high latitudes as well as in major parts of Central Asia, including Mongolia (MARCC, 2009; IPCC, 2007). Already over the last 40 years, substantial increases in air temperature and in the frequency of extreme precipitation events have been observed in the Hövsgöl area in northern Mongolia (Namkhaijanstan, 2006; Nandintsetseg *et al*., 2007). For northern Mongolia, Batima *et al*. (2005) and Sato *et al*. (2007) reported a significant warming accompanied by a decrease in precipitation during the summer within the last 47 years, leading to an increased abundance of droughts over the past decade (Davi *et al*., 2010). During this period, especially after the transition from a socialist to a market-oriented economy since the early 1990s, water demands frequently exceeded the water availability, as exemplary described for the Kharaa catchment by Priess *et al*. (2011).

Although meteorological data are spatially and temporally rare, tree-ring-based hydroclimate reconstructions have shown a high variability of hydroclimatic conditions over the last centuries in northeast Mongolia, with alternating drought and wet conditions (e.g. Hessl *et al*., 2012; Davi *et al*., 2013; Pederson *et al*., 2013). The authors found evidence that most of the 20th century must be characterized as a relatively wet era and that the severe droughts in the early 21st century were not unprecedented. However, the recent changes with the ongoing drying trend are of particular importance regarding the rapid growth of the mining, agricultural and urban sectors (Priess *et al*., 2011; Karthe *et al*., 2013).

The Khentii Mountains in the northeast of Mongolia are situated in the discontinuous permafrost zone, which is one of the most sensitive areas to climate warming in the world (Gunin *et al*., 1999; Yoshikawa *et al*., 2003; Shur and Jorgenson, 2007). The distribution of permafrost in this transition belt between the boreal and dry mid-latitude climates of the Northern Hemisphere is strongly influenced by exposition and vegetation cover, which directly and indirectly influence the surface energy balance (Dulamsuren *et al*., 2005; Dulamsuren and Hauck, 2008). According to the classification presented by Shur and Jorgenson (2007), this region can be characterized as a climate-driven, ecosystem-protected permafrost area, where

permafrost can persist in undisturbed late-successional ecosystems. Thus, a forest-steppe mosaic is prevalent, with southerly exposed steppe slopes that are permafrost free and experience seasonal frost. Here, vertical water percolation is assumed to dominate (Ishikawa *et al*., 2005) and soil moisture has been found to be generally low (Li *et al*., 2007a; Dulamsuren and Hauck, 2008; Liancourt *et al*., 2012). In contrast, northerly exposed slopes are covered with taiga forests and soils are influenced by the presence of permafrost, which acts as an impermeable layer that restricts vertical water infiltration and permits lateral downward water movement beneath the surface (Ishikawa *et al*., 2005).

Regarding the forest-steppe mosaic, the predicted increase in MAAT has the following capabilities: (1) To extend unfavorable conditions for tree growth by the enlargement of steppe zones in presently forested areas. This is due to the fact that the future increase in potential evapotranspiration (ET) is expected to exceed the higher precipitation input in many places in Mongolia (Dulamsuren and Hauck, 2008; MARCC, 2009), resulting in a net loss of forests (Dulamsuren *et al*., 2010b) as tree growth decline and tree mortality are expected to increase (Liu *et al*., 2013). The forest conversion to grassland may further be exaggerated by herbivory small mammals and insects as well as the propagation of tree diseases (MARCC, 2009; Dulamsuren *et al*., 2008; Dulamsuren *et al*., 2010a). (2) To degrade permafrost and increase the thickness of the active layer (IPCC, 2012). This can durably affect local hydrology (Ishikawa *et al*., 2005) and water stress can occur more frequently. The active layer is defined as the soil above the permafrost table that annually freezes and thaws. The depth of the frost table directly controls the rate of subsurface drainage during spring time as horizontal hydraulic conductivity of the saturated organic surface layer decreases exponentially with depth (Quinton *et al*., 2005). Degradation of permafrost alters the permeability and allows precipitation water to percolate deeper. This reduces soil moisture in the organic layer and upper parts of the active layer (Ishikawa *et al*., 2005). (3) To shift the fire regime in boreal forests to a higher frequency of extreme fire years due to an augmentation of future water stress periods alongside increased human activity (Goldammer, 2002; Flannigan *et al*., 2009; MARCC, 2009; Tchebakova *et al*., 2009; Beck *et al*., 2011; Hessl *et al*., 2012; Saladyga *et al*., 2013). Depending on fire severity, wildfires can change hydro-meteorological processes, both immediately and in the long term, as they sustainably alter the ground thermal regime and the distribution of permafrost (Yoshikawa *et al*., 2003). Irreversible changes might occur if permafrost degrades or if combustion penetrates the insulating organic surface layer of the taiga (Hinzman *et al*., 1991; Harden *et al.*, 2006). As the organic surface layer is reduced or removed, surface albedo

decreases, soil thermal conductivity rises, the active layer thickness increases and permafrost degradation accelerates. Simultaneously, soil moisture in the upper layer decreases (Brown, 1983; Hinzman *et al*., 1991; Yoshikawa *et al*., 2003; Ishikawa *et al*., 2005). Regrowth of taiga following wildfires might, therefore, be hindered or possibly not occur at all. Burned forests may take up to 200 years or more to regenerate (Goldammer, 2002; Harden *et al*., 2006).

To our knowledge, few studies exist that deal with soil moisture distribution in a semi-arid forest-steppe ecotone (e.g. Dulamsuren and Hauck, 2008). A substantial number of studies examine the history and the effects of forest fires in permafrost regions in Alaska (e.g. Yoshikawa *et al*., 2003; Harden *et al*., 2006; Bond-Lamberty *et al*., 2009; Flannigan *et al*., 2009; Barrett *et al*., 2011; Beck *et al*., 2011) and few in Siberia and Mongolia (e.g. Tchebakova *et al*., 2009; Zhang *et al*., 2011; Hessl *et al*., 2012; Lopez *et al*., 2012; Saladyga *et al*., 2013). However, no study was carried out that highlights the effects of a recent forest fire on soil moisture distribution in the semi-arid and discontinuous permafrost zone of northern Mongolia.

The objective of the present study is to examine the soil moisture distribution and dynamics as well as the physical soil variables along a transect from a southerly exposed, permafrost-free steppe slope across a river floodplain to northerly exposed permafrost sites, which are covered by pristine, lightly and heavily burned forest.

Our aims were to:

- identify the most important controlling factors with regard to soil moisture distribution in a mountainous headwater area characterized by discontinuous permafrost and heterogeneous vegetation cover

- explore the effects of a wildfire on soil warming and soil moisture dynamics

- derive informations about possible effects of a wildfire on permafrost distribution

2.2. Materials and Methods

2.2.1. Study Site

The study sites are located in the Sugnugr Basin in the Khentii Mountains, approximately 60 km northwest of the Mongolian capital Ulaanbaatar (Figure 1). The Khentii range is an alpine-type massif which stretches over the majority of northeastern Mongolia; it peaks at about 2800 m a.s.l. in the upper parts of the Sugnugr basin. The Sugnugr has been shown to contribute significantly to the discharge of the Kharaa (Menzel *et al*., 2011), the latter draining an area of 15 534 km^2, including the western slopes of the Khentii Mountains and the dry steppe. Therefore, the Sugnugr plays an important role in the water supply of the rural population which is mainly concentrated in the steppe lowlands.

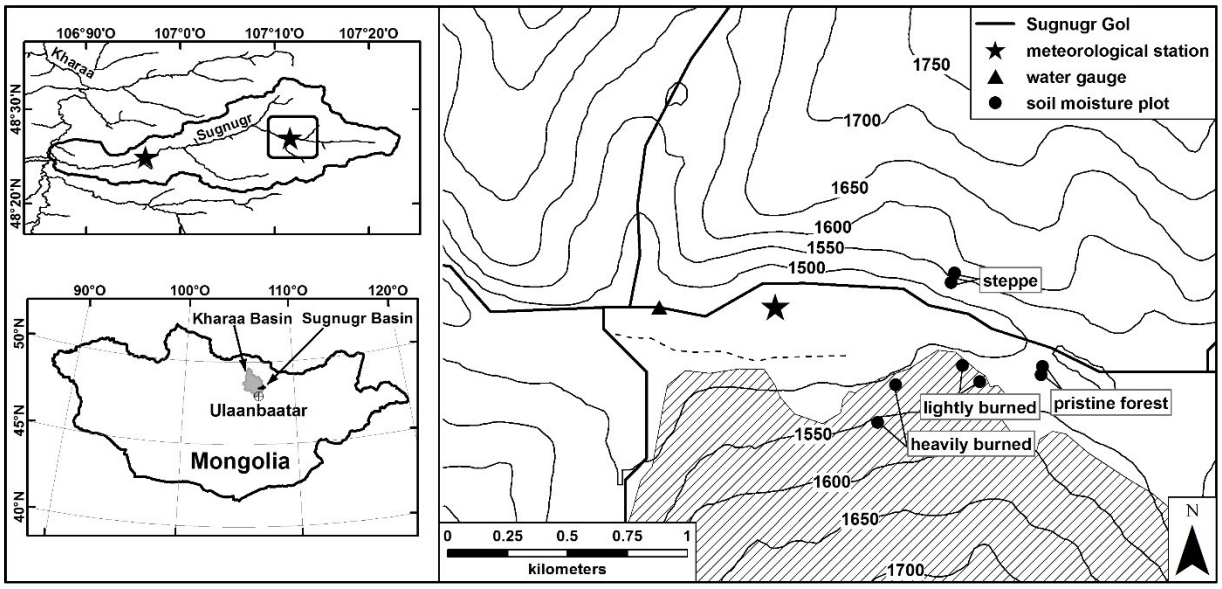

Figure 1: Topographic map of the Sugnugr basin, Mongolia. Shown are the positions of the lower (small map) and upper study site (detailed map).

Climate is highly continental and semi-arid with mean annual precipitation amounts ranging between 250 and 400 mm, of which 70 % fall during the summer months (Menzel *et al*., 2011). The Sugnugr basin has a geological composition of granite and gneiss bedrock and is primarily sedimentary in the floodplain. The river course is mainly east-west directed; it thus subdivides the catchment into southerly and northerly exposed slopes, separated by the river's floodplain.

The lower meteorological station, at an elevation of 1193 m a.s.l. (48°24'55"N, 106°56'21"E) is situated in the vicinity of a settlement were a small number of herdsman live (Figure 1). The

upper site in the headwaters, at an elevation of 1483 m a.s.l. (48°26'55"N, 107°11'41"E) (Figure 2), is virtually unaffected by direct human impacts due to its remote location and poor accessibility. Although forest fires can frequently occur during dry periods in Mongolian boreal forests (Hessl *et al*., 2012), the study site was unaffected by forest fires since, at least, the beginning of the 1960s as shown by satellite images (CORONA and LANDSAT, Chapter 6). Due to a forest fire at the upper site in 2007, which destroyed considerable areas of taiga stands with different intensities (lightly burned at the boundary areas, heavily burned at the center) on the northerly exposed slope, the effects of fire on soil moisture dynamics and ecosystem functioning could be investigated. Until today, the heavily burned area is very sparsely covered with vegetation as succession hardly proceeded.

Figure 2: View over the research area at the upper site. The steep left slopes are steppe vegetated, whereas slopes on the right are covered with burned and pristine taiga.

At the upper study site (Figure 1 and Figure 2) the southerly exposed steppe slope is approximately 27.5° down slope and 31.5° up slope. It is characterized by herb-rich grasslands and dry, relatively warm soils without an organic surface layer. Shallow silty soils underlain by small boulders below a depth of 0.2 m prevail. The northerly exposed slopes exhibit cool and moist soil conditions and are covered by dense taiga consisting mainly of *Pinus Sibirica, Larix Sibirica* and *Betula Platyphylla* and a thick organic layer of mosses and small shrubs, predominantly *Ledum palustre* and *Vaccinium vitis-idaea*. Soils are dominantly silt-loam, which is gradually replaced by coarse gravel and small boulders below a depth of approximately 0.1 to 0.2 m. The slope is 11.5° to 12.0° and the thickness of the organic layer above the mineral

horizon, both on the down- and up-slopes, averages 0.15 ± 0.04 m (n = 30). In contrast, there are major differences of the organic layer in the heavily burned forest. A dry, mostly dead leaf litter layer exists at the surface, with only a very sparse cover of vital mosses and shrubs, averaging a thickness of 0.05 ± 0.03 m (n = 30) down slope and 0.03 ± 0.02 m (n = 30) up slope. Thereby, the mineral horizon is partly exposed. The slope at the heavily burned forest ranges from 11.5° down-slope to 14.5° up-slope. The lightly burned forest has similar slope and soil characteristics as the pristine forest and the thickness of the organic layer ranges from 0.07 ± 0.03 m (n = 20) down-slope to 0.09 ± 0.02 m (n = 20) up-slope.

2.2.2. Instrumentation and Measurements

A meteorological station at the lower site recorded (15 min intervals) air temperature, relative humidity (HMP155, Vaisala) and precipitation (1 min intervals) (Pluvio², Ott), among other parameters, with a CR3000 datalogger (Campbell Scientific). Before the main station was put into operation on 16 June 2011, a meteorological station (WXT5500, Driesen & Kern; weather transmitter WXT520, Vaisala) recorded standard meteorological parameters since October 2010.

At the upper site, field measurements were carried out during the summer months of 2011 and 2012. A meteorological station (WXT5500, Driesen & Kern; weather transmitter WXT520, Vaisala) was installed in the floodplain from 25 June to 26 August 2011 and from 28 May to 3 September 2012. It measured standard meteorological parameters at 2 m above $^2/_3$ of the vegetation height at 15 min intervals. Moreover, net radiation (1 min intervals) and soil temperature (15 min intervals) at a depth of 0.05, 0.1, 0.2 and 0.5 m were recorded. Due to datalogger failure, precipitation measurements are lacking from 14 July to 18 August 2012. During this period, precipitation recorded at the lower site was modified using altitude dependent linear interpolation.

Volumetric soil water content (VWC) was measured at the upper site from 5 July 2011 until 3 September 2012 across three transects. Transect points were installed at the upper and lower slopes of the steppe, as well as in the heavily burned and lightly burned forest. Additionally, VWC was measured at two sites in the floodplain. At each site, frequency domain reflectometery (FDR) sensors (10HS, Decagon Devices) were buried at depths of 0.05, 0.1 and 0.3 m in triple replicates to capture the influence of soil heterogeneity. A datalogger (EM 50, Decagon Devices) recorded VWC at 15 min intervals with an accuracy of ± 3 % using the

standard 10HS sensor calibration equation. On 3 June 2012, the measuring points situated in the lightly burned forest were shifted toward the pristine forest, which allowed a better evaluation of the impact of forest fires. Over rainless days following precipitation events, soil drying rates were calculated as exponential decay (Liancourt *et al*., 2012). Four suitable periods could be identified in summer 2011 and seven periods in summer 2012. Soil hydraulic conductivity ($K_{f(unsat)}$) was determined on several occasions at each site using a minidisk infiltrometer (Decagon Devices) with different suction rates (Zhang, 1997). Suction rates of 2.0 and 0.5 cm were chosen to examine the $K_{f(unsat)}$ of the soil matrix and of the macropores, respectively.

Soil temperature was measured manually across the transects on 17 August 2011 to determine spatial differences. Boreholes were drilled with an Edelman driller (Eijkelkamp) in, at least, triple replicates. After drilling, soil temperature was immediately measured, using a Pt1000 sensor (Greisinger), at 5 cm intervals down to a maximal depth of 0.85 m, as far as boulders and frozen soils allowed. To assess spatial and temporal differences in temperature distribution across the transects, temperature sensors (DS1922L-F5, iButton) were installed in summer 2012 at the upper sites of the three transects, which continuously recorded soil temperature at hourly intervals from 23 June 2012 to 3 September 2013. Three replicates at depths of 0.05, 0.1 and 0.3 m at each site, and additionally at a depth of 0.5 m at the heavily burned forest, accounted for soil heterogeneity.

2.2.3. Laboratory Analysis

To determine the water retention characteristics, undisturbed soil samples (100 cm^3) were taken from the upper and lower steppe, lightly burned and heavily burned sites at depths of 0.05, 0.1 and 0.3 m, directly adjacent (within 0.3 m) to the FDR probes, in June 2011. The analysis was performed using a pressure plate apparatus. VWC was measured gravimetrically during the drying phase at nine increments of pressure head, ranging from 0.01 m (near saturation (θ_s)) to 160 m (permanent wilting point (θ_r)). Water retention curves were fitted applying the van Genuchten (1980) analytical model.

2.2.4. Statistics

The aim of the statistical analysis using the statistics software R (http://www.r-project.org) was to ascertain the effects of the slopes with different vegetation types, inclination, exposure and solar radiation on VWC, soil temperature and infiltration capacity (both soil matrix and macropore infiltration) over the observation periods. To distinguish between inter-annual variations, VWC analysis was undertaken separately for the summer periods of 2011 and 2012. The normality of the data was assessed by the Shapiro-Wilk and the Kolmogorow-Smirnow tests and, a log-transformation was applied when required. Sphericity was verified by the Mauchly test and, if necessary, a Greenhouse-Geisser correction (Huynh-Feldt correction for small sample size) was made. A one-way analysis of variance (ANOVA) for repeated measures was applied to examine whether significant differences in the data sets exist. Afterwards, the paired t-test with Bonferroni correction ($\alpha = 0.05$) was used as a post hoc comparison to assess the pairwise differences between the slope sites.

2.3. Results

2.3.1. Meteorological Parameters

During the year 2011 (2012), mean annual air temperature (MAAT) was -1.8°C (-3.0°C) and annual precipitation amounted to 317 mm (391 mm) at the lower site. The mean monthly air temperature varied between -28°C in January (2011 and 2012) and 16°C in August 2011 and July 2012 (Figure 3). The precipitation amount of 220 mm during the summer months (June to August) in 2011 was smaller compared to 275 mm in 2012.

The upper site was generally 2 to 3°C colder during the summer measurement campaigns of 2011 and 2012 than the lower site. A daily mean air temperature of 12.4°C (2011) and 11.3°C (2012) was observed during the measurement periods. Also summer 2011 was substantially dryer with 171 mm of precipitation in comparison to 317 mm in 2012 (25 June, to 26 August, respectively) and mean daily global radiation varied between -221.9 W m^{-2} (2011) and -195.9 W m^{-2} (2012). Fair-weather periods were characterized by daily air temperatures of around 20.0°C, daily relative humidity of 50-60 % and daily net radiation intensities of -190.0 W m^{-2}. These periods alternated with rainy days, with typical average daily air temperatures between 5.6°C (2011) and 2.9°C (2012), daily relative humidity of 90 % and daily net radiation intensities of around 0.0 W m^{-2}.

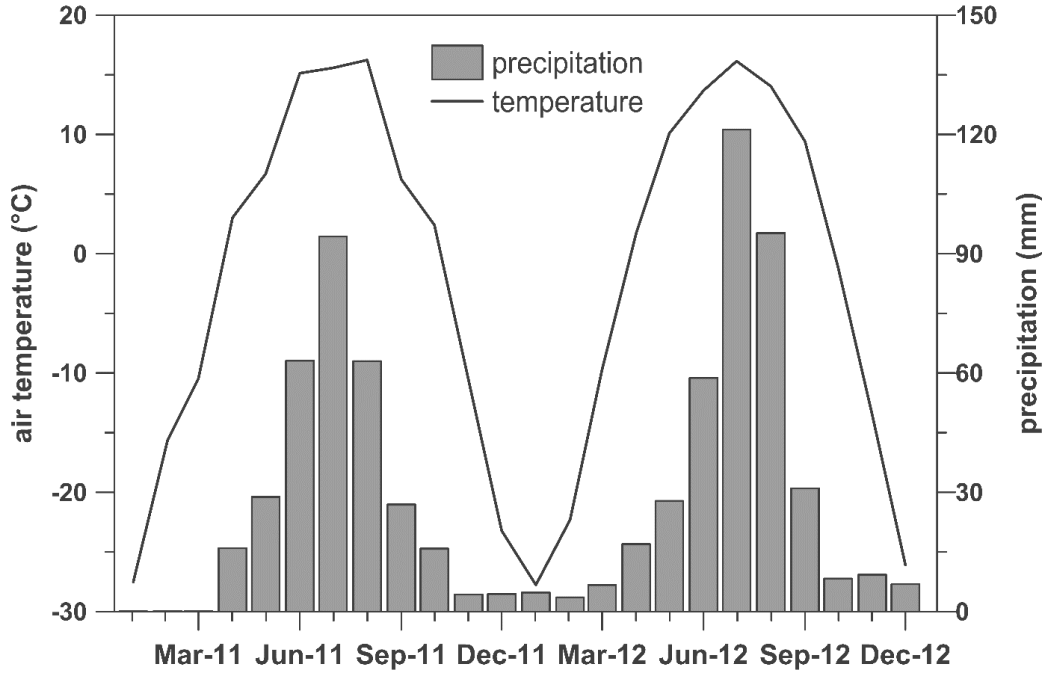

Figure 3: Monthly air temperature (°C) and precipitation (mm) recorded at the lower steppe site from January 2011 until December 2012.

2.3.2. Surface Infiltration

A clear tendency was revealed by the distribution of the measured unsaturated hydraulic conductivity ($K_{f(unsat)}$) (n = 6) across the transects at the upper site (Figure 4). Among all sites, the southerly exposed slope showed the lowest mean measured $K_{f(unsat)}$ values of the soil matrix (0.20 ± 0.08 m d^{-1}, up slope) and of the macropores (0.41 ± 0.18 m d^{-1}, up slope). At the northerly exposed slope, the highest values of $K_{f(unsat)}$ were observed at the pristine forest, mean rates occurred at the lightly burned forest, whereas the lowest rates were measured at the heavily burned forest. Thus, the pristine forest up slope matrix infiltration and macropore infiltration were 2.02 ± 0.65 m d^{-1} and 6.25 ± 2.36 m d^{-1}, respectively. In contrast, at the heavily burned forest up slope matrix infiltration of 0.13 ± 0.12 m d^{-1} and macropore infiltration of 0.40 ± 0.24 m d^{-1} were substantially lower. The observed mean up slope infiltration rates at the lightly burned forest of the soil matrix (n = 4) and of the macropores (n = 3) were 0.35 ± 0.29 m d^{-1} and 0.378 ± 0.29 m d^{-1}, respectively. $K_{f(unsat)}$ values at the down slope sites were similar across the transects and high infiltration rates were measured at the river floodplain.

The results of the ANOVA showed that soil matrix infiltration of the pristine forest was significantly higher compared to the highly burned forest (p = 0.02 up slope and p = 0.04 down

slope) and steppe sites (p = 0.01 up slope and p = 0.04 down slope). Also, the macropore infiltration rates of the pristine forest were significantly higher compared to the heavily burned forest (p = 0.02 up slope and p = 0.00 down slope) and steppe sites (p = 0.03 up slope and p = 0.00 down slope).

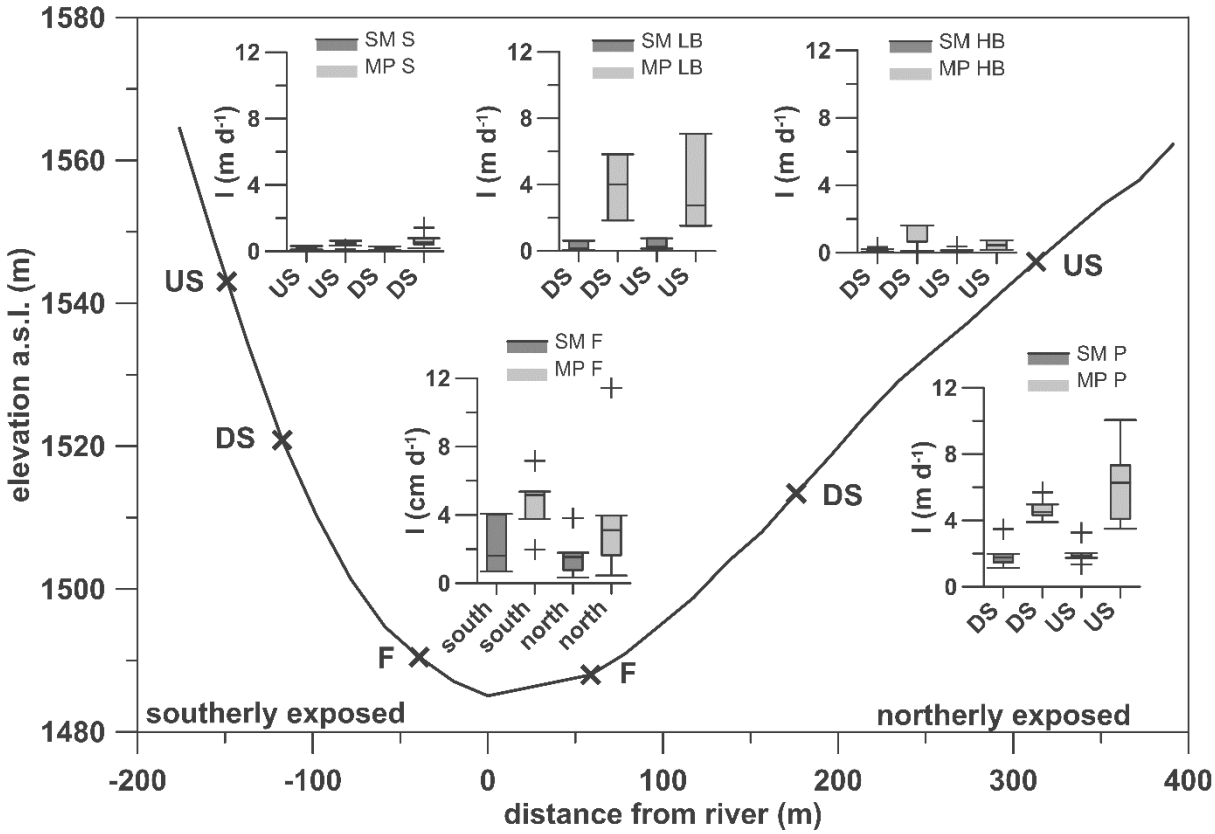

Figure 4: Unsaturated soil matrix (SM) and macropore (MP) infiltration rates (I) of the upslope (US) and downslope (DS) sites of the steppe (S), lightly burned forest (LB), heavily burned forest (HB), pristine forest (P) and the floodplain (F).

2.3.3. Soil Temperature, Soil Moisture and Soil Drying

Soil temperatures showed characteristic, site dependent behavior. During the manual measurements in mid-August 2011 the lowest soil temperatures were observed in the pristine forest. With a mean value of 12.8°C at a depth of 0.3 m, the southerly exposed site was the warmest, followed by the floodplain (11.3°C), the heavily burned forest (7.2°C), the lightly burned forest (4.5°C) and the pristine forest (2.7°C). Additionally, a northerly exposed terrace, vegetated by grasses and shrubs at the slope bottom, was examined. Here, deeper drilling was possible and frozen soils were found at a depth of 0.7 m. During the summer months of 2012,

temperatures were highest at the southerly exposed slope, where also the diurnal amplitude was most pronounced (Figure 5). The heavily burned forest was characterized by higher mean temperatures than the pristine forest (1.5 times, 1.7 times and 2.0 times at depths of 0.05, 0.1 and 0.3 m). Results of the ANOVA revealed significant differences among all slopes (p values < 2.0×10^{-16}).

Table 1: Mean, minimal and maximal recorded soil temperatures (°C) at the up slope sites during the observation period from 23 July to 1 September 2012.

Site	Depth (m)	Mean soil temperature (°C)	Minimum soil temperature (°C)	Maximum soil temperature °C)
Steppe	0.05	16.2 ± 0.5	9.98	21.22
	0.1	16.0 ± 0.3	10.75	20.41
	0.3	14.9 ± 0.3	11.82	17.78
Pristine forest	0.05	7.3 ± 1.5	2.71	11.61
	0.1	5.8 ± 1.6	1.63	9.02
	0.3	4.1 ± 1.6	0.94	6.45
Heavily burned forest	0.05	11.2 ± 1.8	7.17	15.01
	0.1	10.1 ± 2.4	6.87	13.21
	0.3	8.4 ± 2.6	5.63	10.53
	0.5	6.7 ± 2.7	4.07	8.27

At all sites, the mean winter volumetric water content (VWC) was small. During the summer periods of 2011 and 2012, the lowest mean values of VWC were found at the southerly exposed slope at all depths and standard deviation was low. Also the amplitude of the recorded VWC values at this slope was greater, and the response to rainfall events was most pronounced at depths of 0.05 and 0.1 m. Most strikingly, the mean VWCs during the comparison period from 5 July until 3 September were approximately 1.9 times higher at all depths in 2012 than during the dryer summer of 2011. Inter-annual variability and short-term soil moisture dynamics at the northerly exposed slopes were less pronounced and the mean VWC values were higher, with relatively constant high values at the heavily burned forest (Figure 6). Comparing the soils of the pristine and heavily burned forest, it is evident that VWC at a depth of 0.05 m was drier in the pristine forest. The ANOVA revealed VWCs to be significantly different among the slopes at each depth during the summer period 2011 and 2012 (p values < 1.0×10^{-3}).

The determined mean soil drying rates across the transects are depicted in Figure 7. At a depth of 0.1 m, the rates were highest (23 %) at the southerly exposed slopes in summer 2011

and slightly higher (15 %) during summer 2012 compared to the pristine forest (11 %). The smallest mean soil drying rates at a depth of 0.1 m were observed at the heavily burned forest with values of 4 % (3 %) during summer 2011 (2012). Generally, smaller rates were observed during the wetter summer 2012. The drying rates of the lightly burned forest were between the above mentioned rates of the pristine and heavily burned forest during summer 2011.

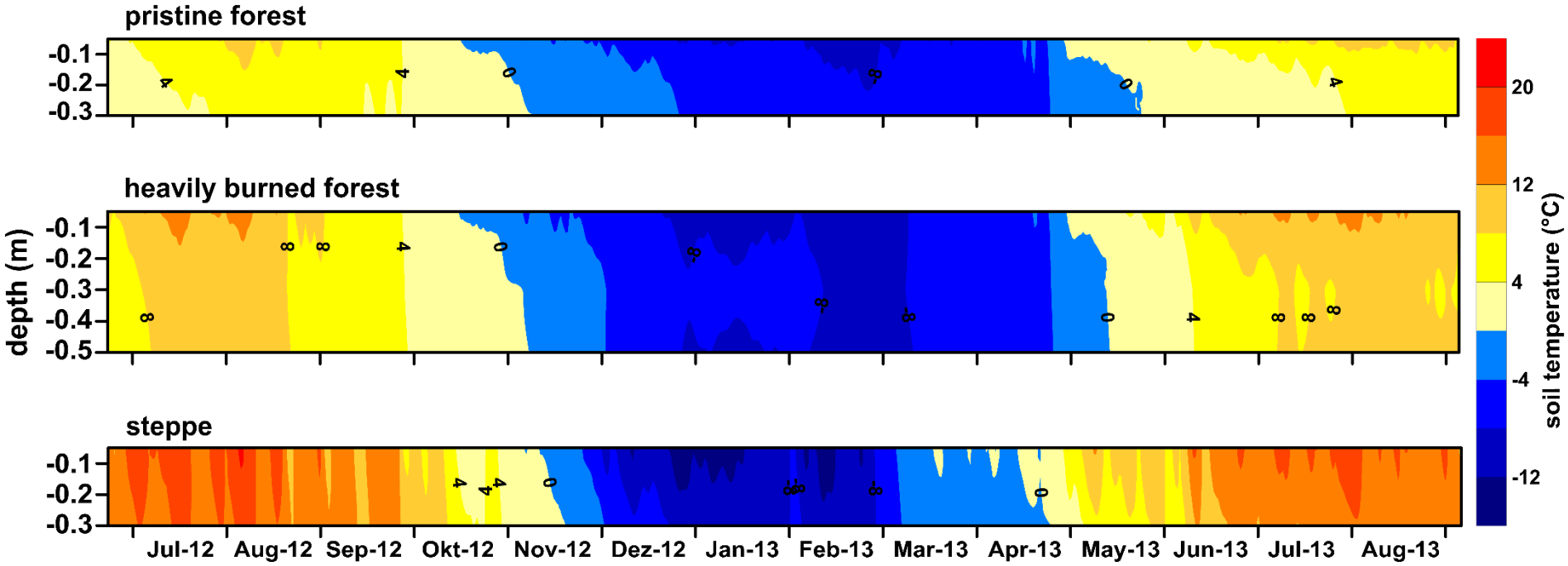

Figure 5: Mean recorded soil temperatures (°C) at the upper slope sites.

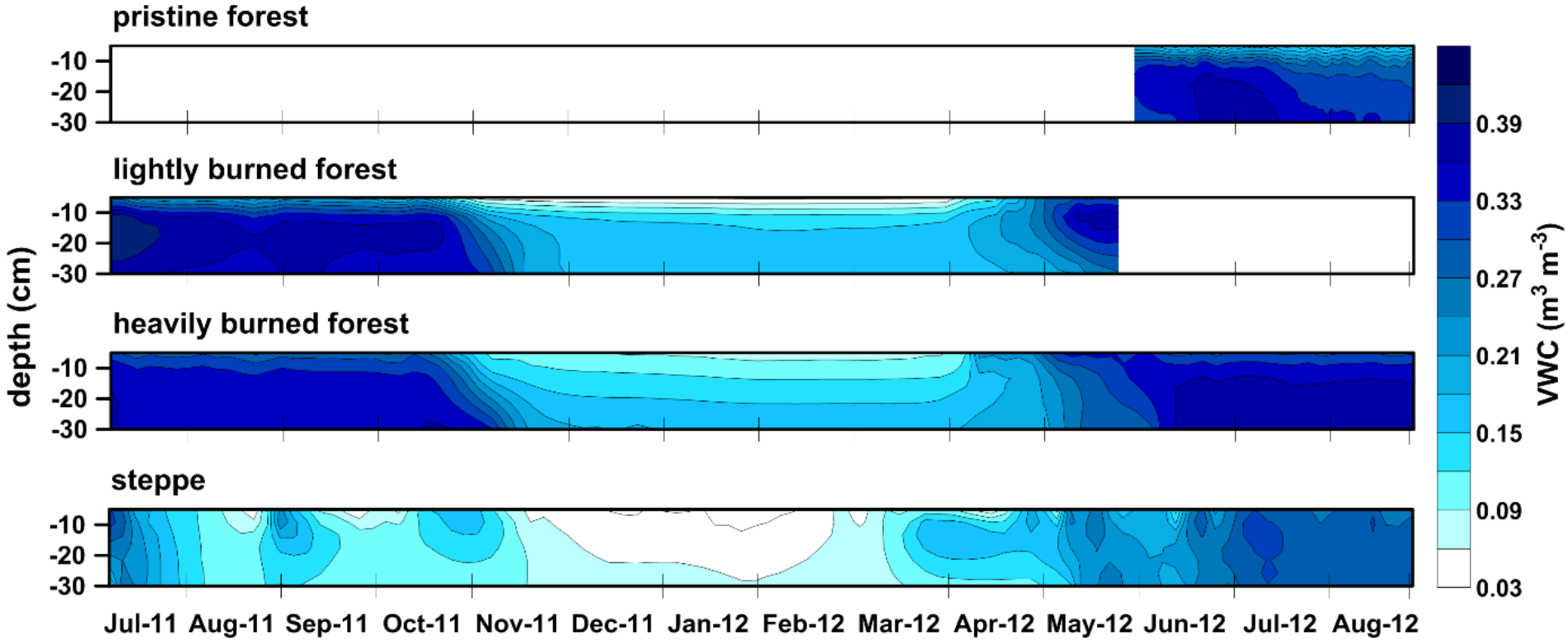

Figure 6: Mean volumetric soil moisture contents (VWC) in m^3 m^{-3} of the down- and up slope sites. FDR sensors of the lightly burned forest were removed at the beginning of June 2012 and installed at the pristine forest.

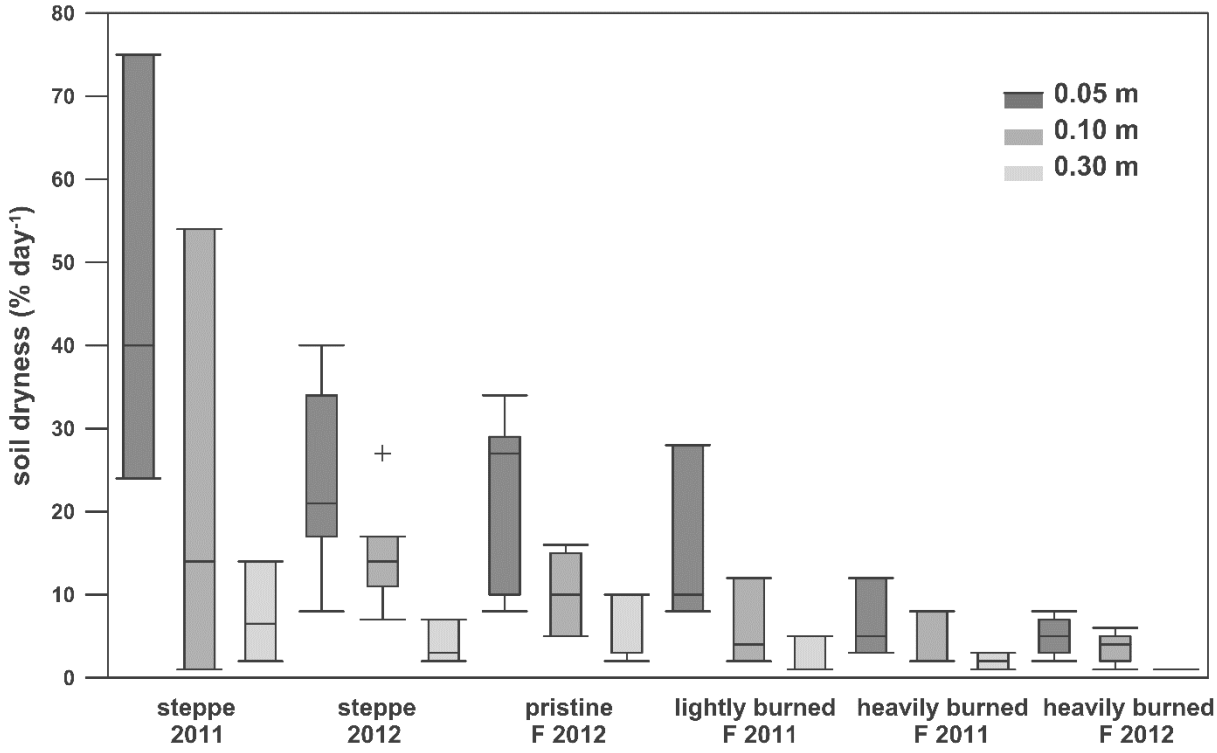

Figure 7: Determined soil drying rates ($‰_v$ d^{-1}) for the summer periods. The lightly burned sites were shifted toward the pristine forest at the beginning of June 2012.

2.3.4. Pressure Plate Analysis

The results of the pressure plate analysis indicate that the residual moisture content (θ_r) at the permanent wilting point (PWP) ranged between 0.07 and 0.11, 0.10 and 0.16 as well as 0.08 and 0.11 m^3 m^{-3} for the upper steppe, lightly burned and heavily burned forest, respectively (Figure 8).

The mean VWC at the upper steppe slope during the dry summer period of 2011 was 0.15 m^3 m^{-3} (Table 2), which corresponds to soil tensions of about 7.6 m. However, minimum VWC at all depths dropped to values below the PWP (> 160 m) during drought periods, resulting in heavily water-stressed conditions. In 2012, during the comparison period from 5 July to 3 September, mean VWCs were considerably higher (0.27 m^3 m^{-3}) and mean soil tensions were around 1.8 m; minimum VWC values were clearly above the PWP (Table 2). However, VWC at a depth of 5 cm was close to the PWP at the end of May and mid-June (Figure 6). Mean and minimum VWC values at both the lightly and heavily burned sites were above the PWP in 2011. Water-stressed conditions did not occur at these sites during the observation period.

Mean VWCs at the pristine forest and the heavily burned sites were 0.25 m^3 m^{-3} and 0.30 m^3 m^{-3} in 2012. As the pristine forest was not analyzed by the pressure plate method, we compared measured VWCs at a depth of 0.05 m with the water retention curve of the lightly burned forest. This analog could be conducted as soils of the pristine forest are comparable to those of the lightly burned forest with regard to the composition of the organic surface layer. As the mean VWC during the summer of 2012 at this depth was 0.15 m^3 m^{-3} (soil tension of 26 m) and even dropped to minimum values of 0.10 m^3 m^{-3} (pressure head >160 m), water-stressed conditions might have occurred. The results for the lower sites were similar across the transects (data not shown).

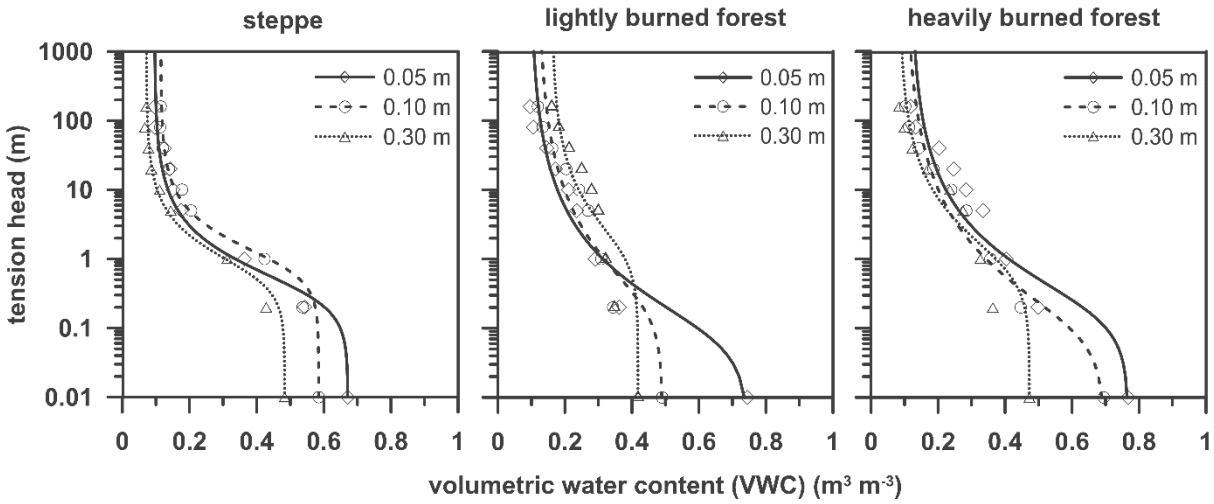

Figure 8: Results of the variation in soil moisture content determined from the pressure plate analysis according to the method proposed by van Genuchten (1980).

Table 2: Mean, minimal and maximal daily volumetric water content (VWC) in m^3 m^{-3} during the observation period from 5 July 2011 until 3 September 2012.

Site	Depth (m)	Mean VWC (m^3 m^{-3}) 2011 / 2012	Minimum VWC (m^3 m^{-3}) 2011 / 2012	Maximum VWC (m^3 m^{-3}) 2011 / 2012
Steppe	0.05	0.15 ± 0.03 / 0.27 ± 0.03	0.03 / 0.23	0.31 / 0.32
	0.1	0.16 ± 0.03 / 0.29 ± 0.02	0.07 / 0.25	0.32 / 0.33
	0.3	0.15 ± 0.03 / 0.29 ± 0.02	0.09 / 0.23	0.27 / 0.31
Heavily burned forest	0.05	0.29 ± 0.09 / 0.30 ± 0.06	0.26 / 0.28	0.31 / 0.31
	0.1	0.33 ± 0.10 / 0.34 ± 0.10	0.32 / 0.33	0.36 / 0.36
	0.3	0.35 ± 0.06 / 0.38 ± 0.03	0.34 / 0.38	0.36 / 0.39
Lightly burned forest (2011) and pristine forest (2012)	0.05	0.21 ± 0.10 / 0.15 ± 0.09	0.18 / 0.10	0.26 / 0.18
	0.1	0.34 ± 0.09 / 0.27 ± 0.09	0.30 / 0.23	0.40 / 0.32
	0.3	0.36 ± 0.05 / 0.35 ± 0.08	0.35 / 0.32	0.39 / 0.39

2.4. Discussion

Significant differences in the distribution of volumetric soil water content (VWC) in time and space across the three transects at the upper site were observed (Figure 6). During drought periods in summer, a clear tendency was revealed from warm and dry soils beneath the steppe vegetation toward cold and wet soils of the taiga forest (Figure 5 and Figure 6). This can primarily be derived from differences in exposition, slope inclination, plant coverage and permafrost distribution (Ishikawa *et al*., 2005; Dulamsuren and Hauck, 2008; Liancourt *et al*., 2012).

2.4.1. Steppe

At the permafrost-free, southerly exposed steppe slopes, intense net radiation resulted in a strong diurnal soil temperature pattern during the summer of 2012, as temperatures increased up to a maximum of 29°C at depth of 0.05 m in the afternoon and declined to a minimum of 7°C in the early morning. The high daily soil drying rates of 47 % at a depth of 0.05 m (Figure 7) and relatively low precipitation resulted in water-stressed periods in 2011, when the VWC temporarily dropped below the permanent wilting point (PWP) (Figure 6). This limitation in plant-available water during drought periods can explain the observation that, on the southerly exposed slopes, conifers are not able to grow and steppe vegetation dominates. This finding is in accordance to the literature (Etzelmüller *et al*. 2006; Heggem *et al*., 2006; Dulamsuren *et al*., 2008). During the wetter summer period of 2012, the VWC was above the PWP and daily soil drying rates were lower (24 % at a depth of 0.05 m) due to higher VWC values and precipitation amounts compared to 2011 (Figure 6 and Figure 7). A similar observed difference in soil drying rates between two years, with smaller values during the wetter year, was reported by Liancourt *et al*. (2012) for a southerly exposed steppe slope in northern Mongolia. In summer 2012, daily actual evapotranspiration (AE) rates peaked at around 6 mm d^{-1} after periods with high precipitation input and thus relative high VWC, whereas actual ET rates gradually declined (< 1 mm d^{-1}) during water-stressed conditions, as examined by Minderlein and Menzel (2015) using the Bowen ratio energy balance method.

Steep slopes and low infiltration rates (Figure 4) reduced the amount and depth of percolating precipitation water. Occasionally, overland flow could be observed during high-intensity precipitation events. The observed low VWCs of less than 0.1 m^3 m^{-3} at the southerly exposed slopes during drought periods are in accordance with the studies of Li *et al*.

(2007a), Dulamsuren and Hauck (2008) and Liancourt *et al*. (2012). However, high daily VWC values > 0.3 m^3 m^{-3}, as observed in our study at the southerly exposed steppe slopes during rainy periods, were not reported earlier.

2.4.2. Pristine Forest

The pristine forest at the less inclined northerly exposed slope exhibited similar soil drying rates as the steppe slope during the growing season of June, July and August 2012 (Figure 7). However, the VWC remained high at a depth of 0.3 m, with only small variations following precipitation events (Figure 6). This can be attributed to the storage of a considerable amount of water in the active layer, which is underlain by the impermeable permafrost (Sugimoto *et al*., 2002; Ishikawa *et al*., 2005; Etzelmüller *et al*., 2006). As soil temperature at a depth of 0.3 m gradually increased from 0.9°C at the end of June to a maximum of 6.5°C at the beginning of August 2012, the underlying permafrost degraded deeper into the mineral horizon and the thickness of the active layer increased (Ishikawa *et al*., 2005; Quinton *et al*., 2005; Heggem *et al*., 2006). Sugimoto *et al*. (2003) observed a maximum thickness of the active layer of 1.2 to 1.5 m at the end of August underneath a larch forest in East Siberia near Yakutsk. Precipitation water, infiltrating at significantly highest rates (Figure 4) into the organic surface layer, now percolated deeper into the soils. The observed decrease in VWC at a depth of 30 cm from mid-July after the soil thawed is coherent with results reported by Takata (2002) and Sugimoto *et al*. (2003). Using a one-dimensional land surface model, Takata (2002) showed that a wet soil zone is formed above the thawing front. This zone moves down as thawing progresses and soils in the upper part are drained. Subsequently, the previous shallow lateral subsurface drainage in the organic layer with high hydraulic conductivity is stopped (Quinton *et al*., 2005), except for excess water during periods with high precipitation input. Mean daily ET rates of the boreal canopy are reported to account for approximately 1.4 to 2.3 mm d^{-1} (Ohta *et al*., 2001; Lopez *et al*., 2008; Ohta *et al*., 2008). The organic surface layer in the pristine forest reduces VWC at the surface during drought periods due to daily ET rates ranging between 0.3 and 1.5 mm d^{-1} (Heijmans *et al*., 2004; Bond-Lamberty *et al*, 2009). This considerable loss resulted in the relatively high soil drying rates and low VWC at the soil surface at a depth of 0.05 and 0.1 m observed for the pristine forest in our study. As water-stressed conditions might occur during drought periods at a depth of 0.05 m, the spreading of forest fires is facilitated (Rowe and Scotter, 1973).

Thawing permafrost plays an important role as a direct source of water for the larch trees during drought periods, as observed by Sugimoto *et al*. (2002). Li *et al*. (2007b) found soil water in the uppermost 0.3 m to be the main source for larch trees in months with little precipitation input. In return, the taiga forest protects the permafrost due to reduced net radiation input through canopy interception and by the thermal insulating capacity of the organic layer (Brouchkov *et al*., 2005; Harden *et al*., 2006; Heggem *et al*., 2006; Zhang *et al*., 2011). Yoshikawa *et al*. (2003) stated that an organic surface layer with a thickness of 0.1 m provides adequate thermal resistance to protect the frozen mineral soil.

2.4.3. Burned Forest

Following deforestation due to wildfire, shadowing, organic layer thickness and albedo are decreased, yielding a greater absorption of shortwave radiation at the ground's surface. Simultaneously, soil properties, such as soil density and moisture, infiltration and evaporation rates, thermal conductivity and heat capacity are altered (Hinzman *et al*., 1991; Yoshikawa *et al*., 2003; Brouchkov *et al*., 2005; Dulamsuren *et al*. 2005; Iwahana *et al*., 2005; Harden *et al*., 2006; Etzelmüller *et al*., 2006). We observed a decrease in vital organic surface cover in the lightly burned area and a removal in most areas of the heavily burned forest. Yoshikawa *et al*. (2003) reported that the ratio of ground heat flux and sensible heat flux to net radiation increased following fire, whereas the latent heat flux decreased. The authors stated that differences in temperature between soils of burned and unburned forests have been shown to correlate with the thickness of the organic and active layer. Therefore, thermal conductivity increases after the organic layer is reduced or removed. This effect could be observed at the heavily burned forest as soil temperatures were significantly higher compared to the pristine forest at all depths ($p < 2.0 \times 10^{-16}$). This is enforced by the prevalent wet soils at these sites as high VWCs are reported to further increase thermal conductivity (Takata, 2002; Harden *et al*., 2006; Shur and Jorgenson, 2007). Depending on fire severity, the above mentioned factors can explain the differences in soil temperature between the northerly exposed sites (Figure 5).

As a consequence of the reduced AE after the removal of the vegetation, significantly highest mean VWCs across the transects were found at the lightly and heavily burned forest in 2011 and 2012, respectively (Figure 6).

Hence, as transpiration came to a virtual standstill, calculated soil drying rates were smallest at the heavily burned sites (Figure 7). This finding is in accordance with Iwahana *et al*. (2005)

who observed soil water retention after one year at a cutover site compared to a reference forest site near Yakutsk, eastern Siberia. Yoshikawa *et al.* (2003), who studied post fire behavior of boreal forests in Alaska, reported short-term soil moisture increases after wildfires as transpiration rates decreased due to the loss of vegetation and long term (more than a decade) drying due to an increasing thickness of the active layer and the recovery of vegetation. The increased soil temperatures of the heavily burned forest clearly indicate enhanced permafrost degradation to deeper depths as we recorded temperature values up to 8°C at a depth of 0.5 m in July and August (Figure 5). Iwahana *et al*. (2005) stated that vegetation removal enhanced ground thawing and therefore increased the thickness of the active layer by 0.14 m after one year. These changes in active layer thickness affect local hydrology. Infiltrating precipitation water now percolates deeper into the warm and more permeable permafrost (Brouchkov *et al*., 2005; Ishikawa *et al*., 2005; Quinton *et al*., 2005), possibly resulting in thermokarst (Iwahana *et al*., 2005) and dryer soils in the long term (Yoshikawa *et al*., 2003). This may further exacerbate permafrost recovery, as the conduction of cold winter temperatures toward the underlying soils is reduced in dry soils (Harden *et al*., 2006). Typically, a time span occurs of between 3 to 5 years after boreal forest fires during which the active layer increases to a thickness that does not completely refreeze the following winter (Brown, 1983). DeBano (2000) reported a near surface hydrophobic layer after burning that can resist surface water infiltration, which is coherent with the significantly lower surface infiltration rates measured in the heavily burned forest compared to the pristine forest (Figure 4). This reduced infiltration capacity might further limit recharge in the active layer following precipitation events and increase hillslope runoff, as the severity of water repellency at lower soil water contents is enhanced, especially during the dry season (DeBano *et al*., 2000).

2.5. Conclusion

This study examined the distribution of different soil parameters in a semi-arid forest-steppe ecotone. In particular, the effects of a recent forest fire in 2007, which was characterized by different burn intensities, in the Khentii Mountains in northern Mongolia were investigated. The hydroclimatic conditions in this region have been shown to undergo frequent changes over the last 300 years (Pederson *et al*., 2013). However, the current climatic conditions can sustainably alter this fragile ecosystem, which can be considered to be representative of other semi-arid mountainous areas in northern Mongolia. Considering the increasing anthropogenic and natural disturbance regime, as for example by wild food gatherers, increasing MAAT and

drought conditions, these are likely to result in declined tree growth and increasing tree mortality (Dulamsuren *et al*., 2010b; Liu *et al*., 2013), as well as in a propagation of forest fires (Hessl *et al*., 2013). Therefore, the forest cover and the distribution of the coupled permafrost-forest system are decreasing. Once permafrost is degraded, water stress generally increases on the long-term while the vegetation regime shifts towards deciduous species, especially *Betula* (Otoda *et al*., 2012). Therefore, the forest composition may change as a consequence of wildfire, as the post-fire tree species composition depends on seed supply and soil surface conditions (Johnstone and Chapin, 2006). Although our results show an increase in soil moisture four and five years after a forest fire, the study of Yoshikawa *et al*. (2003) gives a strong hint towards long-term drying and expansion of steppe areas (Dulamsuren *et al*., 2010b), that is adapted to water limitation during drought periods.

As mountain forests form the main water generating areas in the forest-steppe ecotone (Karthe *et al*., 2013; Minderlein and Menzel, 2015), their future development must be of special interest, especially considering the growing demand for water in urban, agriculture and mining development (Priess *et al*., 2011; Karthe *et al*., 2013; Pederson *et al*., 2013). Hence, longer observational studies of soil moisture distribution and of the rate of vegetation change following forest fires in the forest-steppe ecotone of northern Mongolia are necessary.

CHAPTER 3

Effects of wildfire on runoff generating processes in northern Mongolia

3.1. Introduction

In The Kharaa River Basin, situated north-west of the Khentii Mountains in northern Mongolia, water demands from urban, agricultural and mining sectors frequently exceeded the water availability during the last decades (Priess *et al*., 2011). The Kharaa River is part of the Selenga-Baikal drainage system. The Selenga has a basin area of 477 000 km² and drains major parts of the mountain and arid-land permafrost of Mongolia. Especially after the transition from a socialist to a market-orientated economy in the 1990s frequently occurred and water shortage has intensified (Davi *et al*., 2013; Pederson *et al*., 2013). Considering the ongoing rapid economic growth, a detailed understanding of the most important freshwater generating processes in the headwaters is of crucial importance to successfully address future water supply (Karthe *et al*., 2015). The problem of water shortage is aggravated by the observed increase in mean annual air temperature (MAAT) (Davi *et al*., 2010; Törnqvist *et al.*, 2014) during the last decades in Mongolia. Higher MAAT increases potential evapotranspiration (PE) and thus affects water scarcity in semi-arid regions. In addition, wildfire magnitude and frequency during drought periods is favored (Onodera and van Stan, 2011), possibly resulting in substantial ecological and hydrological changes (Kopp *et al*., 2014).

The semi-arid discontinuous permafrost zone of the Khentii Mountains is characterized by high climate variability and strong ecosystem vulnerability against air temperature and precipitation changes. A detailed description of permafrost characteristics in the Khentii Mountains is given by Ishikawa *et al.* (2005). The authors state that the hydrologic regime in this mountainous forest-steppe ecotone differs greatly, depending on exposure, vegetation distribution and the presence or absence of permafrost. Permafrost distribution is climate-driven and ecosystem-protected and thus persists beneath undisturbed late-successional ecosystems (Shur and Jorgenson, 2007). The observed increase in MAAT has the capability to result in soil warming, permafrost degradation (e.g. Osterkamp, 2007; Zhao *et al.*, 2010; Törnqvist *et al.*, 2014) and hence to cause distinct changes of the hydrological regime (Ishikawa *et al*., 2005; Woo *et al*., 2008). Although Minderlein and Menzel (2015) identified taiga forests to be the main source of freshwater in the transition zone between steppe and taiga, still little is known

about the factors governing freshwater generation in this data scarce region, and how they are affected by wildfires.

However, hydrological analogies from similar physiographic and hydrological settings in North America can be derived from a number of process studies: the presence of permafrost and the depth of the active layer, a soil zone above the permafrost that annually freezes and thaws, have been shown to control runoff pathways during stormflow (Carey and Woo, 2000, 2001a, 2001b; Petrone *et al*., 2007). These studies found stormflow runoff to be controlled by a two-layer flow system, with: (i) quickflow in a highly conductive organic surface layer and along the organic-mineral interface; (ii) slowflow in the mineral horizon. However, in a permafrost environment seasonal dynamics differ as the position of the frost table governs the proportion of hillslope runoff divided into quick- and slowflow. Hence, the contribution of quickflow is highest in early summer, resulting in pronounced runoff responses (Yamazaki *et al*., 2006). While the thickness of the active layer increases during summer, slowflow dominates the hydrological response. Tracer techniques applied in early summer at a taiga covered north facing (Nf) slope in the Sugnugr Basin within the Khentii Mountains, showed full infiltration and quickflow runoff above the mineral layer (Lange *et al*., 2015).

Although forest fires frequently occur during dry periods in Mongolian boreal forests (Hessl *et al*., 2012), the Sugnugr Basin has been unaffected by forest fires since, at least, the beginning of the 1960s, as shown by satellite images (CORONA and LANDSAT, Chapter 6). However, a forest fire in 2007 destroyed considerable areas (~30 % of the forest stands). Until today, the heavily burned area is very sparsely covered with vegetation as succession hardly proceeded.

Wildfires have significant impacts on hydrological, geomorphological and biogeochemical processes (DeBano, 2000; Yoshikawa *et al*., 2003; Dulamsuren *et al*., 2005; Petrone *et al*., 2007; Onodera and van Stan, 2011). In the study area, the combustion of the organic surface layer has been shown to result in increased soil temperatures and permafrost degradation (Kopp *et al*., 2014). If the active layer increases to a thickness that does not completely refreeze during the following winter, a talik is formed on the long-term. A talik is defined as a layer of unfrozen soil above the permafrost, characterized by a greater thawing depth during the warm period than the amount refreezing during the winter. This allows soils to be drained throughout the year, causing them to dry out (Hinzman *et al*., 2003). Hence, post-fire taiga regrowth is limited (Tchebakova *et al*., 2009) and the vegetation regime shifts towards deciduous species (e.g.

Betula) and an increasing abundance of grassland species (Hinzman *et al*., 2003; Dulamsuren *et al*., 2005; Dulamsuren and Hauck, 2008; Tchebakova *et al*., 2009).

The objectives of this study were to increase our knowledge about freshwater generating processes in this data scarce region within northern Mongolia, located between the boreal and dry mid-latitude climates of the northern hemisphere. Dominant seasonal hydrological processes at a hillslope covered by both, pristine and burned taiga were investigated. Furthermore, seasonal streamflow dynamics were identified on the catchment scale by runoff analysis and hydrograph separation.

We hypothesize that:

- due to the thick organic surface layer, taiga forests have the capability to absorb a significant amount of precipitation water, before lateral drainage along dominant flowpaths emerges

- in the burned taiga, hillslope runoff is immediately activated following precipitation events. Dominant flowpaths are dislocated towards deeper depths as soil temperature increased and permafrost degraded

- the thickness of the active layer controls seasonal runoff processes following precipitation events.

3.2. Study Site

The study basin is located within the western Khentii Mountains in northern Mongolia in the headwater of the Sugnugr River (48°26'56"N, 107°11'17"E, at the basin outlet), about 60 km north-west of the Mongolian capital of Ulaanbaatar (Figure 9). With a mean specific runoff of 2.2 l $(s*km^2)^{-1}$ the Sugnugr River is a major tributary of the Kharaa River, which is part of the Selenga-Baikal drainage system (Menzel *et al.*, 2011). The study basin drains an area of approximately 100 km^2 and ranges in elevation from 1466 to 2687 m a.s.l., averaging at 2000 m a.s.l.

The Sugnugr River drains from east to west, resulting to a high degree in north facing (Nf) and south facing (Sf) slopes. It is defined as a small siliceous highland river dominated by coarse substrate, characterized by high fluctuations in discharge over the year with pronounced

discharge peaks in spring after snow melt and in late summer and ice cover from October until April/May (Hofmann *et al.*, 2015). Soils in the catchment are generally shallow with underlying crystalline rocks, mainly gneiss and granite. River valleys are covered by alluvial deposits and permafrost is found under Nf-slopes and at higher elevation but is absent beneath steppe vegetated Sf-slopes. The warm, dry and silty soils at the Sf-slopes are vegetated with herb-rich grasslands (Figure 9a). On the Nf-slopes, cool, moist and stone-rich silt loam soils are covered with a thick organic surface layer 0.15 ± 0.04 m (n = 30), dominated by *Ledum palustre*, *Vaccinium vitis-idaea* and mosses (Figure 9b). Here, widespread taiga forests (*Pinus Sibirica, Larix Sibirica* and *Betula Platyphylla*) have developed. All slopes are frequently intermitted by bedrock outcrops and ridges are round-topped. Above the tree line of approximately 2200-2300 m, slopes are covered with scree. In 2007 and 2011, wildfires destroyed large areas (~30 %) of the taiga forest within the basin. As a consequence, trees and the organic surface layer have been disturbed to a high degree (Figure 9c).

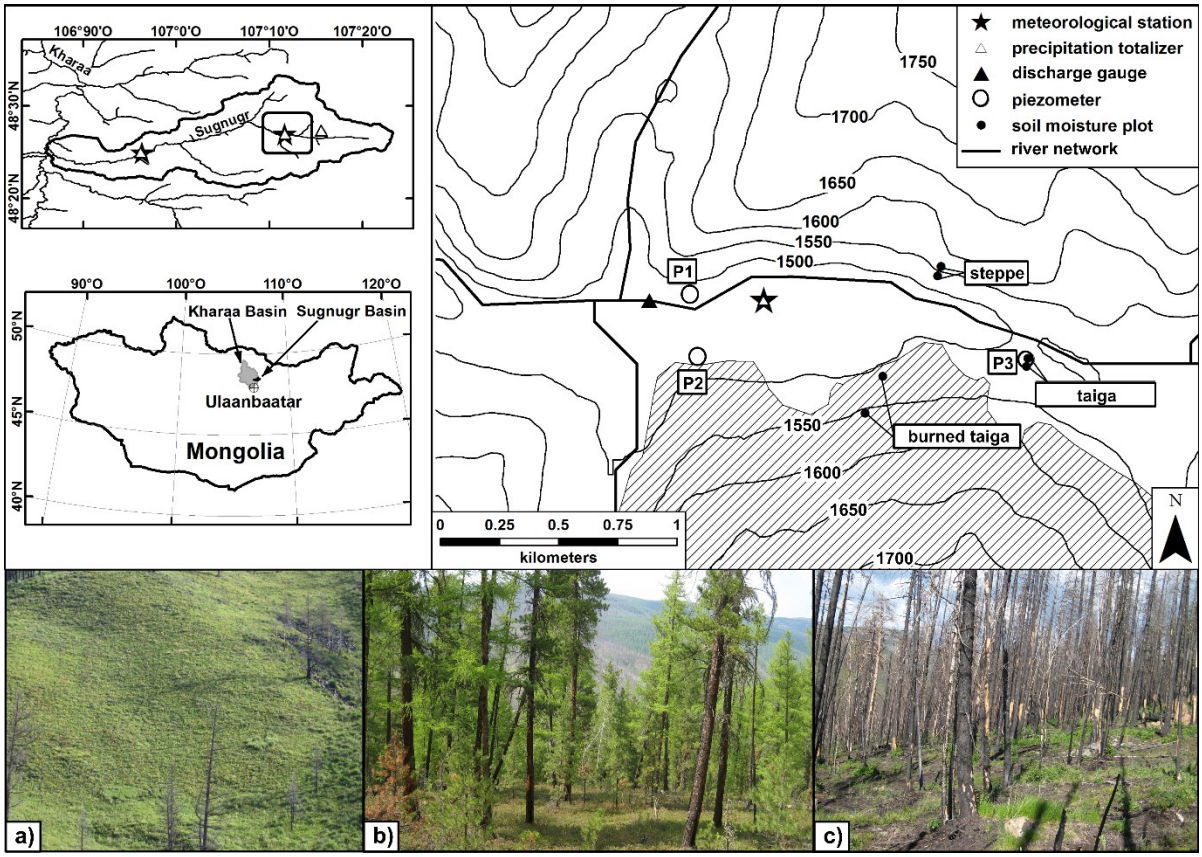

Figure 9: Study catchment (small map) and instrument locations (detailed map) within the Sugnugr Basin, northern Mongolia. The three main vegetation types steppe (a), taiga (b) and burned taiga (c) are shown.

In 2011 and 2012, measured annual air temperature at the meteorological station situated ca. 20 km downstream at an elevation of 1193 m a.s.l. (Figure 9), was -1.8°C and -3.0°C, averaging at -27.5°C and -27.7°C in January and 15.6°C and 16.1°C in July. Annual precipitation summed up to 317 mm in 2011 and 391 mm in 2012. Approximately 70 % of the yearly precipitation falls during the summer months; ≤ 5 % occur during the winter months (Kopp *et al*., 2014; Hülsmann *et al.*, 2015). These conditions correspond to a highly continental, semi-arid climate.

3.3. Materials and Methods

Instrumentation was operated from 22 June - 28 August 2011 and from 29 May - 3 September 2012. A meteorological station (WXT5500, Driesen & Kern) recorded precipitation, global radiation, air temperature, relative humidity, air pressure, wind speed and direction at 15 min intervals at an elevation of 1483 m a.s.l.. For one month (14 July to 18 August 2012) missing rainfall records were interpolated by linear regression using data from the meteorological station situated downstream (Figure 9). A detailed list of instruments operated at the two meteorological stations is given in Table 1 of Minderlein and Menzel (2015). Areal precipitation of the study basin was calculated by applying a precipitation gradient of 12.6 % per 100 m, which was determined from the records of the two meteorological stations. To specify the gradient in isotopic ratio of the summer precipitation, three precipitation totalizers (RS200, UMS) were installed at 1193, 1483 and 2048 m a.s.l.

3.3.1. Hill Slope Runoff

To examine the seasonal dynamic of lateral subsurface flow, three piezometers (P) were installed (2.5 cm inner diameter, continuously screened) (Figure 10) to record water stage and water temperatures in 15 min intervals (Levelogger, Solinst). In June 2011, P1 was installed in the riparian aquifer of the floodplain at depth of -1.78 m and P2 at the base of the burned slope within the mineral horizon at depth of -0.62 m. In June 2012, P3 was installed at the taiga slope at depth of -0.33 m. Installation depth was limited by frozen mineral soils. Recordings in P2 and P3 hence represent slope groundwater. VWC of the steppe, taiga and burned taiga were recorded (10HS, Decagon Devices) at 15 min intervals (EM50, Decagon Devices) across transects from the Sf-slope towards the floodplain into the Nf-slope, as described in detail in Kopp *et al*. (2014). The specific water retardation capacity (VWC_i) is described by the mean

increase in VWC of the three soil moisture recording depths (-0.05, -0.1 and -0.3 m) (equation 1). VWC_i was calculated for the taiga and burned taiga at the Nf-slope. It provides a measure for the retardation of precipitation water by the organic surface until the emergence of subsurface flow was observed at the corresponding piezometer.

$$\overline{VWC_{i,t}} = \overline{VWC_t} - \overline{VWC_0} \qquad (1)$$

where $\overline{VWC_0}$ is the mean volumetric soil water content before the event and $\overline{VWC_t}$ is the mean increase in volumetric soil water content during stormflow.

3.3.2. River Runoff

At the outlet of the study basin runoff and stream temperature were recorded continuously at 15 min intervals (Levelogger, Solinst). To derive informations about streamflow origin during peak flow, electric conductivity (EC) was recorded (3310, WTW) in 15 min intervals during field stays in 2012 (Figure 10).

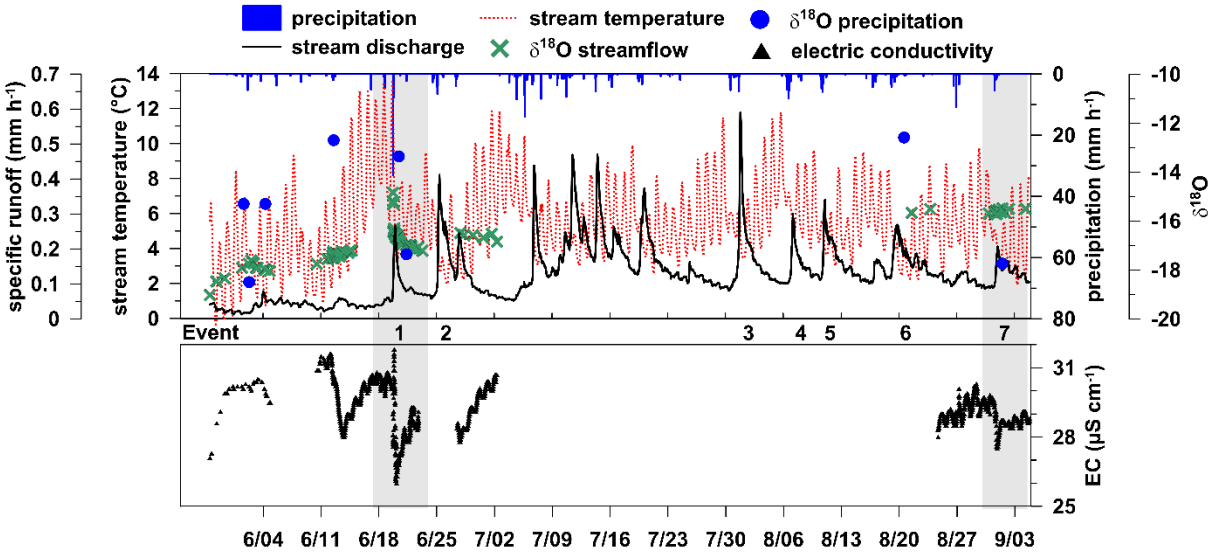

Figure 10: Time series of precipitation, runoff, water temperature, EC and $\delta^{18}O$ at the basin outlet in 2012. The numbers 1 – 7 represent the selected stormflow events for hydrograph analysis.

Quickflow and delayed flow for seven selected events in 2012 (Figure 10) were calculated following Lange and Haensler (2012). The resulting volumes of quick flow Q_F [m³] were calculated (i) as a fraction of catchment precipitation PP [m³] yielding R_P [%], and (ii) as a fraction of total event runoff Q_{tot} [m³] yielding R_y [%]. The importance of delayed flow can be expressed by DF_P [%]:

$$DF_p = \frac{(Q_{tot} - Q_F)}{PP} \qquad (2)$$

The recession coefficient α [d^{-1}], which is determined by local hydraulic and geographic conditions, was fitted to the first 4 h of the falling limb of the hydrograph by applying single exponential recession functions (Maillet, 1905). Finally, the antecedent wetness T_{2d}, which represents the amount of rainfall during the two days prior to the event, was calculated.

3.3.3. Sampling

Water samples from the precipitation collectors, piezometers, stream baseflow and frozen soil water were taken in 50 ml PE-bottles and sealed with airtight caps. Two stormflow events were sampled intensively (Table 5, Table 6). Samples were stored at cool and dark places until analysis, which occurred within two months after collection. Analysis for isotopes of hydrogen (^{2}H) and oxygen (^{18}O) were performed at the University of Freiburg, Germany, using a wavelength-scanned cavity ring-down spectroscopy (Picarro L1102-i). The analytical precision for ^{2}H and ^{18}O were ± 1.0‰ and ± 0.2‰ with reference to standard V-SMOW, respectively.

3.3.4. Hydrograph Separation

Two component hydrograph separation was performed to distinguish between pre event and event water fractions (Sklash and Farvolden, 1979) for Event 1 and Event 7 using δ^{18}O as isotopic tracer:

$$Q_T = Q_p + Q_e \qquad (3)$$

$$c_T^{t_i} Q_T = c_p^{t_i} Q_p + c_e^{t_i} Q_e \qquad (4)$$

$$\frac{Q_p}{Q_T} = \frac{(c_T^{t_i} - c_e^{t_i})}{(c_p^{t_i} - c_e^{t_i})} \quad (5)$$

where Q_T is the total runoff, Q_p and Q_e are the pre event and event runoff components and $c_p^{t_i}$ and $c_e^{t_i}$ are the concentrations of the observed tracer t_i.

Pre event baseflow samples were used to estimate c_p, and averaged event rainfall samples were used for c_e, which were modified using a digital elevation model and the determined gradients to calculate the amount of catchment rainfall and the corresponding isotopic signature. The Gaussian standard error method as presented by Genereux (1998) was applied to estimate the uncertainty of hydrograph separation for $\delta^{18}O$:

$$W_{f1} = \left\{ \left[\frac{c_e - c_T}{(c_p - c_e)^2} W_{c_p} \right]^2 + \left[\frac{c_T - c_p}{(c_p - c_T)^2} W_{c_e} \right]^2 + \left[\frac{1}{(c_p - c_e)} W_{c_T} \right]^2 \right\}^{1/2} \quad (6)$$

where W represents the uncertainty in the variable specified in the subscript p, e and T, which refer to the pre event, event and discharge water components, respectively. f represents the mixing fraction and c is the tracer concentration.

3.4. Results

3.4.1. Hillslope Scale

3.4.1.1. Piezometer Water Characteristics

In 2012, the measured frost table depth within P1 (floodplain) increased from -1.00 m (28 May) to -1.50 m (30 June) (Figure 11 a), corresponding to a melting rate of 1.4 cm d^{-1}. Before 19 June, liquid water in P1 was absent. Thereafter, a permanently saturated layer developed with water levels ranging between -0.60 and -1.40 m.

In P2 (burned taiga), frost table depth increased from -0.13 m at the end of May to below -0.40 m in mid July. This corresponds to a melting rate of 0.7 cm d^{-1}. Recorded water levels can be split in two phases, before and after mid July (Figure 11). During Phase 1, the water level remained close to the surface. In Phase 2, the water level dropped below the recording depth; now pronounced hydrograph peaks were only recorded following precipitation events. Although the general water level dynamics were similar in P2 and P3, the increase in active layer thickness was more enhanced in the burned taiga (P2), as indicated by the subsiding position of piezometer peaks (Figure 12 a-f).

Water temperature in P2 remained around the freezing point until mid of July, but increased during hillslope runoff (Figure 12 a,b). This pattern changed in Phase 2 as the water temperature declined while water levels were rising, reached a maximum as the hydrograph peaked and re-cooled during falling water levels (Figure 12 c-f). Water temperature in P3 was generally increasing during summer as soils warmed, but remained constant during hydrograph peaks (Figure 12).

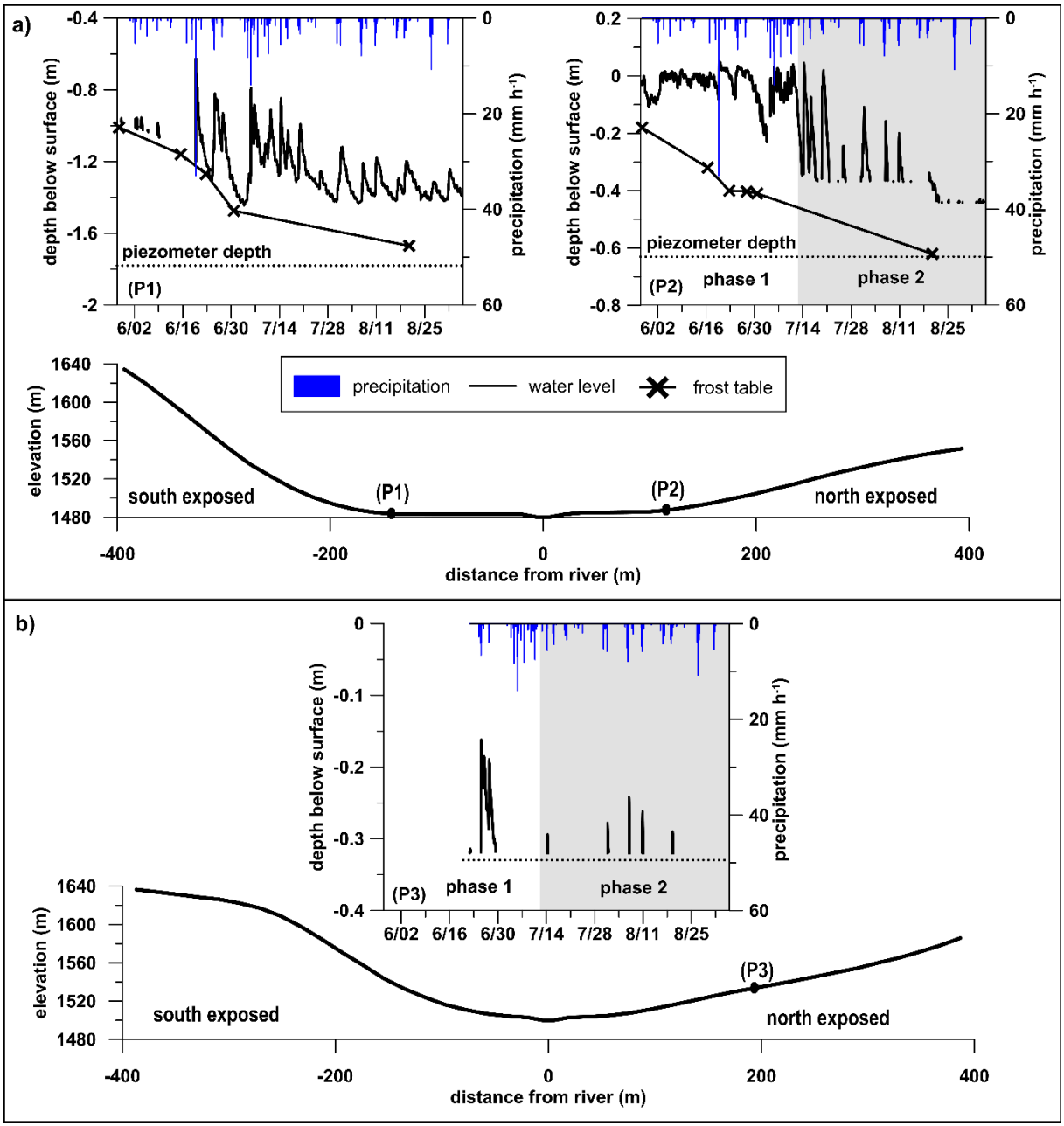

Figure 11: Frost table depth, piezometer water level and precipitation during the summer months of 2012. The cross section across the river valley displays the position of P1 in the floodplain, P2 at the base of the burned taiga (a) and P3 in the taiga (b).

3.4.1.2. Relative Increase in Volumetric Water Content (VWC_i)

Following precipitation events, lateral subsurface flow in P2 and P3 emerged on top of the frost table, after a specific threshold in retardation capacity (VWC_i) was reached (Figure 12).

A VWC_i of 0.05 ± 0.01 m^3 m^{-3} at the taiga and of 0.01 ± 0.01 m^3 m^{-3} at the burned taiga was determined. This finding could be verified during precipitation events between 10 July 2015 and 25 July 2015 (Figure 11), when distinct piezometer peaks were only recorded in P2. During these events, water level increases were not recorded in P3; where the VWC_i (0.02 and 0.04 m^3 m^{-3}) remained below the determined threshold for taiga forests. As a result, it can be derived that a substantial amount of precipitation is stored within the organic surface cover of the taiga, whereas wildfires result in a rapid transition from precipitation water towards the stream.

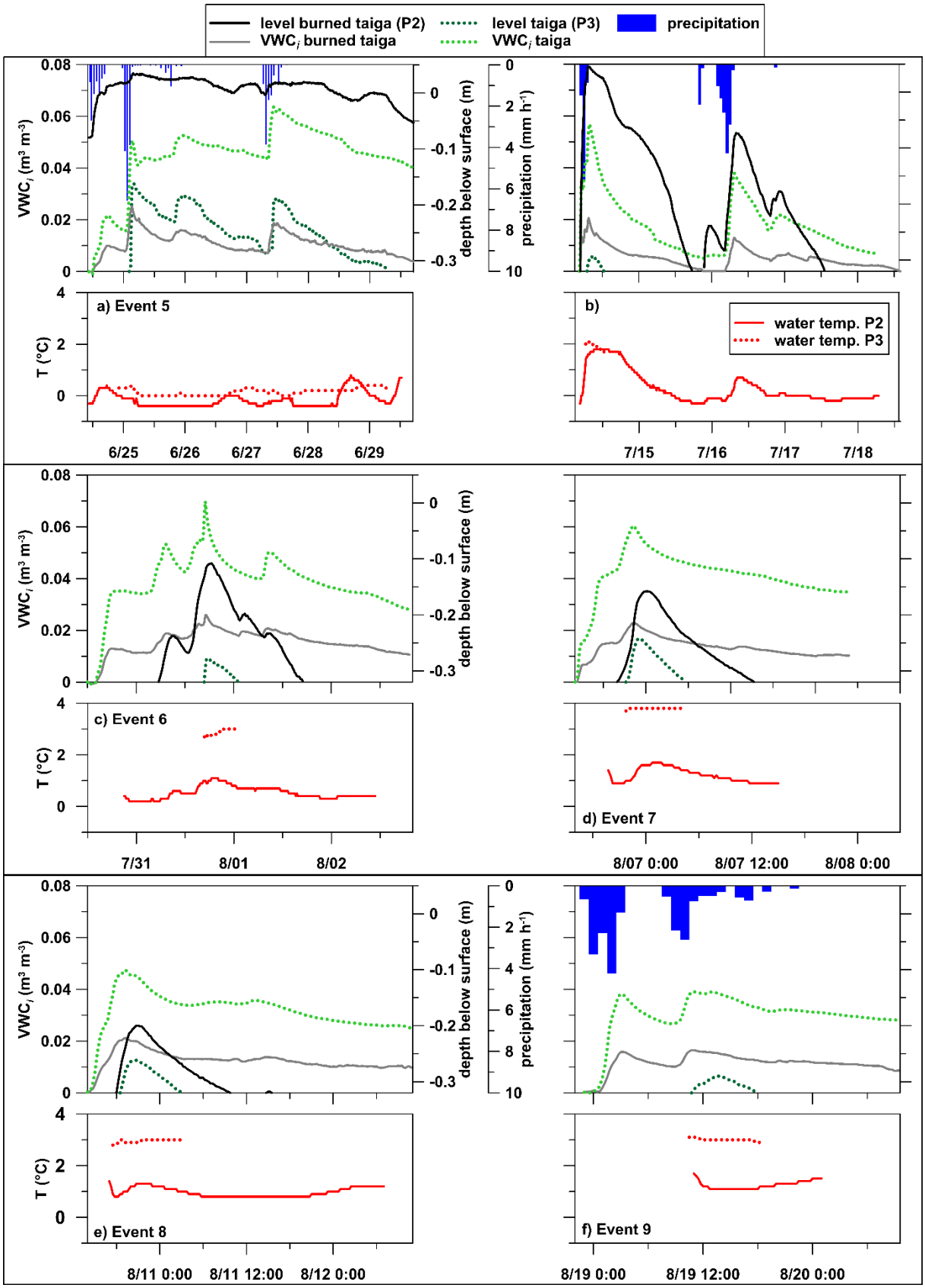

Figure 12: Relative increase in volumetric water content (VWC$_i$), piezometer water level and water temperature (red line) during six recorded events in P2 (burned taiga) and P3 (taiga) at a depth of -0.32 m. Precipitation is missing from 14 July to 18 August 2012.

3.4.2. Catchment Scale

3.4.2.1. Stream Water Characteristics and Hydrological Response Parameters

Precipitation and runoff for selected periods in 2011 and 2012 are shown in Table 3. Streamflow EC in 2012 ranged from 26 µS cm^{-1} during stormflow to 32 µS cm^{-1} during baseflow conditions (Figure 10). Mean EC at P2 was around 50 µS cm^{-1}. Baseflow water temperature was characterized by a diurnal pattern, with minima in the early morning and maxima in the late afternoon. This pattern changed during stormflow events as high runoff rates decreased water temperatures (Figure 10, Figure 14).

Table 3: Precipitation (PP), mean, minimum and maximum daily runoff (Q) and runoff ratios at the catchment outlet for selected time periods.

Date	PP Total (mm)	Q Mean (mm d^{-1})	Q Min (mm d^{-1})	Q Max (mm d^{-1})	Q Total (mm)	Runoff Ratio / modified[a]
22 June – 28 August 2011	173.4 / 201.7[a]	2.0	0.9	10.0	136.4	0.79 / 0.68[a]
22 June – 28 August 2012	331.5 / 385.7[a]	3.7	1.4	8.1	250.8	0.76 / 0.65[a]
28 May – 18 June 2012 (low flow period)	43.9 / 51.1[a]	0.9	0.4	1.4	18.9	0.43 / 0.37[a]
28 May – 3 September 2012	434.2 / 505.2[a]	3.0	0.4	8.1	295.1	0.68 / 0.58[a]

[a]modified by applying the PP gradient of 12.6 % per 100 m

Hydrological response parameters for the stormflow events in 2012 are presented in Table 4. In the course of summer, α declined while DF_p and R_y were generally increasing. This is caused by rising fractions of delayed flow and an overall increase in water storage. Event 1 had low R_p and DF_p, representing the response of a dry catchment within baseflow periods (Figure 10), alongside a shallow active layer (high α). In contrast, Event 3 had maximum R_p and T_{2d} despite the lowest catchment PP, illustrating the response of the catchment under wet conditions. Event 6 and 7 represent the dampened catchment response in late summer, with low α and high DF_p and R_y, controlled by a thick active layer.

Table 4: Characteristics of the seven selected runoff events in 2012.

Event	1	2	3	4	5	6	7
Date	19/06/12	25/06/12	31/07/12	06/08/12	10/08/12	19/08/12	31/08/12
Catchment PP (mm)	73.6	49.2	11.3[a]	18.4[a]	47.8[a]	32.1	21.1
Max. PP intensity (mm/15min)	26.7	5.3	9.5[a]	3.6[a]	9.6[a]	7.0	3.8
Q_{tot} Total flow (m³)	1081127	2758639	2010936	1401912	2282287	2788064	1442803
Peak discharge (m³/s)	7.0	10.9	16.4	8.3	9.5	7.6	5.8
T_{2d} (mm)	10.8	13.8	33.1[a]	3.1[a]	5.3[a]	10.8[a]	0.1
R_p (%)	3.0	13.1	51.2[a]	11.4[a]	6.9[a]	7.9	5.1
R_y (%)	80.3	79.9	71.7	85.3	85.8	91.1	92.6
DF_p (%)	0.1	0.5	1.3[a]	0.7[a]	0.4[a]	0.8	0.7
α (d^{-1})	1.4	1.0	1.5	0.6	1.1	0.5	0.5

[a] based on interpolated precipitation data
T_{2d}: antecedent wetness; R_p: volume of quick flow Q_F as a fraction of Catchment PP; R_y: volume of quick flow Q_F as a fraction of total event runoff Q_{tot}; DF*p*: measure for the importance of delayed flow; α: recession coefficient fitted to the falling limb of the hydrograph

3.4.2.2. Stable Isotopes

The isotopic ratio of all samples was close to the Global Meteoric Water Line (GMWL), indicating a minor influence of evaporation. The observed local altitude effect in summer precipitation was -0.31‰ / 100 m for $\delta^{18}O$ and the isotopic ratio of stream baseflow gradually increased during the observation period (Figure 10, Figure 13). Sampled water at the burned taiga was characterized by a higher isotopic ratio and increased from -16.0‰ to -13.7‰ for $\delta^{18}O$ during summer. The isotopic ratio of frozen Nf-slope water was -17.7‰ (n = 1).

3.4.2.3. Streamflow during Event 1 and Event 7

Precipitation and streamflow parameters of Event 1 and Event 7 are shown in Table 4, Table 5, Table 6 and Figure 14. During Event 1, the measured precipitation totaled 41 mm, with an isotopic signature of -11.7 ‰ for $\delta^{18}O$. The calculated mean catchment precipitation $\delta^{18}O$ ratio was -13.6 ‰ (Figure 14 a,c). Pre event VWC at depth of -5 cm was 0.106, 0.288 and 0.129 $m^3\ m^{-3}$ at the steppe, burned taiga and taiga, respectively. During Event 7, measured precipitation was 14 mm with a $\delta^{18}O$ ratio of -16.1 ‰, yielding a mean catchment $\delta^{18}O$ of -17.9 ‰ (Figure 14 b,d). Pre event VWC in depth of -5 cm was 0.220, 0.288 and 0.112 $m^3\ m^{-3}$ at the steppe, burned taiga and taiga, respectively.

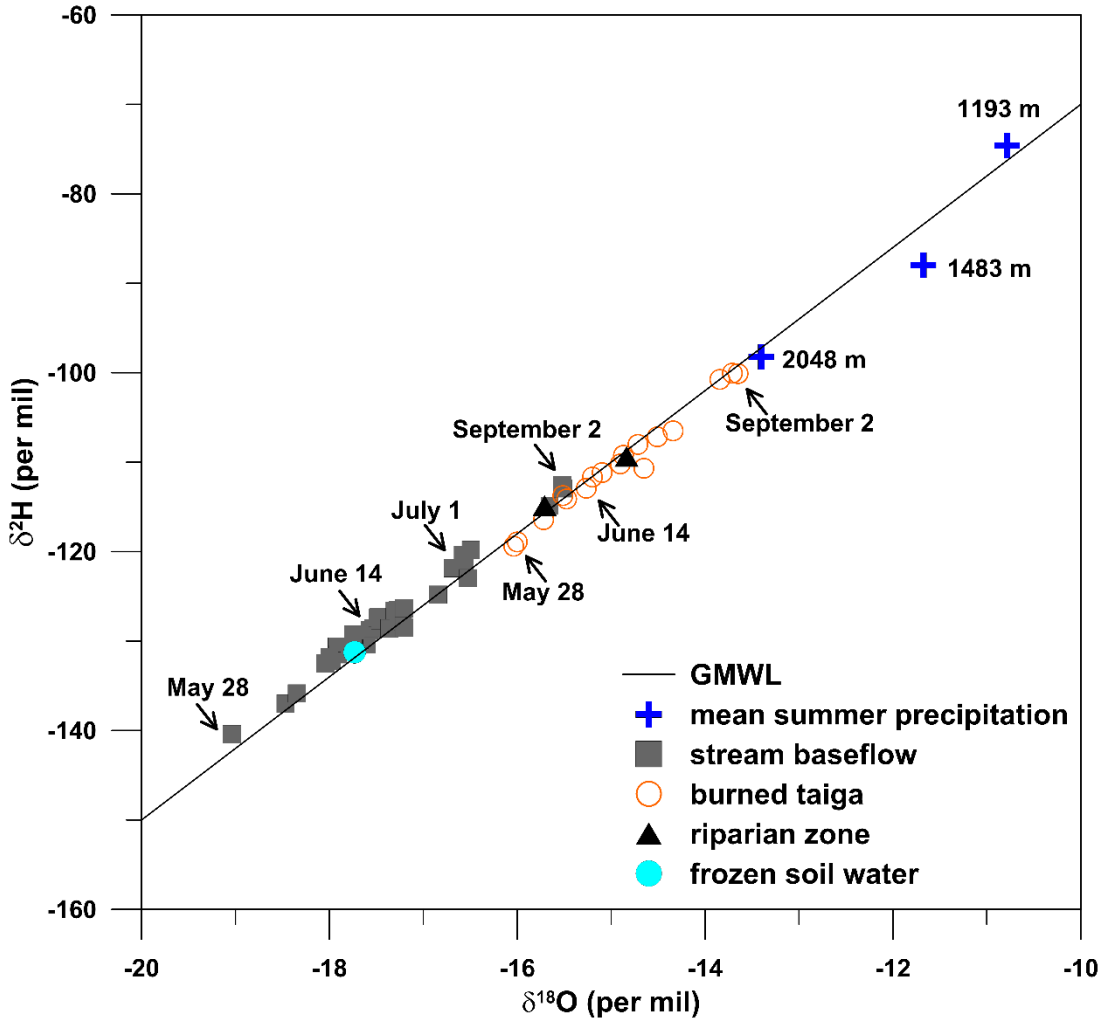

Figure 13: Temporal increase in $\delta^{18}O$ and $\delta^{2}H$ in stream baseflow and burned taiga slope water during summer, supplemented by isotopic signatures of frozen soil water, riparian zone water (P1) and averaged summer precipitation at different elevations.

Table 5: Precipitation, stream water characteristica ($\delta^{18}O$, $\delta^{2}H$, Q, EC and T) and VWC_i following the onset of Event 1 (19 June, 17:00).

Time after onset (h)	PP (mm)	stream isotopic ratio ^{18}O / ^{2}H (‰)	Q ($m^3 s^{-1}$)	EC ($\mu S\ cm^{-1}$)	Stream T (°C)	VWC_i vital / burned ($m^3\ m^{-3}$)
0 h	0	-17.2 / -128.5	1.53	30.2	12.93	0.00 / 0.00
0.5 h	23.2	-	2.03	27.8	12.05	0.06 / 0.03
1.0 h	9.8	-14.9 / -108.3	2.61	27.7	11.41	0.05 / 0.03
2.0 h	7.9	-15.3 / -111.0	2.95	29.7	9.96	0.06 / 0.02
4.0 h	0.1	-16.3 / -118.8	5.91	31.6	6.19	0.05 / 0.02
6.0 h	0	-16.5 / -121.9	7.37	29.9	4.57	0.04 / 0.01
12.0 h	0	-16.6 / -121.7	5.44	26.7	3.37	0.04 / 0.01
24.0 h	0.8	-16.9 / -124.8	3.00	27.3	7.43	0.02 / 0.01
48.0 h	2.9	-17.1 / -125.6	2.36	28.0	7.24	0.01 / 0.01
72.0 h	0	-17.1 / -126.6	2.02	28.5	7.21	0.01 / 0.01

Table 6: Precipitation, stream water characteristica ($\delta^{18}O$, $\delta^{2}H$, Q, EC and T) and VWC_i following the onset of Event 7 (31 August 12:00).

Time after onset (h)	PP (mm)	stream isotopic ratio ^{18}O / ^{2}H (‰)	hillslope isotopic ratio ^{18}O / ^{2}H (‰)	Q ($m^3 s^{-1}$)	EC ($\mu S\ cm^{-1}$)	Stream T (°C)	VWC_i vital / burned ($m^3 m^{-3}$)
0 h	0	-15.7 / -114.5	-	2.52	29.5	5.14	0.00 / 0.00
0.5 h	0.3	-	-	2.51	29.3	5.12	0.00 / 0.00
1.0 h	0.7	-	-	2.62	29.3	5.10	0.00 / 0.00
2.0 h	5.2	-15.7 / -114.8	-13.4 / -98.6	2.63	28.9	5.06	0.02 / 0.00
4.0 h	2.8	-15.7 / -115.0	-13.4 / -98.9	3.00	28.9	4.90	0.03 / 0.01
6.0 h	1.6	-15.6 / -114.2	-13.5 / -98.9	3.85	28.8	4.68	0.04 / 0.01
12.0 h	3.2	-15.6 / -113.2	-13.5 / -98.8	5.30	27.9	3.54	0.04 / 0.01
24.0 h	0.4	-15.5 / -113.0	-13.7 / -99.5	4.06	28.7	4.27	0.04 / 0.01
48.0 h	0	-15.5 / -112.9	-13.7 / -100.1	3.61	28.4	5.20	0.03 / 0.01

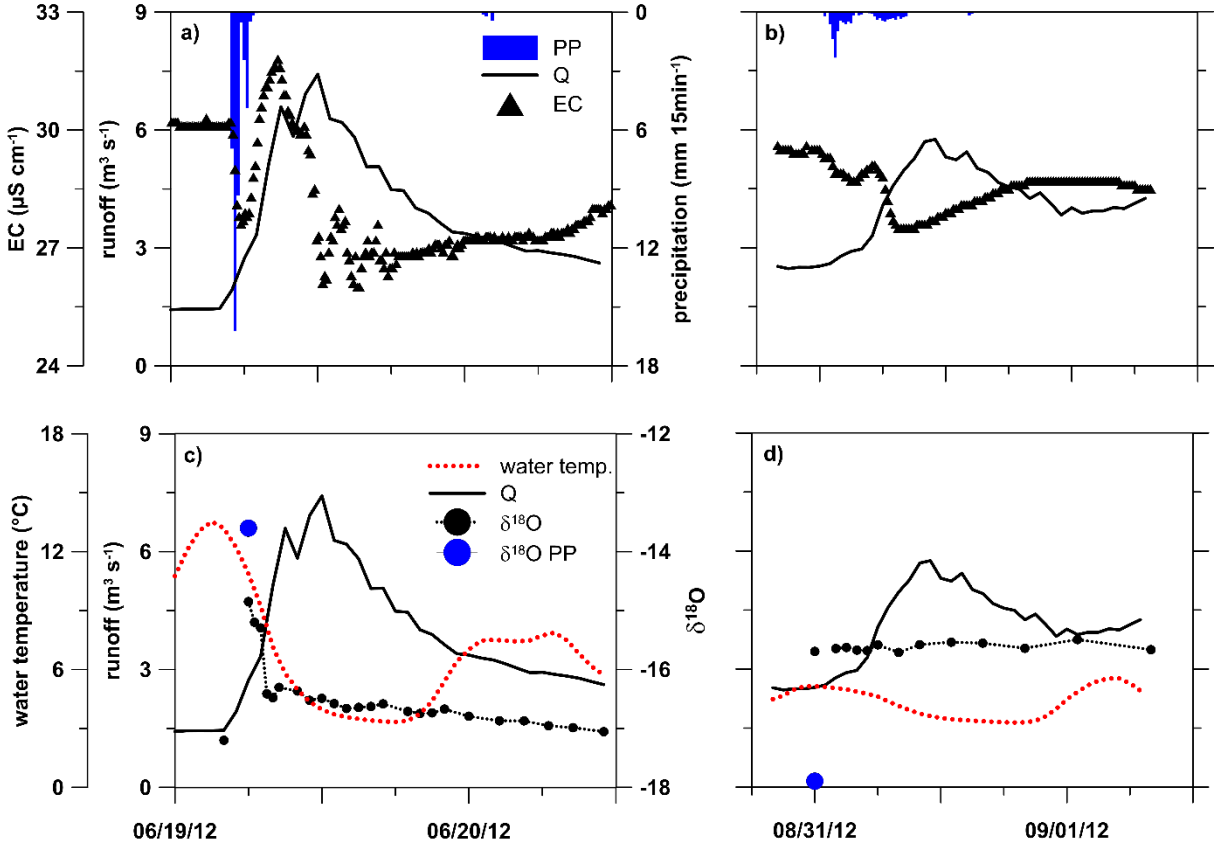

Figure 14: Runoff (Q), Electric Conductivity (EC) and precipitation (PP) during Event 1 (a) and Event 7 (b). Water temperature, mean $\delta^{18}O$ ratio of the catchment precipitation (blue circle) and river runoff (black circle) of Event 1 (c) and Event 7 (d) are shown.

3.4.2.4. Hydrograph Separation

Results of two-component hydrograph separation using $\delta^{18}O$ showed a total event water contribution of 22 % during the first 24 h of Event 1. The maximum event water fraction of 70 % occurred at the beginning of the hydrograph peak and declined towards the end of Event 1. The calculated averaged daily error (Eq. 6) for $\delta^{18}O$ ranged between 0.4 % (day 1) and 8.9 % (day 4). For Event 7, hydrograph separation applying $\delta^{18}O$ could not be performed successfully as the difference between c_{pe} and c_T was in the range of the analytical error and the precipitation isotopic signature was close to frozen soil water.

3.5. Discussion

Our observations support the development of a general conception of runoff processes in a remote study area in northern Mongolia. However, due to the relatively small number of observations, both in time and space, the large spatial heterogeneity within the basin could not be accounted for. For example, no investigations exist from the extended scree areas at higher elevations, although it is evident that they contribute to runoff formation. However, the main intention of the presented study was to demonstrate the differences in runoff processes between taiga and burned taiga, and how they interact towards runoff formation at the catchment scale.

3.5.1. Runoff Processes at the Hillslope Scale

3.5.1.1. Taiga

In permafrost areas, slopes with an organic surface layer above the mineral horizon are characterized by a two-layer flow system (Carey and Woo, 2001b), which is controlled by the thickness of the active layer (Ishikawa *et al*., 2005). Quickflow occurs in the organic layer and along the organic-mineral interface (Carey and Woo, 2000; Lange *et al*., 2015). Slowflow dominates in the underlying mineral layer, which is characterized by hydraulic conductivities that are several orders of magnitude lower than that of the organic surface layer (Carey and Woo, 2001b; Carey and Quinton, 2005). Quickflow is activated when the retardation capacity of the organic surface layer is reached. Thus, runoff is generally reduced as large amounts of water are retained in the organic layer prior to saturation (Carey and Woo, 2001a). In our study, this effect could be observed by the threshold in VWC_i of 0.05 $m^3\ m^{-3}$, above which lateral subsurface flow was observed during the summer period.

In early summer, precipitation water infiltrates at high rates into the organic surface layer, resulting in quickflow when frost table depth is shallow (Figure 15 a). Low water temperatures in P3 at the end of June indicate quickflow on top of the frost table (Figure 12 a). In the course of summer, soil temperatures increased, soil moisture declined and the active layer subsided deeper into the mineral layer (Kopp *et al*., 2014). Now slowflow became dominant, while quickflow was only observed occasionally (Figure 11 b, Figure 15 b).

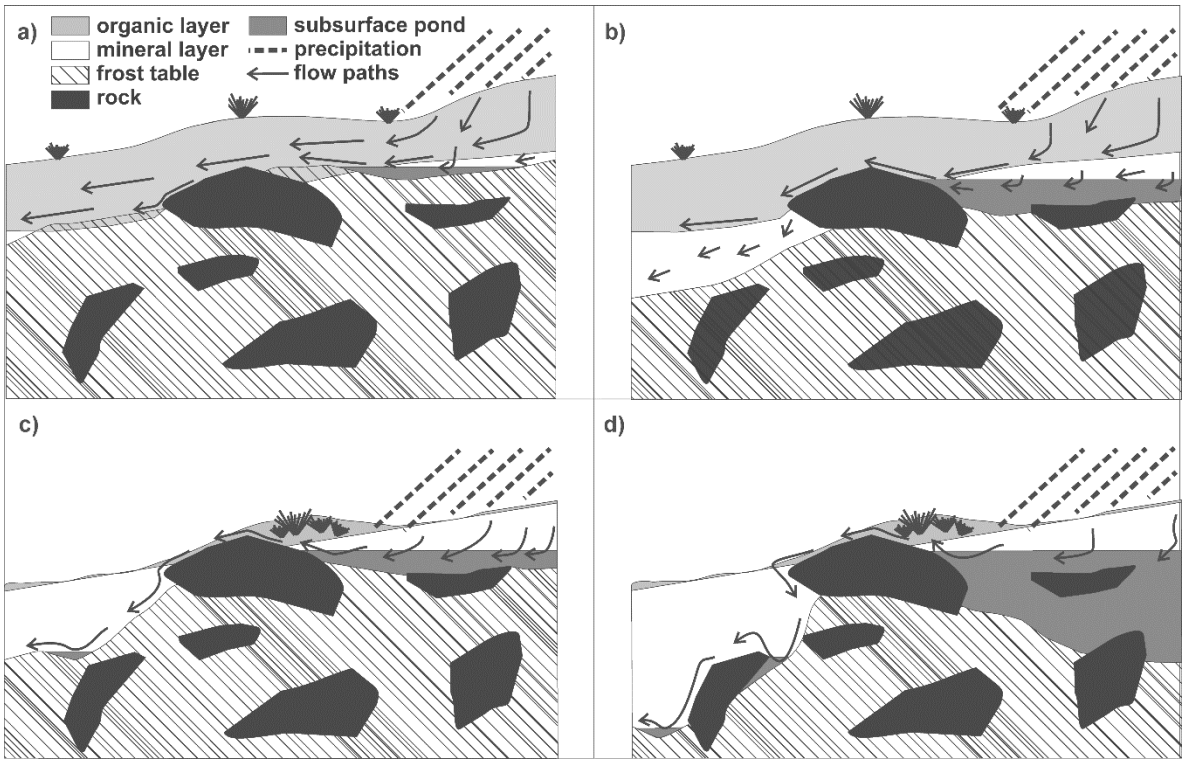

Figure 15: Schematic scheme showing the position of the active layer above the frost table and dominant runoff pathways during stormflow in the taiga in early (a) and late summer (b) and in the burned taiga in early (c) and late summer (d).

3.5.1.2. Burned Taiga

The small observed VWC_i of 0.01 m^3 m^{-3} in the burned taiga is linked to the combustion of the organic surface layer and consequently to a loss of the water retardation capacity. Kopp *et al*. (2014) observed small post-fire soil drying rates and mineral soils near saturation throughout the summer period. These conditions favor heat convection and result in an increase in active layer thickness and enhanced permafrost degradation (Takata, 2002; Shur and Jorgenson, 2007). Post-fire soil temperatures were found to have increased significantly (Kopp *et al*., 2014) and precipitation water infiltrated preferentially into the mineral horizon towards the permafrost

surface (Lange *et al.*, 2015). Cold subsurface water (0.1°C) temporarily returning to the surface was observed at obstacles such as large boulders and areas with a shallow frost table underneath isolated vital organic surface covers (Figure 15 c,d). This is in accordance with Wright *et al*. (2009) who found the phreatic surface to be directly controlled by the position of the frost table.

Regarding the water level and temperature dynamics in P2, it becomes evident that a dislocation of dominant flow paths occurred in the course of summer (Figure 11 a). During Phase 1, the phreatic surface fluctuated between the shallow depth of the frozen layer and the soil surface, with overland flow being recorded during stormflow events (Figure 15 c). Increasing water temperatures during peakflow suggest small active layer depth and a quick transfer of event water (Figure 12 a,b). As soil temperatures and the thickness of the active layer increased, the position of the phreatic surface gradually declined during Phase 2 (Figure 11 a, Figure 12 a-e). Now, an effective drainage network in the mineral layer along the permafrost surface has evolved. Lange *et al*. (2015) observed quickflow in the mineral layer of a burned hillslope, which rapidly increased flow velocities two days after a precipitation event. This indicates the emergence of the above mentioned deep effective drainage network, which became dominant during Phase 2. According to Wright *et al*. (2009), sinks in a heterogenic frost table topography must fill before over spilling water results in lateral subsurface flow. This process can explain the recorded water temperature dynamics in P2 (Figure 12 d-f). Thus, cold pre event water, which is stored in subsurface ponds above the frost table, is mobilized first (Figure 15 d). Subsequently, infiltrating event water temporary increases water temperature until cooler water reaches the piezometer, indicating quickflow on top of the frost table.

3.5.2. Runoff Processes at the Catchment Scale

3.5.2.1. Runoff Mechanisms

Gradually changing hydrological response parameters indicate expanding recession periods and a rising fraction of delayed flow in the course of summer (Table 4). This finding can be explained by an increase in active layer depth and hence water storage capacity (Yamazaki *et al*., 2006). The thawing of the active layer attenuates the hydrologic response and the flux of solutes to the stream (Petrone *et al*., 2007; Woo *et al*., 2008). The observed dynamics of Event 1 and Event 7 reflect the influence of active layer depth on runoff generation, although the precipitation magnitude differed (Figure 14).

Using two component hydrograph separation, a total fraction of event water of 22 % for $\delta^{18}O$ during Event 1 was calculated. These fractions are similar to results reported by Boucher and Carey (2010) for a discontinuous permafrost catchment in north-west Canada. The high event water fraction of 70 % at the onset of Event 1 can be explained by a substantial input of precipitation water into the stream channel and by overland flow from steep Sf-slopes (Lange *et al*., 2015). Overland flow can also be derived by the observed EC dynamics, as concentrations instantaneously declined at the beginning of the event (Table 5). The temporal increase in isotopic signature and EC after 3 to 4 h and decreasing water temperatures must hence be caused by quickflow water draining the taiga vegetated Nf-slopes. Petrone *et al.* (2007) found the permafrost extent within a catchment to control EC dynamics during stormflow, as flowpaths in the organic surface layer increase concentrations of dissolved organic carbon (DOC). Carey and Quinton (2005) argue that event water reaching the stream channel, by pathways other than overland flow, has altered its hydrochemical and isotopic composition. Consecutively declining $\delta^{18}O$, EC values and water temperatures after approximately 12 h (Table 5, Table 6, Figure 14) suggest an increasing fraction of mixed melt- and event water from higher elevated areas.

During Event 7, streamwater response was delayed, mainly due to low precipitation intensities and the damping function of the thick active layer at the end of summer, explaining the low observed dynamics in EC, water temperature and $\delta^{18}O$ (Figure 14 b,d).

3.5.2.2. Isotopic Signature

The observed altitude effect in precipitation isotopic signature of 0.31 ‰ / 100 m is in accordance to the literature (e.g. Tsujimura *et al*., 2007, Leibundgut *et al*., 2009). However, the altitude effect cannot explain the relatively low stream water $\delta^{18}O$ values, compared to the averaged summer precipitation of -13.4 ‰ at 2048 m a.s.l. (Figure 13). As frozen soil water has been found to exhibit distinct lower $\delta^{18}O$ values, and winter precipitation is generally characterized by lower δ values compared to the summer (Tsujimura *et al*., 2007), a high contribution of meltwater must have occurred at the end of May with a gradually decreasing fraction during the summer months, while active layer thickness increased (Figure 13). This finding is supported by decreasing water temperatures during stormflow. These conditions indicate a significant contribution of meltwater to runoff, which possibly originate from permafrost underlain Nf-slopes and from higher elevated scree covered areas.

3.6. Conclusion

This study examined dominant seasonal runoff generating processes by investigating isotopic, hydrometric and hydrochemical data in a headwater of the mountainous Sugnugr River, a tributary of the Selenga River (via the Kharaa and Orkhon rivers). At the catchment scale, the regulative function of active layer depth became evident. In early summer, precipitation is quickly transferred in a shallow active layer towards the river, as indicated by short recession periods. In the course of summer, the active layer subsided deeper into the mineral horizon and slowflow became dominant. At the hillslope scale, a regulative function of the taiga forest on stormflow generation, due to the water retardation capacity of the organic surface layer, could be derived. A wildfire, around five years prior to this study, combusted this layer to a high degree. It reduced the water retardation capacity and enhanced transfer of precipitation water towards the stream along preferential flow paths above the frost table.

Recent investigations indicate slow but steady hydrological changes in the Selenga river regime, with decreasing intra-annual variabilities of river flow (Törnqvist *et al*., 2014). It is assumed that this is a consequence of continued permafrost thaw in a region that experiences over-proportional warming. However, the results of our study indicate wildfires to result in converse hydrological behavior by increasing stormflow and decreasing low-flow conditions.

We consider the current processes of change in the Sugnugr Basin to be representative for a wider region along the Siberian-Mongolian border. The Khentii Mountains belong to the Trans-Baikal Conifer Forest Ecoregion, of which the boreal forest (taiga) is one of its subzones (Johnson *et al*., 2009). This ecoregion is one of the hotspots of forest fires in boreal Eurasia. Although the natural fire-return interval in Mongolia has been estimated to be at least 175 years (Johnson *et al*., 2009), the recent fire pattern affects 14 percent of total forest land annually (Nyamjav *et al*., 2007). For example, the 2015 spring fires in Mongolia and Southern Siberia burned about 40,000 km² of steppe and forest lands. In remote natural systems, the presence of woodworkers, lifestock breeders and wild food gatherers has increased since the breakdown of the socialist economy at the early 1990s (Priess *et al*., 2011). Generally, human abundance aggravates the risk of forest fires (Hessl *et al*., 2012). Burned forests may take up to 200 years to regenerate (Goldammer, 2002) and the recovery of the dominance of late successional conifers after fire can last 400 years (Schulze *et al*., 2005). Hence, the identified changes in the hydrological regime following wildfires will, to all probability, have long-lasting effects on water availability in northern Mongolia.

CHAPTER 4

Identification of runoff variability by applying tracer techniques at a steppe, taiga and burned taiga hillslope in a forest-steppe ecotone in northern Mongolia

4.1. Introduction

Mountainous regions have been identified as important water sources ("water towers") for adjacent lowlands, which is especially true for arid and semi-arid regions (Viviroli *et al*., 2007). Mongolia, a country with growing pressure on its scarce water resources, is a typical example for this concept. Main settlements of the semi-arid lowlands are located along river courses and directly depend on surface water or on groundwater from shallow alluvial aquifers largely recharged by river runoff (Menzel *et al*., 2011). Most streamflow originates from mountainous permafrost regions. The scientific community agrees that permafrost regions are particularly affected by climate change (IPCC, 2007). Recent meteorological measurements indicate that effects in Mongolia might even be greater than that in the high latitudinal regions of the Northern Hemisphere (Wu *et al*., 2011). A rise of global temperature generally leads to permafrost degradation and to an increase of active layer depth, which is defined as the soil zone above a permanent permafrost layer that periodically thaws and re-freezes (Dobinski, 2011). Finally, evapotranspiration is increasing, which facilitates the spreading of forest fires during drought periods (Onodera and van Stan, 2011). As a consequence, accentuated hydrological changes may be expected. Those can only be estimated if present-day hydrological systems are thoroughly understood, which is not the case in Mongolia up to now.

Permafrost helps to retain water resources of forest ecosystems (Iwata *et al*., 2012) and intensifies runoff responses by increased runoff/precipitation ratios (McNamara *et al*., 1998). Woo *et al*. (2008) categorized the hydrology of mountainous permafrost regions to show a large variability in hydrological processes, mainly due to the influence of differences in aspect and elevation. On undisturbed north-facing (Nf) slopes, dominant hydrological processes are well understood from process studies in northern America. Here, an existing permafrost layer acts as a barrier of vertical soil water percolation and promotes lateral subsurface flow in an overlying organic, highly porous active soil layer (e.g. Quinton and Marsh, 1999; Carey and Woo, 2001b). Flow velocities may be enhanced by preferential pathways, such as soil pipes (Carey and Woo, 2000). In general, an analogy to the concept of subsurface stormflow (SFF)

exists, which may be defined as a fast lateral flow of water through the soil above a layer of reduced permeability (Bachmair and Weiler, 2011). An important difference is the seasonal variability: During soil thawing, the permafrost layer descends through the soil profile and the depth of the active layer increases (Carey and Woo, 2001; Dobinski, 2011). This is superposed by an accentuated spatial variability of active layer depth (Wright *et al*., 2009). Hence, one may expect seasonal changes in runoff generation. Thereby, a thin active layer in spring will lead to the most intense runoff response (Carey and Woo, 2001b; Yamazaki *et al*., 2006). Forest fires may combust the insulating organic surface layer, decrease the albedo, increase soil temperatures and therefore the thickness of the active layer (Burn, 1998; Yoshikawa *et al*., 2003). Long-term ecological changes are most significant in areas that completely thaw after forest fires, since they become drier (Swanson, 1996). However, runoff generation processes in recently burned forests on permafrost have not been studied so far.

In mountainous permafrost regions, south-facing (Sf) slopes are often devoid of permafrost (Woo *et al*., 2008). Here runoff generation is less variable throughout the season and mainly depends on rainfall, vegetation, bedrock and (mineral) soil characteristics. In northern Mongolia, Ishikawa *et al*. (2005) found low and rather constant soil moisture values and concluded a dominance of deep water percolation for their Sf study slopes. However, they measured soil moisture profiles only two times and limited their studies to two gravel-rich, sandy sites. On Nf slopes their findings agreed with those of other regions, as they found high but variable soil moisture above permafrost. Heggem *et al*. (2006) and Kopp *et al*. (2014) continuously measured ground surface temperatures (GST) and found highest amplitudes on dry, Sf grasslands. The authors concluded that main controls for GST and hence permafrost distribution were solar radiation, ground surface wetness, winter snow cover and the presence of an organic surface cover, all of them directly or indirectly linked to aspect. For the mountainous, discontinuous permafrost regions of northern Mongolia, we are not aware of systematic hydrological process investigations that include aspect driven differences or areas affected by recent forest fires. And to the best of our knowledge, we do not know about a study that applied artificial tracer techniques on the plot and on the hillslope scale in a permafrost region.

This study addresses the variability of runoff generation processes in a mountainous permafrost region in northeastern Mongolia. By dye tracer experiments we aim to provide evidence for overland flow generation on Sf slopes and for changes of infiltration and runoff patterns on a recently burned Nf slope underlain by permafrost.

4.2. Study Area

The Selenga River, drains an area of 477 000 km^2 to Lake Baikal. The basin is populated by approximately 70 % of the entire Mongolian inhabitants. It is characterized by a cold, continental, semi-arid climate, where mean annual precipitation is below 300 mm and constitutes only 15 % of mean annual potential evapotranspiration (Ma *et al*., 2003). The Khentii Mountains are important headwaters for this river system (Menzel *et al*., 2011). We selected two opposite slopes close to the outlet of a 100 km² basin in the headwater of the Sugnugr River ranging from 1466 - 2687 m a.s.l. at an altitude of approximately 1500 m a.s.l. (Figure 16). Continuous two-year measurements of a nearby meteorological station at 1193 m a.s.l. yielded mean annual precipitation of 354 mm (70 % falling during June-August) and annual air temperatures of -2.4°C, with monthly mean values ranging from - 27.6°C (January) to 15.9°C (July) (Kopp *et al*., 2014). The area is underlain by crystalline rocks (gneiss, granite). Since the main valley drains east to west, entirely different ecosystems have developed on north- and south-facing slopes.

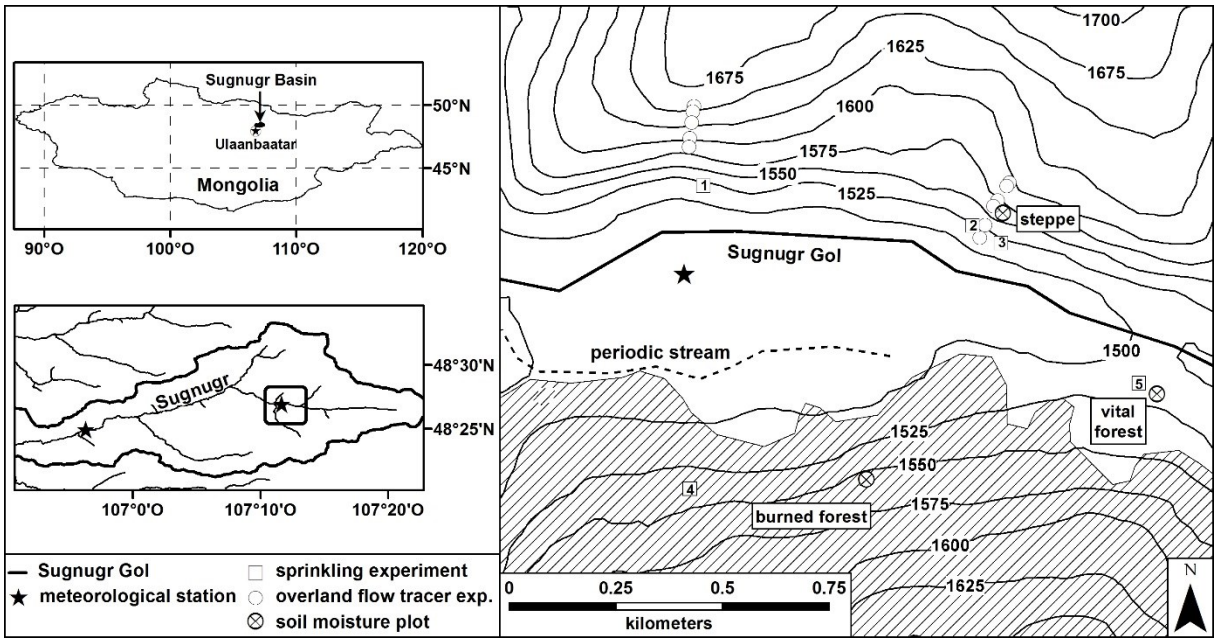

Figure 16: Location map showing the experimental setup and sites of the tracer experiments: overland flow was traced on two south-facing slopes and sprinkling experiments were carried out on five different locations.

On Sf slopes, soils consist of a dry silt-rich mineral horizon (30 – 50 cm) with moderate stoniness. Slopes are steep (50 – 60 %), frequently intermitted by bedrock outcrops and covered by species rich herbaceous grasslands. No organic topsoil and no permafrost layer have developed. The rounded upper slope margins are less steep and forests persisted. On Nf slopes, thick (15 cm) organic surface layers have developed on shallow stone-rich soils. Slopes are less steep (20 – 30 %) and *Pinus Sibirica*, *Larix Sibirica* and *Betula Platyphylla* form widespread taiga forests with an understory of *Ledum palustre*, *Vaccinium vitis idaea* and mosses. A permafrost layer persists throughout the summer and organic soils on top are cool and moist (Kopp *et al*., 2014). Considerable areas were affected by a forest fire in 2007, which led to a substantial loss of the organic surface layer. Until today, forest regrowth is limited.

4.3. Materials and Methods

4.3.1. Tracer-aided sprinkling experiments

Combined sprinkling and dye tracer experiments have been widely used to visualize processes of infiltration and water fluxes in the unsaturated zone, e.g. hydrophobicity or preferential flow paths through macropores (Flury *et al*., 1994; Weiler and Naef, 2003; Bogner *et al*., 2009). Brilliant Blue is the most frequently used tracer in these experiments due to its low ecotoxicity and good visibility against most soil colors (Flury and Fluehler, 1994). We dissolved 50 g of tracer in 15 l of water to fill a backpack sprayer. Prior to sprinkling, vegetation was cut to a few cm. Then sprinkling lasted for 17 – 20 min on 1.5 m^2 soil plots yielding 10 mm of artificial rainfall with a mean intensity of 30 – 36 mm h^{-1}. This sprinkling intensity fell into the range of natural rainfall, since in a three-month summer (11 June to 4 September 2012) measured 15-minute rainfall five times exceeded 8 mm, and twice 10 mm. Immediately after sprinkling, vertical soil profiles were dug starting from the lower end of the plot. Stained and unstained parts were documented on leveled photographs and manually digitized.

4.3.2. Tracing overland flow on south-facing slopes

Close to the tracer experiments, soil moisture was measured by frequency domain reflectometry (FDR) sensors (10 HS, Decagon Devices, Inc.) at soil depths of 5, 10 and 30 cm in triple replicates (Figure 16), as described in detail by Kopp *et al*. (2014). To document overland flow we chose a qualitative method which was used by Lange *et al*. (1998) to investigate infiltration pathways in a dry arid channel and by Steinmann (2010) to study

overlandflow connection on a Mediterranean hillslope. Preventing wind-blown dispersal, 30 tea bags were filled with a total amount of 500 g powder of the fluorescent tracer naphtionate and distributed equally spaced along a 20 m slope-parallel section on two southfacing slopes, S1 and S2 (Figure 1).

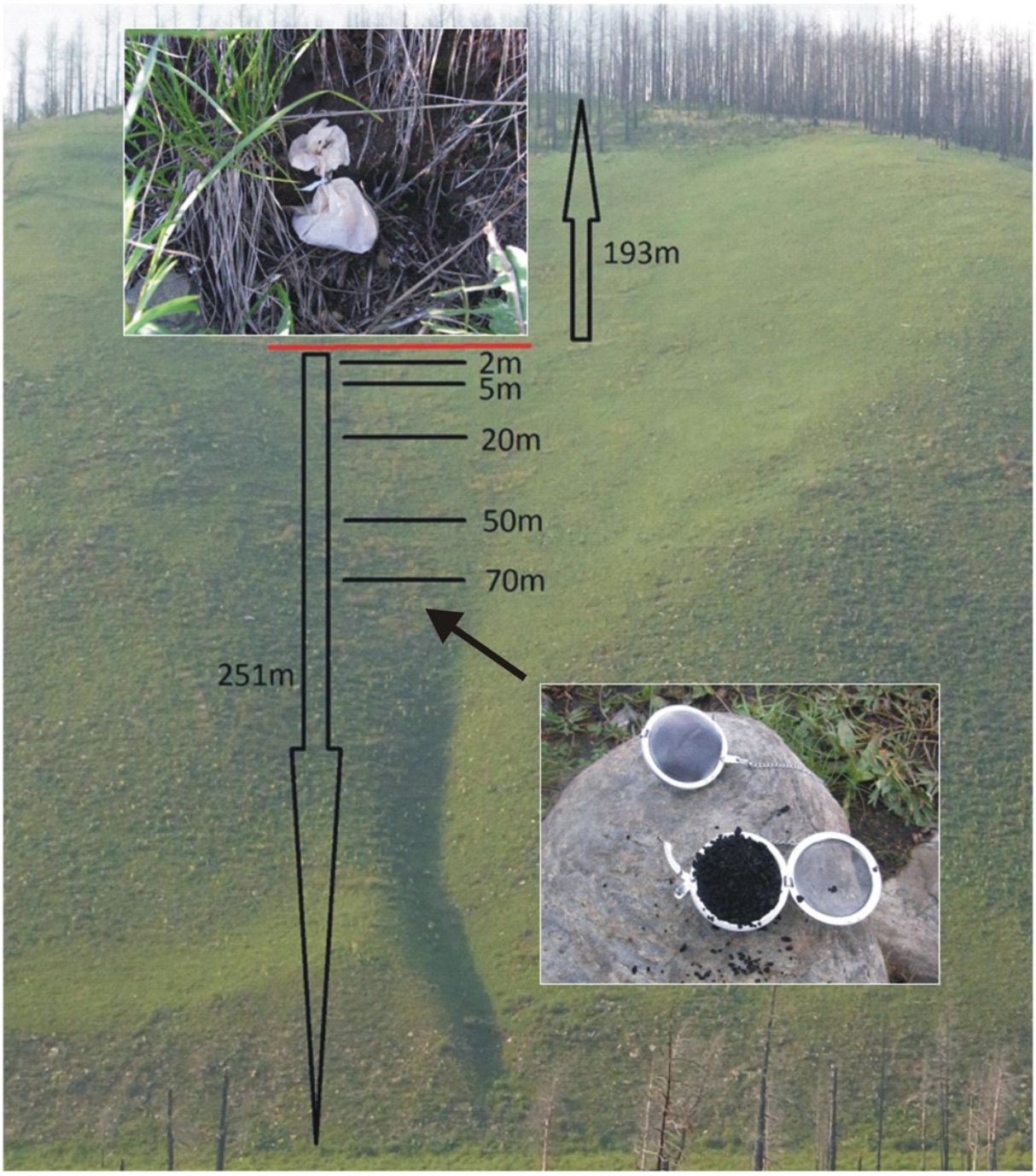

Figure 17: View of the setup for overland flow tracing on the southern slope S2 showing tea bags with naphtionate powder and tea balls with charcoal; red line: tracer section, black lines: section of charcoal with distance to tracer section.

Downslope, horizontal 10 m sections of five steel tea balls were distributed each containing approximately 10 g of charcoal. Where possible, charcoal samples were located in visible runnels to catch occurring overlandflow from upslope sections. We placed five to six charcoal sections at distances of 2 – 135 m (S1) and 2 – 70 m (S2) downslope the tracer section (Figure 17). On occasions of overland flow, the tracer was dissolved by flowing water and adsorbed in the charcoal sections. The charcoal samples were collected, separately packed in plastic bags and aluminium foil and brought to the tracer laboratory of Freiburg University, Germany, for analysis. In the laboratory, tracers were eluted from the charcoal following a protocol by Wernli (2011). A 2.7 g subsample of oven-dried (60°C) charcoal was put into a 1:3 solution of ethanol and ammoniac. After three days the entire leachate was extracted, filtered and filled into a fluorescence cuvette. A fluorescence spectrometer (Perkin Elmer LS 50B) recorded the fluorescence spectrum of the sample. Only samples with a clear fluorescence peak in the characteristic wavelength of naphtionate, which plotted above the background of the entire spectrum, were treated as positive samples. Those were calibrated by the following procedure (Lange *et al*., 1998): pure charcoal was placed in standard naphtionate solutions and analysed according to the above protocol. A comparison of field samples with these standards yielded semi-quantitative equivalent concentrations [mg/g charcoal].

4.4. Results

4.4.1. Tracer-aided sprinkling experiments

On the dry south-facing slopes (profiles 1-3, Figure 18), stained soil was only observed at the uppermost 5 cm of the profiles. Small fingering of the wetting front occurred but no signs of preferential flow were found. Even stones (profile 3) and a large plant root (profile 2) did not change this uniform pattern. On the wet, almost saturated northern slope (profiles 4-5) the tracer quickly infiltrated and blue water seeped out at the base of both profiles, which were delimited by a shallow permafrost layer. At the burned site (profile 4) the infiltration occurred preferentially through a thin combusted organic and stony mineral layer, while an intact organic layer induced uniform infiltration at the unburned site (profile 5).

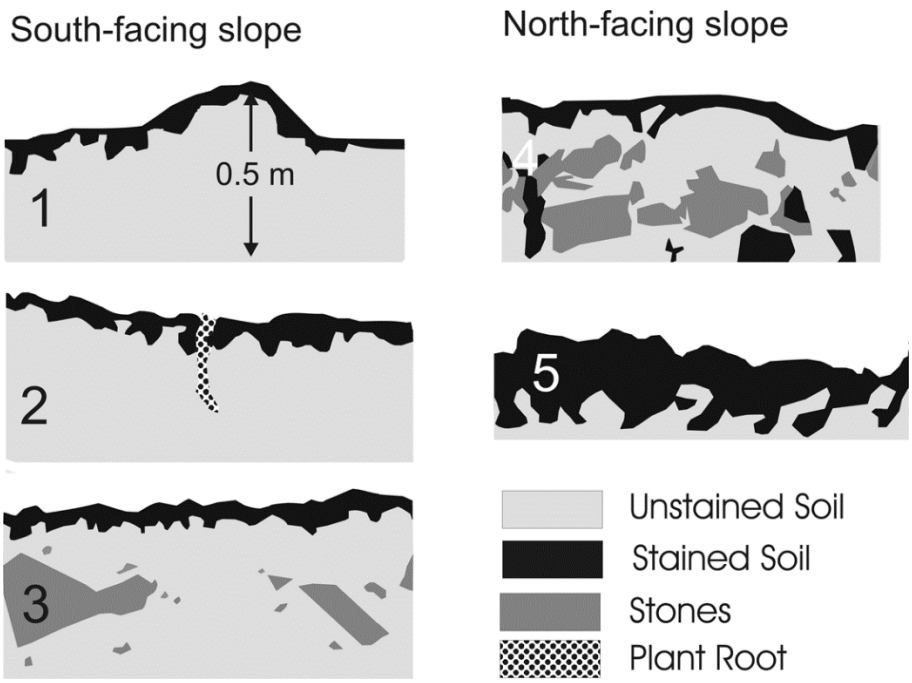

Figure 18: Results of the sprinkling experiments; profiles 1-3 on south-facing slopes, profiles 4 and 5 on north facing slopes with a thin combusted organic surface layer at a burned site (profile 4) and an intact organic surface layer at an unburned site (profile 5).

4.4.2. Tracing overland flow on south facing slopes

Tracer bags and charcoal samples were distributed on two slopes on 30 June 2012. From each section, five charcoal samples were collected on three separate days, two on 20 July, two on 04 August and one on 02 September 2012. From 53 collected charcoal samples the laboratory analysis yielded 30 scans (15 from each slope) that showed clear naphtionate maxima in the spectrometer scan (Figure 19). No clear dependency on exposition time or distance from the tracer section could be found. On both slopes, one sample contained high tracer concentration which necessitated dilution during laboratory analysis.

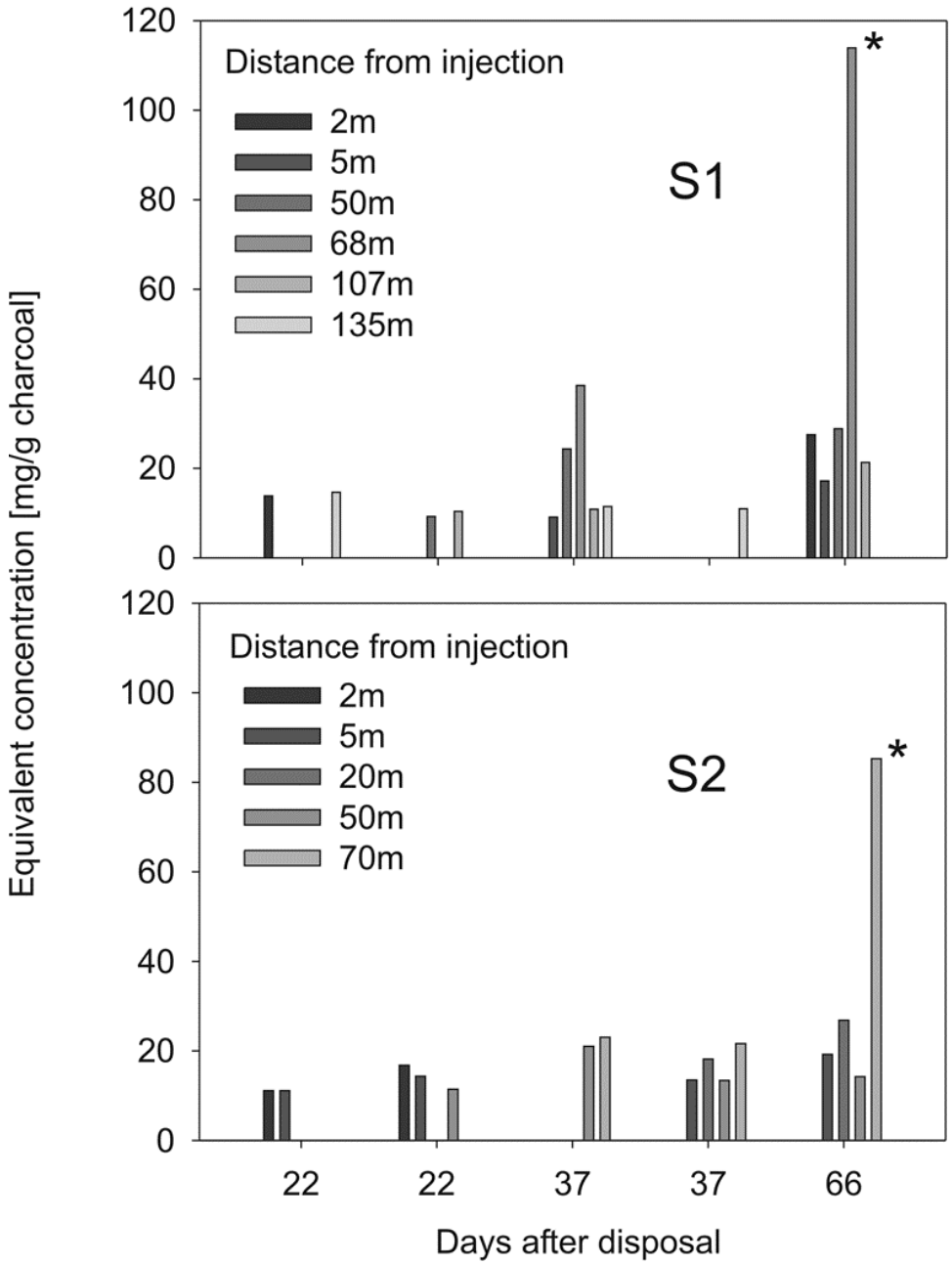

Figure 19: Equivalent naphtionate concentration in collected charcoal samples on two south-facing slopes, samples with high concentration are indicated (asterisk).

4.5. Discussion

4.5.1. Runoff generation on south-facing slopes

All three plots selected for brilliant blue sprinkling experiments had the same vegetation (herbaceous grassland), were dry and devoid of an organic soil layer. The silty mineral soil was homogeneous (profile 1), contained a large plant root (profile 2) or many stones (profile 3).

Despite these differences, experimental results were similar: No signs of preferential flow were observed and infiltration was dominated by homogeneous infiltration into the first 5 cm of the soil matrix (Figure 18). This behavior is contrary to similar experiments in temperate climate which are usually dominated by preferential flow through macropores (Weiler and Naef, 2003; Bogner *et al*., 2008). We attribute our findings to reduced biological activity under the harsh, dry and cold Mongolian climate.

We did not observe significant overland flow on our plots during the sprinkling experiments. This observation seems to contravene the results of the naphtionate-charcoal experiment, which provided evidence for tracer transport by at least one overland flow event (Figure 19). Rainfall data measured at the study area suggested that rainfall is unevenly distributed in time and, typically for semi arid regions, falls in single events lasting for several hours only (Figure 20). Two of these events exceeded 10 mm in one hour, four others exceeded 15 mm in four hours. All events caused distinct moisture increases in the uppermost 10 cm of the soil, while the reaction at a depth of 30 cm was clearly damped. Both the sprinkling experiments and the tracer/charcoal distribution were carried out during a relatively dry period. The event with the highest intensity occurred on 19 June 2012, where 41 mm of rainfall fell within three hours. This event triggered visible overland flow and small landslides on south facing slopes at several locations (Figure 21), but occurred eleven days prior to tracer/charcoal distribution. Nevertheless, it seems plausible that at least one of the following events was large enough to generate overland flow as well. All these results suggest that steep, south-facing slopes should not be excluded from runoff generation as one might infer from the results of Ishikawa *et al*. (2005). We mainly attribute these differences to soil characteristics and slope steepness. While Ishikawa *et al*. (2005) measured soil moisture on sandy soil profiles at approximately 10 % slopes, our study area was silt dominated and located on much steeper slopes (50-60 %).

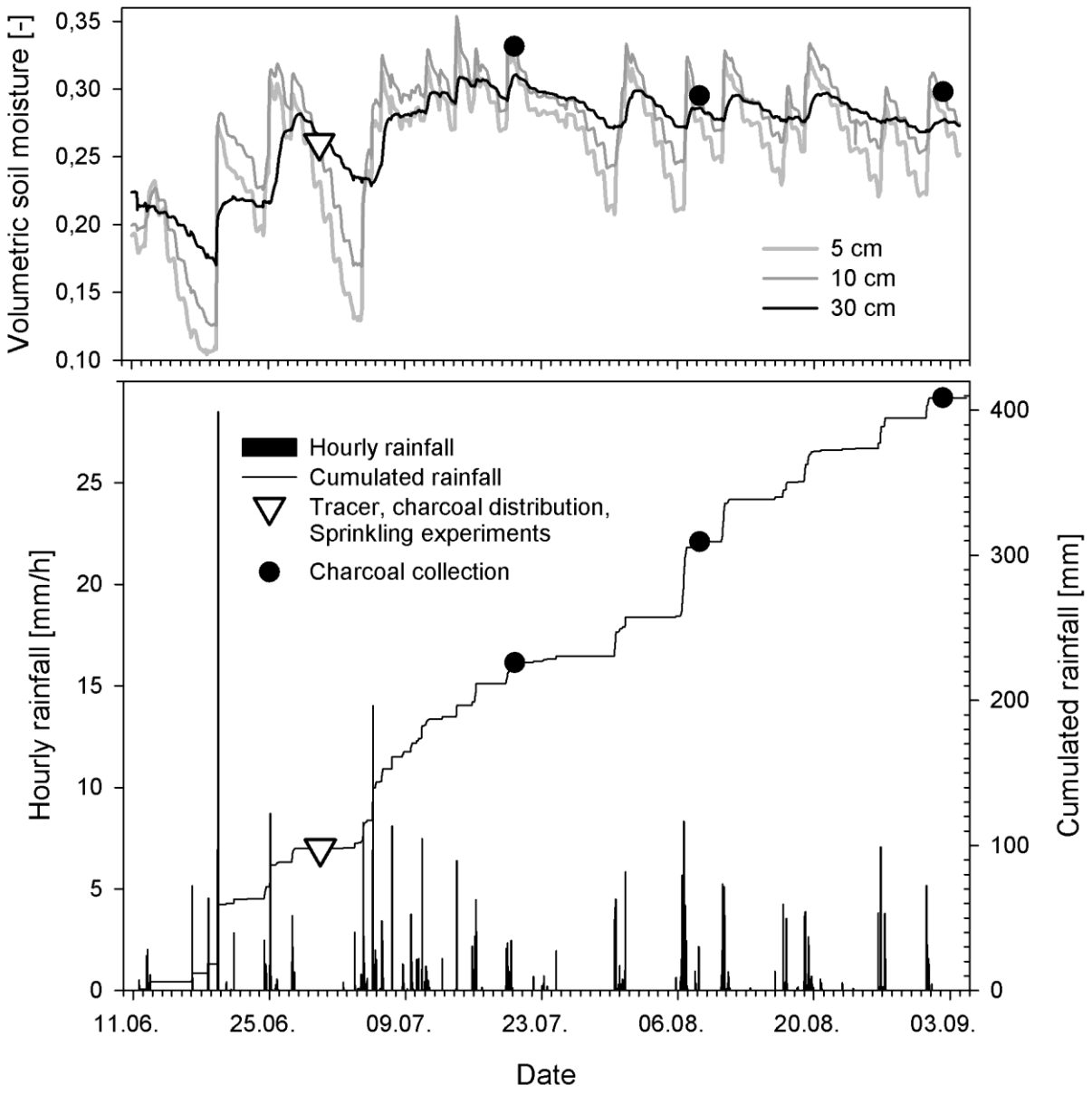

Figure 20: Rainfall characteristics, soil moisture readings and timing of the tracer tests on the south-facing slopes.

Figure 21: Observed overland flow at the bottom of a south-facing slope following the high intensity event of 19 June 2012.

4.5.2. Runoff generation on north-facing slopes

In general, the tracer results on the north facing slopes covered with pristine forest agree with other process studies on slopes underlain by permafrost (e.g. Quinton and Marsh, 1999; Carey and Woo, 2000; 2001). Precipitation water rapidly infiltrated into a moist soil horizon resulting in quick SSF on top of the permafrost layer. In our sprinkling experiments this could directly be observed by tracer seepage on top of the permafrost layer, which indicated lateral subsurface flow. A recent forest fire changed the pattern but had no measurable impact on the magnitude of infiltration. On an unburned profile, a wet organic layer promoted rapid uniform infiltration, while preferential infiltration pathways dominated the thawed mineral horizon of the burned profile.

A high magnitude rainfall event on 19 June 2012 resulted in long-lasting saturation of deeper soil layers, which activated the permafrost SSF system on the burned slope. Lange *et al*. (2015) illustrated short-term SSF changes with the help of repeated tracer injections that were simulated by a Multi-Flow Dispersion model. The authors found a pronounced short-term variability with rather slow dispersive velocities (0.16 m h^{-1}), which switched to preferential flow with 20 times quicker flow (3.24 m h^{-1}). This observed subsurface flow system on top of a permafrost layer is similar to subglacial drainage (e.g. Schuler *et al*., 2004). Also not directly

studied, field observations suggest that an intact organic layer at pristine sites might have isolated the SSF-system, damped short-term fluctuations and caused a more spatially uniform subsurface runoff response.

Figure 22: Upslope view of a 55 m hillslope section with observed preferential sub-surface flow and return flow; inserted photographs show details and measured water temperature.

4.6. Conclusions

Different artificial tracer techniques documented the variability of runoff response on two opposite slopes in a steep permafrost environment, northeast Mongolia. On north-facing slopes, tracer-aided sprinkling experiments showed rapid infiltration through a wet soil layer down to the permafrost. After profile excavation, stained water seeped out at the bottom of the profile suggesting a general aptitude for subsurface stormflow (SSF). The pattern of infiltration was different: While we observed homogeneous infiltration into an intact organic layer at an unburned profile, infiltration was preferential at a burned site where an organic layer was thin and combusted. Measurements of water temperature proved the role of the permafrost layer as a base horizon for SSF. As this study only provides insights into runoff generation five years after a forest fire, further studies are needed to elucidate long-term effects of forest fires in this sensitive ecosystem. On two south-facing slopes the applied tracers remained in the uppermost 5 cm of a silt rich mineral soil horizon. No signs of preferential infiltration could be found, which suggested reduced biological activity under a harsh climate. Instead, direct observations and distributed tracers and charcoal samples provided evidence for the occurrence of overlandflow. These findings have a bearing for water resources management, since existing studies in the region have so far limited runoff generation to slopes with existing permafrost.

4.7. Acknowledgements

I am grateful to Dr. Jens Lange, who supervised the tracer experiments presented in this chapter. A complete summary of the results of the tracer experiments, supplemented by repeated tracer injections of uranine and naphtionate, has been published by Lange *et al*. (2015). Finally, some of the credit for this chapter must be given to Matthias Bents who conducted most of the tracer experiments and sampling as part of his diploma thesis.

CHAPTER 5

The HBV-D Model

The following section about the HBV-D model is based on the work of Daniel Schwandt (2003).

5.1. Introduction

The HBV (Hydrologiska Byråns Vattenbalanssektionsmodell) model is a conceptual, hydrological model used for rainfall / runoff modelling. It was developed at the Swedish Meteorological and Hydrological Institute (SMHI) in Stockholm, and was first applied successfully in spring 1972. Responsible for the conception and further development of the HBV model was Sten Bergström. Due to its rather simple but sound concept the HBV model needs comparatively few input data, while a variety of problems can be addressed. Hence, it is not surprising the HBV model became one of the most popular hydrological models for a variety of hydrological problems worldwide, e.g. flood modelling and the modelling of environmental change effects on runoff characteristics (Bergström, 1995).

Since then, the model has been revised at the SMHI, and a new version, the HBV-96 model was published in 1996 (Lindström *et al*., 1997). Almost simultaneously, starting in 1995, Nils Roar Sælthun developed the "Nordic" HBV model. Besides new functionalities, a variety of features of the individual HBV versions used in Nordic countries have been incorporated. For example, the "Nordic" HBV model (Version 3.24; 1999) contains a simple vegetation parameterization including interception, temperature based evapotranspiration equations, lake evaporation and routing and additional functions for climate change simulations (Sælthun, 1999).

In 1997, the version 3.15 of the "Nordic" HBV-Model was revised by Valentina Krysanova at the Potsdam Institute for Climate Impact Research (PIK). This new version became known as the HBV-D model. It now allowed the simultaneous modelling of up to 100 subbasins while applying an unlimited number of meteorological stations (Krysanova *et al*., 1999). Since 1998, the HBV-D model was modified at the PIK by Lucas Menzel. From then on, up to 15 different land-use classifications could be incorporated and the potential evapotranspiration on a daily basis could be calculated. This version has been used in a variety of investigations on the effects of climate change on runoff formation in Germany (Menzel and Bürger, 2002; Schwandt, 2003;

Menzel *et al.*, 2006). It has also been successfully applied in data scarce catchments in northern Mongolia (Törnros and Menzel, 2010).

5.2. Model Concepts and Components

HBV-D is a conceptual model for rainfall – runoff modelling (Figure 23). Hence, physical processes are comprised in a simplified form, complemented by empirical processes with the aim to represent complex processes by rather simple equations and parameters. Therefore, often no direct connection between parameters used in the model and measurable physical parameters exists (Schwandt, 2003).

The HBV-D model can be subdivided into four sub-models: the snow model, the soil model, the dynamic model and the routing model (Bergström 1992). It is further subdivided into altitude zones and a precipitation and temperature reference height is calculated from the single altitudes of each meteorological station and their weighting factors. By applying the corresponding gradients, precipitation and temperature for each altitude zone is calculated. Both, the precipitation and the temperature gradient can be defined in the parameter file of the HBV-D model. Additionally, a precipitation correction can be applied to account for measurement losses (interception, evaporation etc.) (Schwandt, 2003).

5.2.1. The Snow Model

Once temperature falls below a defined threshold, precipitation accumulates evenly as snow. When exceeding a uniform snow cover of 20 mm, further snow input is unevenly distributed, depending on the vegetation type. This is achieved by applying a lognormal distribution, which is defined in the vegetation file. The degree / day method is used for snow melting: once temperature exceeds a threshold for snow melt, the snow melts according to the defined rate of mm/degree/day. When the proportion of melt water reaches a defined ratio, melt water is released from the snow cover, contributing to runoff. Below the melt threshold temperature, liquid water in the snowpack will refreeze. However the rate of refreezing is less effective than the rate of melt (Sælthun, 1999*;* Schwandt, 2003).

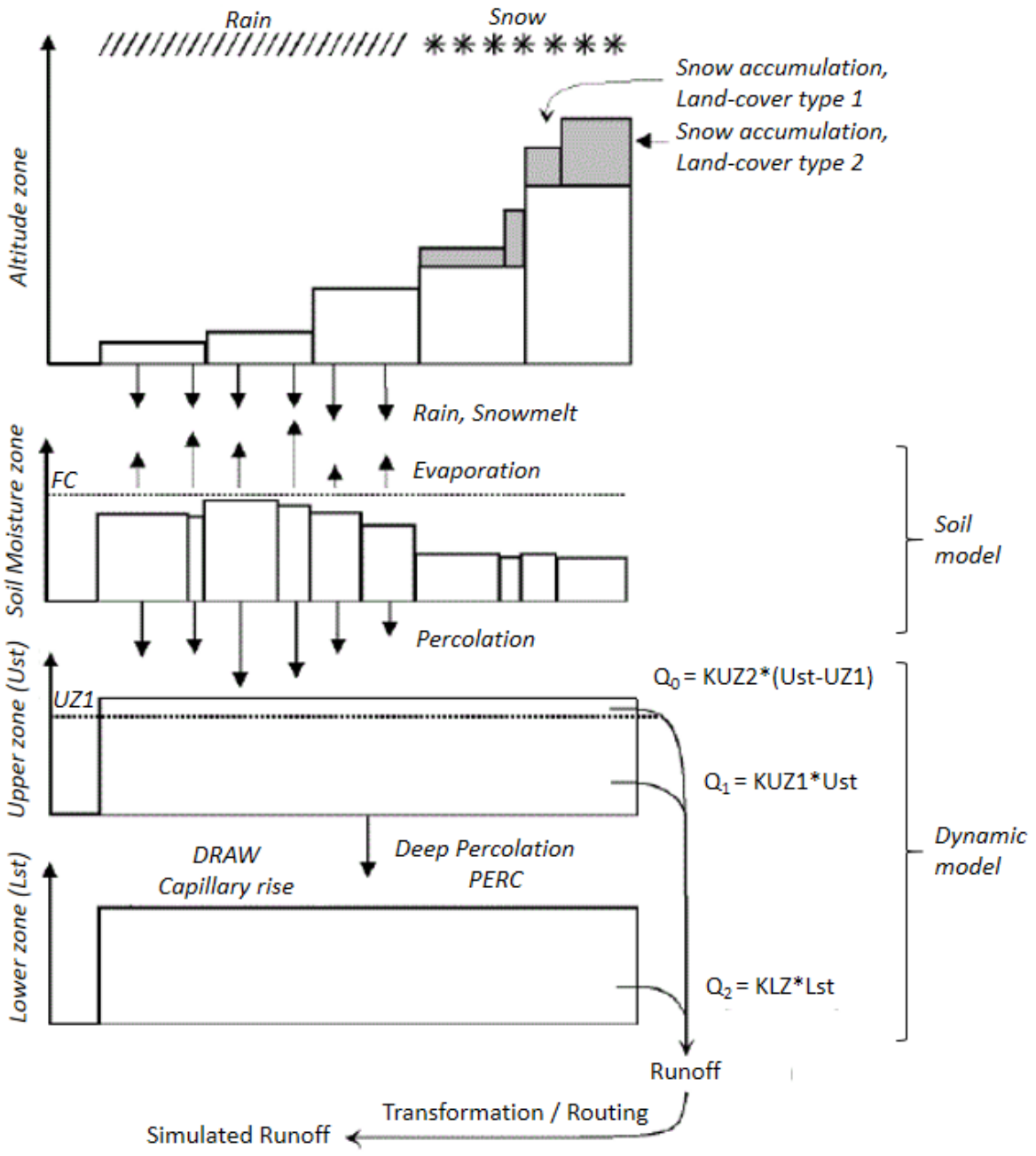

Figure 23: Simplified concept of the HBV-D model (modified following Schwandt 2003).

5.2.2. The Soil Model

The soil model with its soil moisture zone is the central part of the HBV-D model. However, the naturally heterogeneous and very complex soil system is represented by a very simplified abstraction. The whole catchment area is considered to be represented by a mixed-soil system, which can hold a maximum amount of water (FC). Single soil types and classes cannot be displayed. Soil moisture is a result of precipitation and melt water percolation as well as

capillary rise. Actual evapotranspiration (AE) as well as the percolation to the dynamical upper zone of the model is a function of the actual soil moisture content (SM). Water percolated through the soil moisture zone is not delayed, and water is only removed by evapotranspiration. The rate of AE is controlled by SM. For every land-cover type, a specific soil water content is defined (LPDEL). Once SM is equal or exceeds LPDEL, AE is equal to the potential evapotranspiration (PE). Below this factor, AE is less than PE (Figure 24 a). As long as water is in the interception storage, AE of the soil moisture zone is reduced by a factor, which is dimensionless and smaller than one (Sælthun, 1999). The calculation of PE in HBV-D is controlled by temperature. For temperatures above 5°C, the Blaney-Criddle equation (Schrödter, 1985) is applied. For temperatures below 5°C, the Iwanow equation, modified by Menzel, is used (Schwandt, 2003).

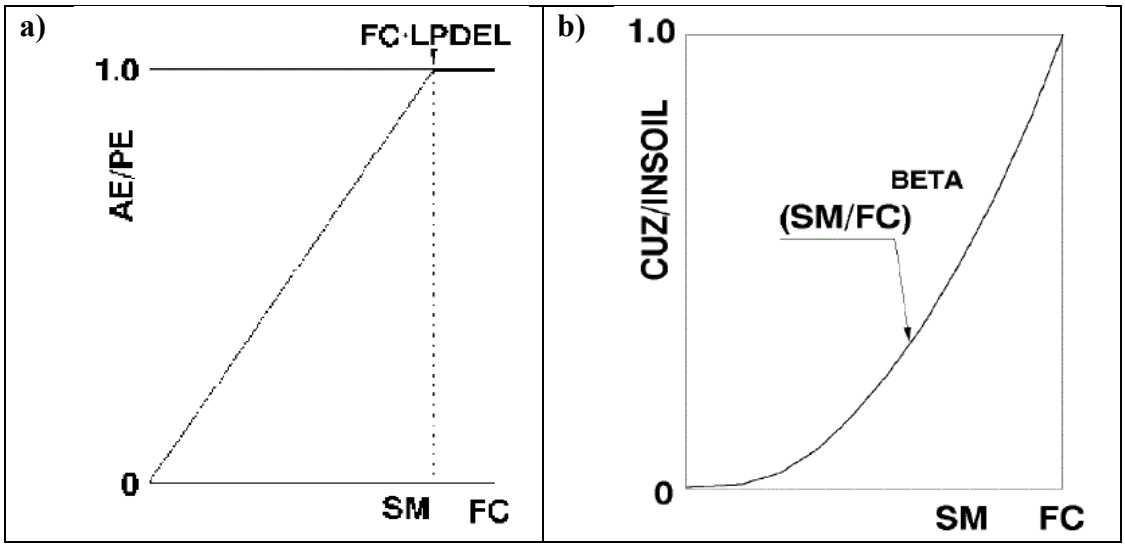

Figure 24: Actual Evapotranspiration as function of soil moisture content (a,) and output from the soil moisture zone as function of soil moisture content (b,) (Sælthun, 1999).

As long as SM is equal to FC, the complete precipitation and melt water input (INSOIL) percolates from the soil moisture zone into the reservoir of the upper zone (CUZ). When SM is below FC, only a proportion of soil water percolates into the upper zone of the dynamic model. This proportion is controlled by the ratio of SM to FC, in relation to the exponential parameter BETA (Figure 24 b) (Sælthun, 1999).

5.2.3. The Dynamic Model

Percolating water from the soil moisture zone is subdivided within the dynamic model into fast (Q_0), slow (Q_1) and very slow (Q_2) runoff components (Figure 23). As long as the upper zone storage is filled, it looses water by deep percolation (PERC) at a constant rate (mm d^{-1}) to the lower zone. Simultaneously, a nonlinear two-fold dynamic reaction, controlled by three parameters, regulates fast und slow runoff components: as long as the upper zone is filled above the threshold for fast runoff (UZ1), the constant KUZ2 controls Q_0, while the constant KUZ1 controls Q_1. Below UZ1 only Q_2 prevails. The lower zone storage represents the groundwater storage. It is filled by PERC from the upper zone, and loses water by capillary rise (DRAW) and Q_2, regulated by the constant KLZ (Sælthun, 1999; Schwandt, 2003).

5.2.4. The Routing Model

Total runoff, as a result of the three different runoff components (Q_0, Q_1 and Q_2) of the dynamic model can be accelerated or delayed by the routing model. This can be achieved by three different routing methods: lake routing, smoothing with fixed weights and smoothing with discharge dependent weights (triangular unit hydrograph) (Sælthun, 1999; Schwandt 2003). The aim of the routing model is to achieve a good fit between measured and simulated river runoff.

CHAPTER 6

Hydrological modeling of land-cover change effects on runoff response in the forest-steppe ecotone in the discontinuous permafrost zone of northern Mongolia

6.1. Introduction

The Khentii Mountains in the northeast of Mongolia are situated within the discontinuous permafrost zone, which is one of the most sensitive areas to climate warming in the world (Gunin *et al*., 1999; Yoshikawa *et al*., 2003). The distribution of permafrost in this transition belt between the boreal and dry mid-latitude climates of the Northern Hemisphere is strongly influenced by exposition and vegetation cover, which directly and indirectly influence the surface energy balance (Dulamsuren *et al*., 2005; Dulamsuren and Hauck, 2008). According to the classification of Shur and Jorgenson (2007), this region is characterized as a climate-driven, ecosystem-protected permafrost area, where permafrost persists in undisturbed late-successional ecosystems. Thus, a forest-steppe mosaic has emerged in this alpine region, with southerly exposed (Sf) steppe slopes that are permafrost free and experience seasonal frost and northerly exposed (Nf) permafrost underlain taiga stands.

An ongoing warming trend of 1.7°C since the second half of the 20th century has been observed by Batima *et al*. (2005). For the near future, an increase in mean annual air temperature (MAAT) is predicted to occur by 2°C in summer and 1°C in winter (Sato *et al*., 2007). Higher MAAT will increase the evaporative demand and lead to prolonged drought periods during summer. Hence, the frequency and duration of low-flow periods will most likely extend. Under current climatic conditions, evapotranspiration exceeds precipitation in the steppe areas (Minderlein and Menzel, 2015). The authors argue that the majority of stream discharge is generated by old successional forests. Under a warming climate, the frequency and severity of wildfires has been hypothesized to increase (Flannigan and Van Wagner, 1991), leading to a regime with a higher frequency of extreme fire years (Beck *et al*., 2011). Liu *et al.* (2013) found wildfire occurrence to have increased during the last decade in Inner Asia. The fire-return interval in Mongolia has been estimated to at least 175 years by Johnson *et al*. (2009). In remote natural systems, the presence of woodworkers, lifestock breeders and wild food gatherers has increased since the breakdown of the socialist economy at the early 1990s and the transition to a market-oriented economy (Priess *et al*., 2011). In general, human abundance aggravates the

risk of forest fires (Hessl *et al*., 2012). Especially under natural conditions where fuel is not removed, forest fires can destroy considerable amounts of the taiga forest. The moisture condition of the fire fuels is among the regulating factors of wildfires (Rowe and Scotter, 1973).

Wildfires have been shown to significantly affect soil moisture dynamics (Kopp *et al*., 2014) and hydrological processes in the Khentii Mountains (Lange *et al*., 2015; Kopp *et al*., 2016). Thus, land-cover changes in the upper reaches of the Kharaa River in the Khentii Mountains are of particular relevance, as they were identified to be the main water source ("water towers") for the lower catchment area (Menzel *et al*., 2011; Hofmann *et al*., 2015; Karthe *et al*., 2015).

In this study, the conceptual HBV model has been applied to simulate the effects of land-cover changes on the hydrological regime of four sub-catchments in the headwaters of the Sugnugr catchment, a major tributary to the Kharaa River. The model is characterized by a simple structure (Figure 23, Chapter 5), that abstracts physical characteristics of a catchment and that is complemented by empirical processes. Bergström (1992) defined conceptual models to represent physical characteristics of a catchment. This structure makes the model, besides its low input data demand, suitable to simulate remote catchments where knowledge about runoff generation processes is rare. It has been successfully applied in Central Europe (e.g. Menzel and Bürger 2002; Menzel *et al*. 2006), as well as in many areas around the world, including Alaska (Hinzman and Kane, 1992), Scandinavia (Lindström *et al*., 1997) and Mongolia (Törnros and Menzel, 2010). The model performs well in cold regions, as the parameters that control simulated runoff are also the parameters that govern the natural system: snowmelt, soil moisture and surface runoff (Carr, 2003). Although permafrost was not explicitly incorporated in the HBV model, Hinzman and Kane (1991) reported a successful abstraction of permafrost by setting the percolation parameter (PERC) equal to 0. PERC regulates the percolation of water from the upper soil zone to the lower zone, and hence to the groundwater reservoir. In regions of discontinuous permafrost, groundwater contribution can be accounted for by setting PERC to the lower end of the reported scale of 0.6 – 1.1 mm d^{-1} (Schwandt, 2003), which is usually used when setting up the HBV model. The semi-distributed version of the model (HBV-D) (Krysanova *et al*., 1999) allows the sub-division of the catchment into elevation zones, each exhibiting individual land-cover proportions. Hence, this version has been proofed to perform well in heterogeneous and alpine catchments characterized by steep gradients in elevation, thus exhibiting distinct vegetation zones.

Yet, little is known about the effects of land-cover change on freshwater generation in the Kharaa River Basin (Karthe *et al*., 2015). Therefore, a detailed understanding of the most important freshwater generating processes in the headwaters is of crucial importance to successfully address future water supply (Karthe *et al*., 2014). To approach this knowledge gap, the aim of this study is to simulate the natural runoff of four chosen sub-catchments in the headwater of the Sugnugr catchment. Effects of land-cover changes, namely wildfire, on the hydrological regime were simulated by applying two different scenarios. Scenario 1 is designed to represent pristine and undisturbed natural conditions, while Scenario 2 is designed to represent a severely disturbed system with all forested areas burned.

We hypothesize that:

- in pristine environments, the hydrological regime is characterized by dampened hydrographs. Rainfall is stored within the vegetation, resulting in reduced stormflow, while water is continuously draining the vegetation zone during drought periods, increasing low-flow runoff.

- due to the loss of the water storage capacity, burned forests result in increased stormflow. Consequently, low-flow runoff is decreasing.

6.2. Study Site

The study area is located within the Khentii Mountains in northern Mongolia in the headwater of the Sugnugr River, an important tributary of the Kharaa River. It is situated about 60 km north-west of the Mongolian capital Ulaanbaatar (Figure 25). The sub-catchments vary in terms of elevation, size and vegetation cover (Table 7, Table 11).

The climate of the Khentii Mountains is characterized by the Asiatic anticyclone in winter, which usually has its center southwest of Lake Baikal and causes dry and cold winters. In summer, warm air masses from the south flow into northern Mongolia. These result in the formation of cyclones when they meet the cold air from Siberia (Dulamsuren and Hauck, 2008). This gives rise to a highly continental semi-arid climate with annual precipitation of less than 400 mm, of which almost 90 % fall during the hydrological summer (May to October), while only 10 % fall during the hydrological winter (November to April) (Figure 26).

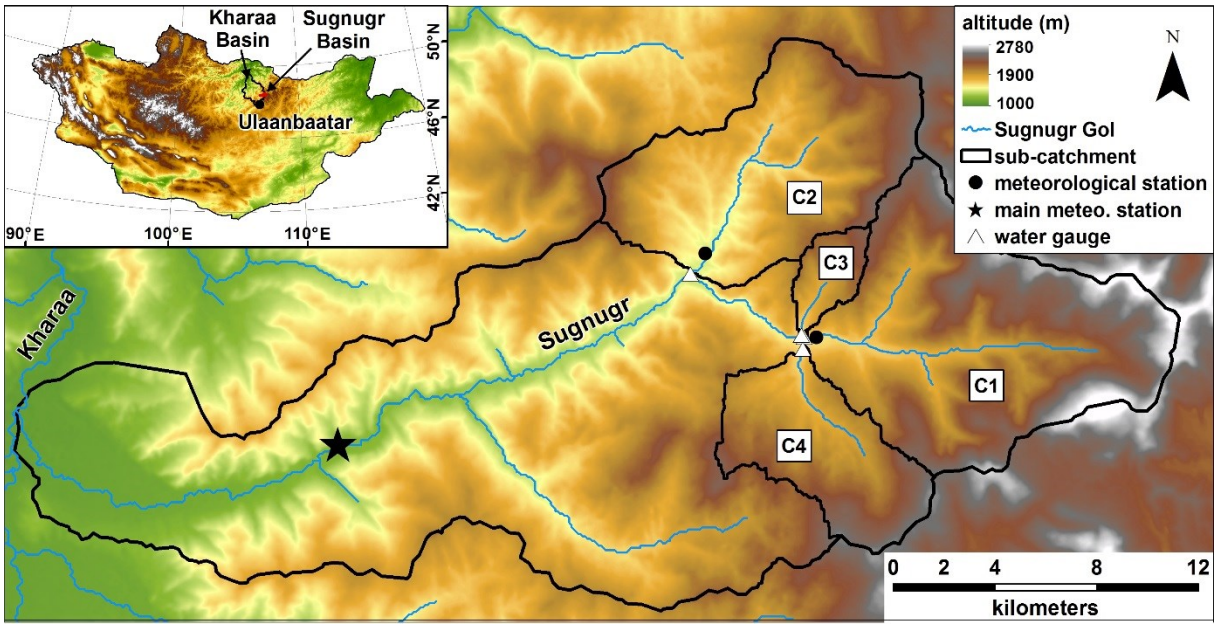

Figure 25: The location of the Sugnugr Basin within Mongolia (small map) and of the four sub-catchments (C1, C2, C3 and C4) within the Sugnugr Basin.

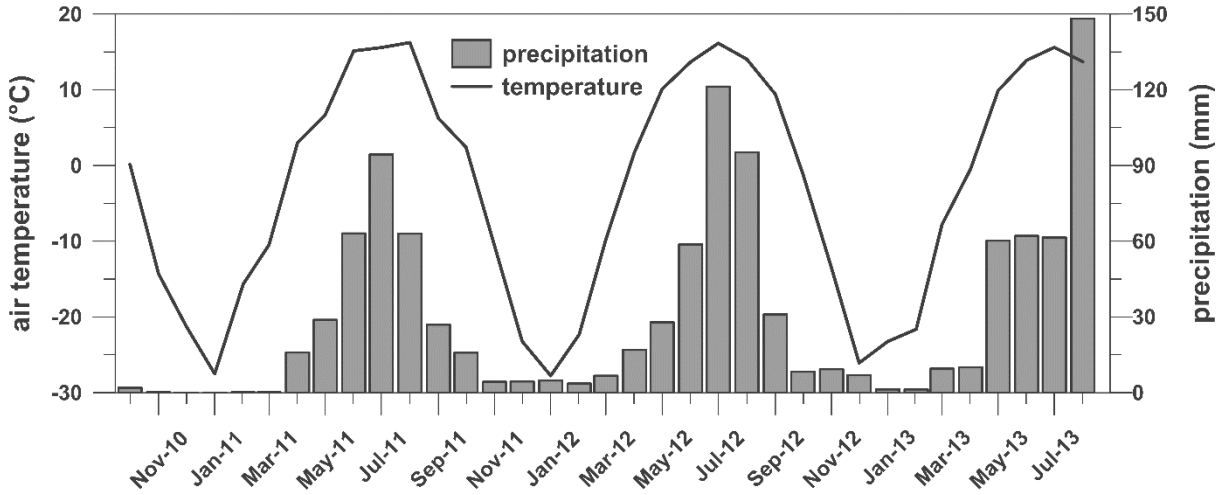

Figure 26: Monthly air temperature (°C) and precipitation (mm) recorded at the main meteorological station from October 2010 until August 2013.

In the Khentii Mountains, permafrost exists beneath old successional north exposed taiga stands and in the high mountains, but is absent at south exposed slopes (e.g. Etzelmüller *et al*., 2006; Heggem *et al*., 2006; Kopp *et al*., 2014). Soil differs at the study site depending on exposition, vegetation and hydrological conditions. Silty material is prevalent at the south-exposed sites and silt loam dominates at both forested and burned forest sites. At each site, at depths between 0.1 and 0.2 m, soil is underlain by coarse gravel and small boulders. The

Sugnugr Basin has a geological composition of granite and gneiss bedrock and is primarily sedimentary in the floodplain close to the rivers.

Field studies have shown that upper soil temperatures (0 – 0.3 m) four and five years after a wildfire have increased significantly compared to a pristine forest site (Figure 5, Chapter 2) at C1. Thus, active layer depth has increased, while permafrost subsided to deeper depth, possibly resulting in thermokarst (Iwahana *et al*., 2005). These conditions allow precipitation water to percolate deeper and stormflow runoff has been observed to occur within the mineral horizon on top of the frost table (Figure 15, Figure 18). Under pristine conditions, stormflow is dominated by quickflow within the organic surface cover and slowflow in the mineral layer (Carey and Woo 2000, 2001a, 2001b; Petrone *et al*., 2007).

Table 7: Catchment characteristics of the four sub-catchments.

Catchment characteristics	C1	C2	C3	C4
Mean elevation (m a.s.l.)	1997	1715	1813	1878
Elevation at basin outlet (m a.s.l.)	1466	1336	1482	1469
Maximum basin elevation (m a.s.l.)	2687	2321	2155	2371
Basin area (km²)	100.2	72.3	7.9	36.1

6.3. Materials and Methods

6.3.1. Instrumentation and data availability

Runoff and field data were obtained over a period of two consecutive summers from mid-June to end of August 2011 and from end of May to the beginning of September 2012. During these periods, runoff was repeatedly manually measured with a current meter (F1, SEBA) at the outlet of each study basin. Water level and temperature were recorded in intervals of 15 min by pressure transducers (Levelogger Junior, Solinst), thus allowing the specification of rating curves for each sub-catchment and each year (2011: C1 and C2; 2012: C1, C2, C3 and C4) (Figure 29 e - Figure 31 e). The resulting specific daily runoff, as a result of catchment size and individual rating curves, was used for the calibration and validation of the models.

A meteorological station (main station) was installed at a south exposed hillslope close to the entry of the Khan Khentii Strictly Protected Area (1193 m a.s.l., 48°24'55"N, 106°56'21"E). It measured standard meteorological parameters besides a variety of additional parameters, as

described in detail by Minderlein and Menzel (2015). Additionally, two temporary meteorological stations (WXT5500, Driesen & Kern) were installed in the headwaters of the Sugnugr catchment. Station 1 was installed approximately 20 km upstream from the main station at a south exposed hillslope close to the outlet of C2 (1396 m a.s.l., 48°28'46"N, 107°8'13"E). Station 2 was installed approximately 25 km upstream from the main station (1483 m a.s.l., 48°26'55"N, 107°11'41"E) in a river floodplain close to the outlet of C1. Both stations recorded standard meteorological parameter at 15 min intervals from 22 June to 28 August 2011 and from 29 May to 3 September 2012. For one month (14 July to 18 August 2012), missing rainfall records at both stations were interpolated by linear regression using data from the main meteorological station situated downstream. The determined precipitation gradient between the meteorological stations was 12.6 % per 100 m.

6.3.2. Land Cover Classification

Remote sensing methods were applied to derive the dominant land-cover types within the Sugnugr catchment and the four sub-catchments from the 1960s until 2011. To distinguish between slope and plain vegetation, a DEM (Digital Elevation Model) in a resolution of 30 m was used (www.terrainmap.com). The threshold for slopes was 10° inclination.

LANDSAT mosaic images (www.earthexplorer.usgs.gov) from 10 September 1990 and 20 September 2011, with a ground resolution of 30 m, were used for land cover classification. Clouds and cloud shadows were virtually absent in both images. The vegetation index (NDVI = Normal difference vegetation index) was determined (Jensen, 2005) and the land-cover classification was subsequently derived from the LANDSAT image using standard routines of the ERDAS IMAGINE software.

To derive informations about wildfires prior to the 1990s, georeferenced black-and-white CORONA (www.earthexplorer.usgs.gov) satellite images with a ground resolution of 12 m (28 July 1962) and of 2 m (31 October 1965) were used. Although a vegetation index cannot be determined from black-and-white photographs, the CORONA images were suitable for a visual comparison with the LANDSAT images.

6.3.3. Hydrological Modeling

The conceptual rainfall / runoff model HBV-D was developed at the Potsdam Institute for Climate Impact Research (PIK), Germany (Krysanova *et al*., 1999) and represents a revised version of the lumped Nordic HBV model (Bergström 1992; Lindström 1997). The HBV-D model allows to deal with sub-catchments, which are subdivided into hydrological response units (HRUs) consisting of elevation zones with prevailing land-cover classification proportions. The low data input demands (daily precipitation and air temperature, monthly values of potential evapotranspiration) as a result of the simple model structure (Figure 23), make the model suitable for data scarce regions, as for example the mountainous areas in northern Mongolia.

The HBV-D model was applied to simulate runoff from the four sub-catchments C1, C2, C3 and C4 from November 2010 to August 2013. Each elevation zone covers 100 m in altitude and is characterized by an individual composition of land-cover proportions. The effects of land-cover changes in the four sub-catchments on the hydrological regime were simulated and compared to the mean runoff in 2011 and 2012.

6.3.3.1. Model Calibration

In the HBV-D model, fifteen different land-cover types are classified. However, to represent the conditions in the study area, the land-cover type "nothing" (no. 15), was modified to the land-cover type "burned forest". As far as possible, results and processes from the field studies in 2011 and 2012 (Kopp *et al*., 2014; Kopp *et al*., 2016) were implemented into this newly defined conceptional vegetation class (Table 8).

Table 8: Excerpt of the vegetation file of the HBV-D model.

Type	no	ICMAX	CXREL	TSDIFF	CVSNOW	FCREL	LPDEL	EPVAR
Coniferous forest	7	6.0	0.7	0.0	0.5	1.5	0.6	1.0
Deciduous forest	8	4.0	0.7	0.0	0.5	1.5	0.6	1.0
Burned forest	15	0.9	1.3	0.0	0.3	1.9	0.9	1.0

ICMAX: Interception storage (mm); CXREL: Correction Factor on Temperature Index; TSDIFF: Adjustment on Zero Melt Temperature Threshold (°C); CVSNOW: Coefficient of Variation of Snow Distribution; FCREL: Adjustment of Maximum Soil Moisture Content; LPDEL: Specific Soil Water Content Regulating the Fraction of Actual to Potential Evapotranspiration; EPVAR: Correction Factor for Potential Evapotranspiration

The summer of 2012 was chosen as calibration period, as the maximum deviation between highest and lowest daily runoff was less pronounced, and therefore less influenced by a single high runoff event as was exemplarily observed in June 2011 (Figure 29 b,c). Both stormflow peaks and low-flow conditions were present in the calibration period, allowing the calibrated model to be considered more stable. The hydrographs for each model run were examined separately both, visually and by calculating efficiency criteria with in order to obtain the optimum fit. The final parameterizations, as a result of the calibration process, are shown in Table 9. It illustrates where differences in the model structure occur between the sub-catchments. Of course, different parameterizations can result in the same quality of the obtained fit. Therefore, the parameterization used was combining our knowledge about the physical system, the model structure and the quality of the efficiency criteria. As far as possible, certain parameterizations were used for all models (threshold temperature, snowmelt index).

The year 2011 was used for validation of the two sub-catchment models C1 and C2. As runoff hydrographs for the two sub-catchments C3 and C4 only exist from mid of June until the beginning of September 2012, these two models were not validated.

Table 9: Final parameterizations as a result of the calibration of the four HBV-D models.

Model Parameter	C1	C2	C3	C4
threshold temperature (°C)	-3.0	-3.0	-3.0	-3.0
Snowmelt index (m*(deg*d)$^{-1}$)	6.0	6.0	6.0	6.0
field capacity (mm)	115	184	280	127
BETA (non-linearity in soil water zone)	1.21	1.12	2.08	1.20
threshold quick runoff (mm)	18.0	24.0	10.0	37.0
Quick time constant – upper zone	0.083	0.082	0.088	0.083
Slow time constant – upper zone	0.066	0.076	0.066	0.058
Slow time constant – lower zone	0.011	0.018	0.034	0.013
Groundwater recharge (mm*d^{-1})	0.61	1.19	1.25	0.50
Evapotranspiration constant (mm*(deg*d)$^{-1}$)	0.042	0.043	0.040	0.041

6.3.3.2. Modeling of Land-Cover Scenarios

Since the beginning of the 21st century, significant areas within the Khentii Mountains have been burned by wildfires (Karthe *et al*., 2015). This is especially true for the headwaters of the Sugnugr catchment, as could be observed during field campaigns and as a result of the land-cover classification applying remote sensing methods.

To investigate the effects of wildfires on the hydrological regime, two scenarios were applied using the calibrated HBV-D model of each sub-catchment:

- Scenario 1 is designed to represent a hydrological regime which is unaffected by wildfires. To this end, the vegetation cover observed in 1990 was applied.

- Scenario 2 is designed to determine the response of a severely burned catchment. To this end, all areas in Scenario 1 classified as forest were classified as burned forest.

6.4. Results

6.4.1. Land Cover Classification

Different land-cover classifications could be derived from the LANDSAT images using the ERDAS IMAGINE software. A reliable differentiation between vegetation and alpine scree was achieved and vegetation could be further subdivided into different classes. As a result, five main classes were derived: forest, burned forest, open shrub, steppe and alpine scree. The results could be ground-truthed by known land-cover types within the research area during field campaigns.

For the year 1990, total percentage of the different individual land-cover classifications for each sub-catchment is shown in Table 10. Shrubs were found to be the dominant vegetation type below an elevation of 1200 m a.s.l. Basically, this vegetation type is limited to flood plains in the vicinity of the rivers. South exposed hill slopes are covered with steppe vegetation from the basin outlets until an elevation of approximately 1800 m a.s.l. To some extent, both shrubs and steppe vegetation is abundant at higher elevation zones. The abundance of forest vegetation increases with elevation and is up to 90 % between 1500 to 2000 m a.s.l. The proportion of alpine scree exceeds 75 % above 2300 m a.s.l. (Figure 27 a) and reaches a maximum of 85 % above 2500 m a.s.l.

Wildfires in 2007 and 2011 destroyed considerable forest stands (~14 %) of the Sugnugr Basin (Figure 27 b). The extent of the burned forest stands varies between the sub-catchments from 15 % in C4 to 82 % in C3 (Table 11). The proportion of other vegetation types varied only to a minor degree.

Table 10: Vegetation cover of the four sub-catchments in 1990.

Vegetation cover in 1990	C1	C2	C3	C4
Forest (%)	59.7	83.8	89.6	87.5
Steppe (%)	6.0	5.4	2.8	2.7
Shrub (%)	5.0	7.9	6.1	5.0
Alpine scree (%)	29.3	2.9	1.5	4.8

Table 11: Vegetation cover of the four sub-catchments in 2011.

Vegetation cover in 2011	C1	C2	C3	C4
Forest (%)	44.0	53.0	12.5	73.3
Burned forest (%)	17.4	33.6	82.0	15.4
Steppe (%)	5.5	4.1	1.9	2.2
Shrub (%)	4.5	6.8	2.3	4.3
Alpine scree (%)	28.6	2.6	1.3	4.8

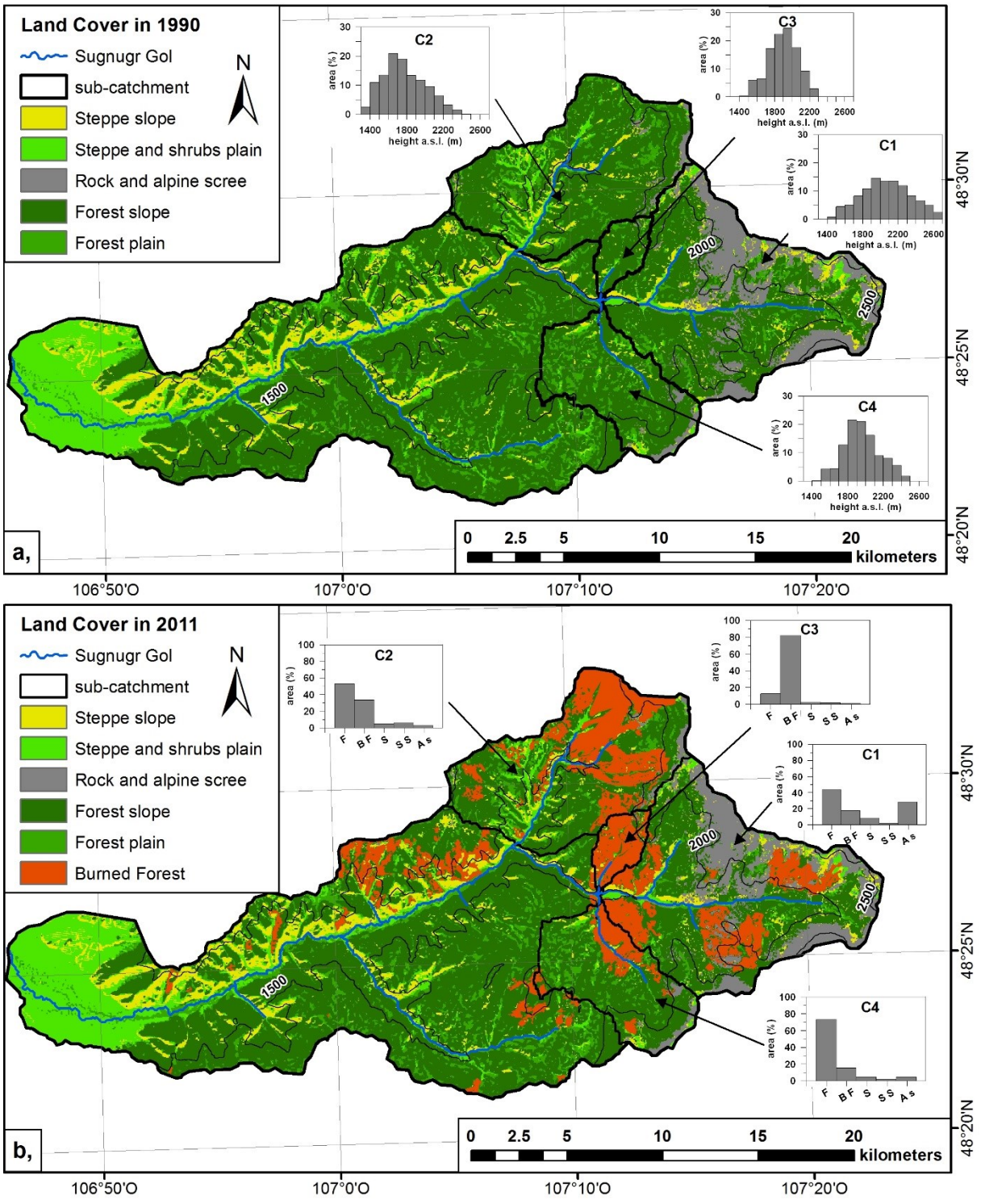

Figure 27: Vegetation cover of the Sugnugr Basin and the four sub-catchments in 1990 (a,) and 2011 (b,). Small Graphs show the elevation distribution (a,) and the vegetation distribution (b,) of each sub-catchment (F = Forest, BF = Burned Forest, S = Steppe (slope), SS = Steppe and Shrub (plain) and As = Alpine scree).

The comparison of the black-and-white CORONA images with the LANDSAT images revealed an insignificant change in vegetation distribution for the Sugnugr catchment between the 1960s and the 1990s. Most strikingly, no indications for wildfires prior to the 1960s were found.

6.4.2. Hydrological Modeling

6.4.2.1. Model Calibration and Validation

The overall runoff variability in the sub-catchments C1 and C2 made it difficult to calibrate the HBV-D models for the summer months of 2012 (Table 12). By calculating the logarithmic Nash-Sutcliffe coefficient, the high impact of stormflow is avoided and the weight of lower values on the efficiency criteria is increased (Krause *et al*., 2005). With a logarithmic Nash-Sutcliff coefficient of 0.70 of the C1 model, the quality of the achieved calibration can be considered to be satisfactory. The calibration quality of the lower elevated C2 was little less, as reflected by a logarithmic Nash-Sutcliffe coefficient of 0.61. In general, the parameters of the soil model had the biggest influence on the simulated hydrograph during calibration.

While runoff during the validation period of the dry summer 2011 was low, two consecutive stormflow events occurred in the beginning of July. Due to the focus of the modeling work on low flow conditions, an insufficient reproduction of the flood event had to be accepted. Although low-flow conditions were generally simulated in good agreement with the observations (Figure 29 b, Figure 30 b), this single stormflow event had a distinct effect on the calculated Nash-Sutcliff coefficient of the validation (Table 12). In general, runoff in 2011 tended to be underestimated while the simulated runoff in 2012 overestimated the observed mean runoff (Table 13).

Table 12: Efficiency criteria for the calibration period in summer 2012 (C1, C2, C3 and C4) and the validation period in summer 2011 (C1 and C2).

Efficiency Criteria	C1	C2	C3	C4
Log Nash-Sutcliffe coefficient (NS)	0.64	0.64	NA	NA
Log NS 2011 (validation period)	0.36	0.41	NA	NA
Log NS 2012 (calibration period)	0.70	0.61	0.57	0.51
Nash-Sutcliffe coefficient (NS)	0.51	0.39	NA	NA
NS 2011 (validation period)	0.23	0.25	NA	NA
NS 2012 (calibration period)	0.61	0.37	0.32	0.38
Root Mean Square Error (RMSE)	1.20	0.62	NA	NA
RMSE 2011	1.37	0.62	NA	NA
RMSE 2012	1.06	0.62	0.83	1.08
Correlation coefficient (R^2)	0.72	0.63	NA	NA
R^2 2011	0.57	0.62	NA	NA
R^2 2012	0.80	0.67	0.60	0.62
$Q_{sim} - Q_{obs}$ (mm)	3.1	-4.4	-2.5 (2012)	-5.8 (2012)

Table 13: Mean daily simulated and observed runoff of the four sub-catchments during the observation periods and the simulated mean daily runoff for 2011 and 2012.

Observed and simulated runoff (mm d^{-1}) during the observation periods	C1	C2	C3	C4
Q_{obs} / Q_{sim}	2.60 / 2.62	1.13 / 1.15	NA	NA
Q_{obs} / Q_{sim} 2011	2.01 / 1.88	0.86 / 0.80	NA	NA
Q_{obs} / Q_{sim} 2012	3.01 / 3.13	1.35 / 1.36	2.41 / 2.38	2.56 / 2.49
Simulated runoff (mm d^{-1}) in 2011 and 2012				
Q_{sim} (mm*d^{-1})	1.08 ± 0.39	0.49 ± 0.18	0.70 ±0.25	0.76 ±0.34
Q_{sim} 2011 (mm*d^{-1})	0.83	0.37	0.52	0.53
Q_{sim} 2012 (mm*d^{-1})	1.34	0.62	0.87	0.99

The mean specific discharge of each sub-catchment is mainly determined by the mean catchment elevation and therefore the amount of precipitation (Figure 28). Thus, the differences in vegetation composition are influencing the mean specific discharge to a minor degree. However, Figure 28 shows an increase in annual specific runoff of 8 % in C3, compared to the moderately burned C1, C2 and C4 sub-catchments. This can be attributed to the fact that 82 % of the catchment area are severely burned. During the summer half year (May to October), the

specific runoff is approximately 14 % higher than expected from the mean catchment elevation, while it is -160 % lower from December to April.

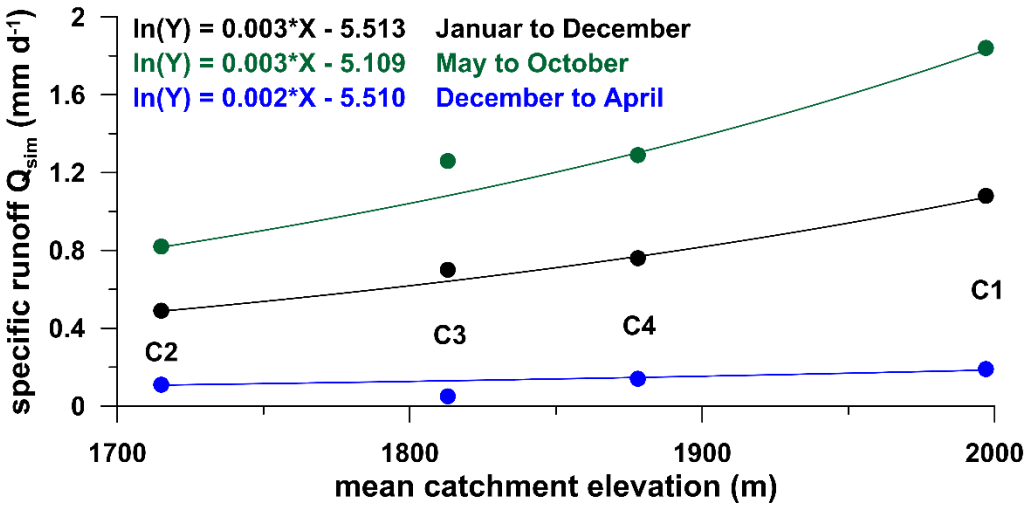

Figure 28: Mean simulated specific runoff of the four sub-catchments in relation to the mean catchment elevation (black: yearly, green: May to October, blue: December to April).

During winter, only small specific runoff rates were simulated for each sub-catchment, which declined to a minimum below 0.1 mm d^{-1} in February and March (Figure 29 to Figure 31). The presence of year-round baseflow could be verified during field stays, as remains of aufeis formations, up to a thickness of 2 m within the river channel, were observed close to the outlet of C1 in the beginning of June 2012.

Sub-catchment C1, with an area of 100.2 km² and a mean elevation of 1995 m a.s.l, is the largest and highest elevated among the four sub-catchments. It's furthermore characterized by the highest altitude difference, as it ranges from 1466 m to 2687 m, resulting in a broad variety of vegetation types and the highest total proportion (28.6 %) of alpine scree (Table 11, Figure 27).

With a simulated specific runoff of 0.4 and 1.1 mm d^{-1}, the modeled snowmelt in April is low, compared to 2.1 and 4.1 mm d^{-1} during summer 2011 and 2012, respectively (Figure 29 a). Taken together, the C1 model did very well at simulating the overall runoff level and baseflow conditions. This applies to both years, the relatively dry year of 2011 and the relatively wet year of 2012. Due to a lack of long-term observational data, it is unknown which year is representative for this region. The cumulative difference between the simulated and observed runoff was -10 mm in 2011 and +10 mm in 2012 (Figure 29 b, c).

However, the observed dynamics of the stormflow events could not be simulated satisfactorily. This might be caused by an inadequate implementation of the observed quick response times in the model, as well as by the lack of input data from higher elevated areas. For example, occasional thunderstorms, that were often limited in their extent to the summits, were observed during field stays in summer. These were not recorded by the meteorological station close to the outlet of the sub-catchment C1.

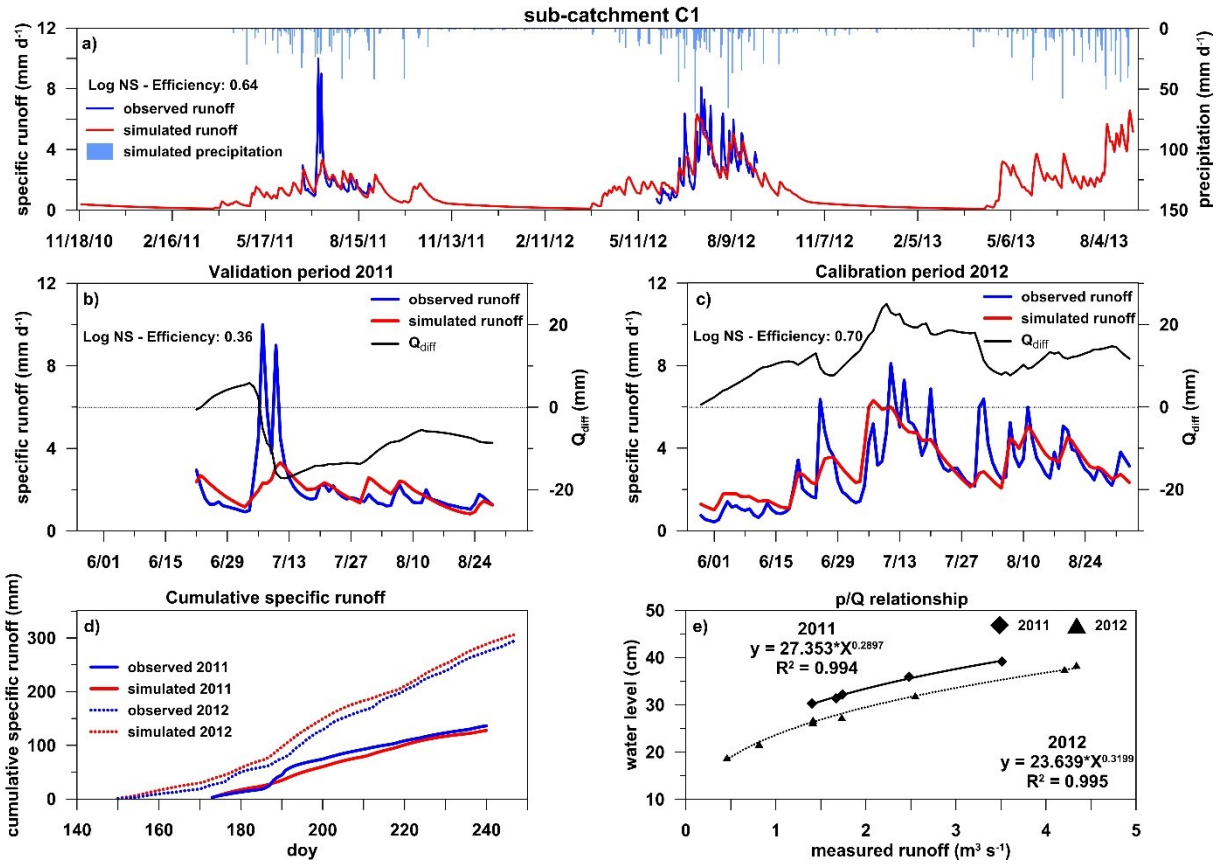

Figure 29: Overview of the model results applying the HBV-D model in the sub-catchment C1.

Sub-catchment C2, which covers an area of 72.3 km², is the second largest among the four sub-catchments. With a mean elevation of 1715 m a.s.l., ranging from 1336 m to 2321 m a.s.l., it is characterized by a less distinct altitude difference compared to C1. As a consequence, vegetation cover is less heterogeneous, and only 2.5 % of the total catchment area exhibits alpine scree (Table 11, Figure 27).

With a simulated specific runoff of 0.1 and 0.3 mm d^{-1}, the modeled snowmelt in April is low compared to 0.9 and 1.8 mm d^{-1} during summer 2011 and 2012, respectively (Figure 30 a).

Taken together, the C2 model did very well at simulating the overall runoff level and baseflow conditions for both summers. The cumulative difference between the simulated and observed summer runoff was -4 mm in 2011 and ±0 mm in 2012 (Figure 29 b,c). However, similar to the C1 model, the observed dynamics of the stormflow events could not be simulated satisfactorily.

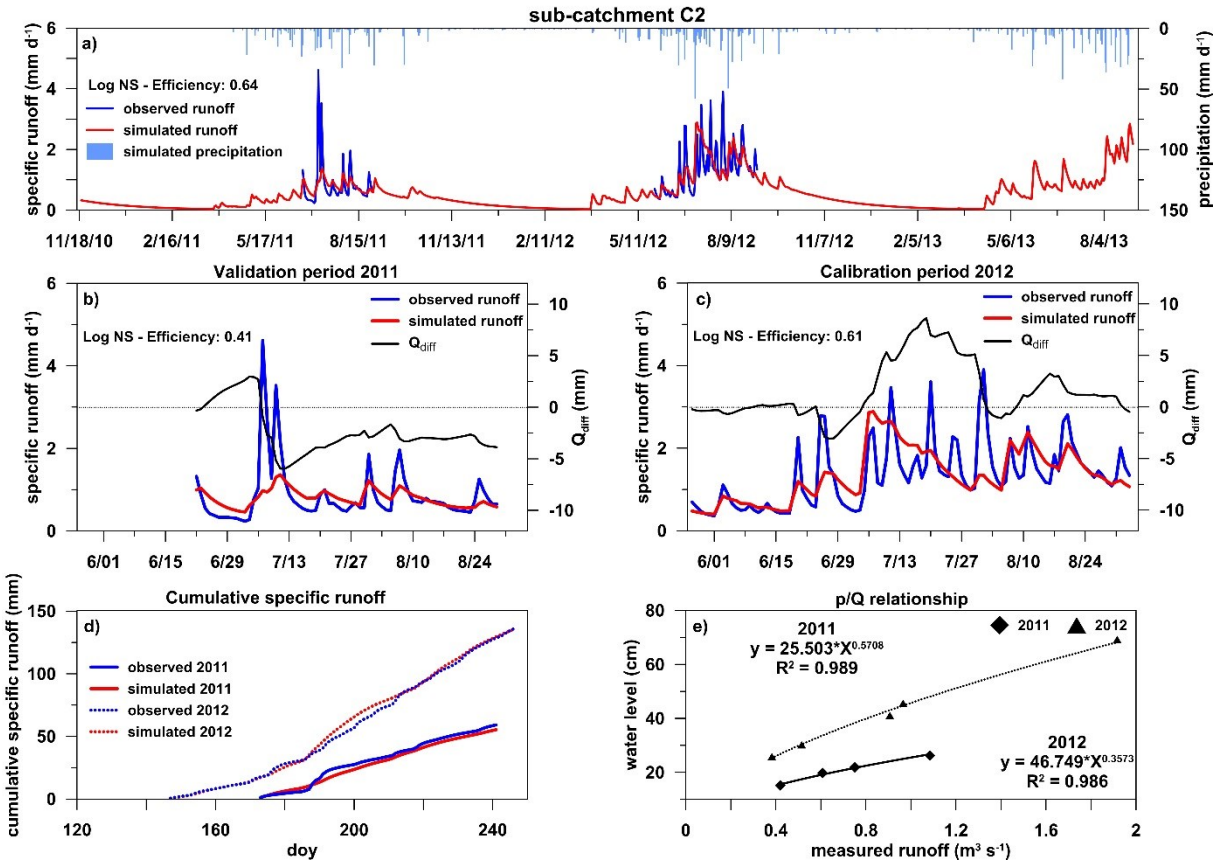

Figure 30: Overview of the model results applying the HBV-D model in the sub-catchment C2.

With a catchment area of 7.9 km² and 36.1 km², C3 and C4 are smaller than C1 and C2. They are characterized by a similar mean elevation of 1813 m (C3) and 1878 m a.s.l. (C4). C3 ranges from 1482 m to 2155 m a.s.l. and C4 from 1469 m to 2371 m a.s.l. While 1.3 % of the catchment area of C3 is covered by scree, 4.8 % of the higher elevated C4 sub-catchment is covered by scree. However, extent of burned areas differs between the two sub-catchments. In the C3, 12.5 % of the total area are covered by pristine forest and 82 % of the area is classified as burned forest. In C4, 73.4 % of the total area are covered by pristine taiga, with only 15.4 % of the area burned (Table 11, Figure 27 b). These differences in vegetation cover were reflected by the observed and modeled hydrographs during summer to a certain degree. Although the mean

elevation of C4 is higher, mean specific runoff from both catchments is about equal (Table 13, Figure 31 d), indicating an increase in runoff following wildfires in C3. Both models did very well at simulating the overall runoff level for the summer of 2012. However, while baseflow conditions were simulated in reasonable agreement with observations for C3, baseflow was slightly overestimated for C4 (Figure 31 c). The cumulative difference between simulated and observed summer runoff was -3 mm at C3 and -6 mm at C4 (Figure 31 b,c). The observed higher snowmelt in C4 can be attributed to higher catchment elevation and hence greater snowpack accumulation during winter.

Similar to the C1 and C2 sub-catchments, runoff dynamics of single stormflow events could not be simulated satisfactorily. However it has to be kept in mind that the determined p/Q relationship is based on only four manual runoff measurements (Figure 31 e), which might result in a misleading hydrograph in terms of peakflow and low-flow.

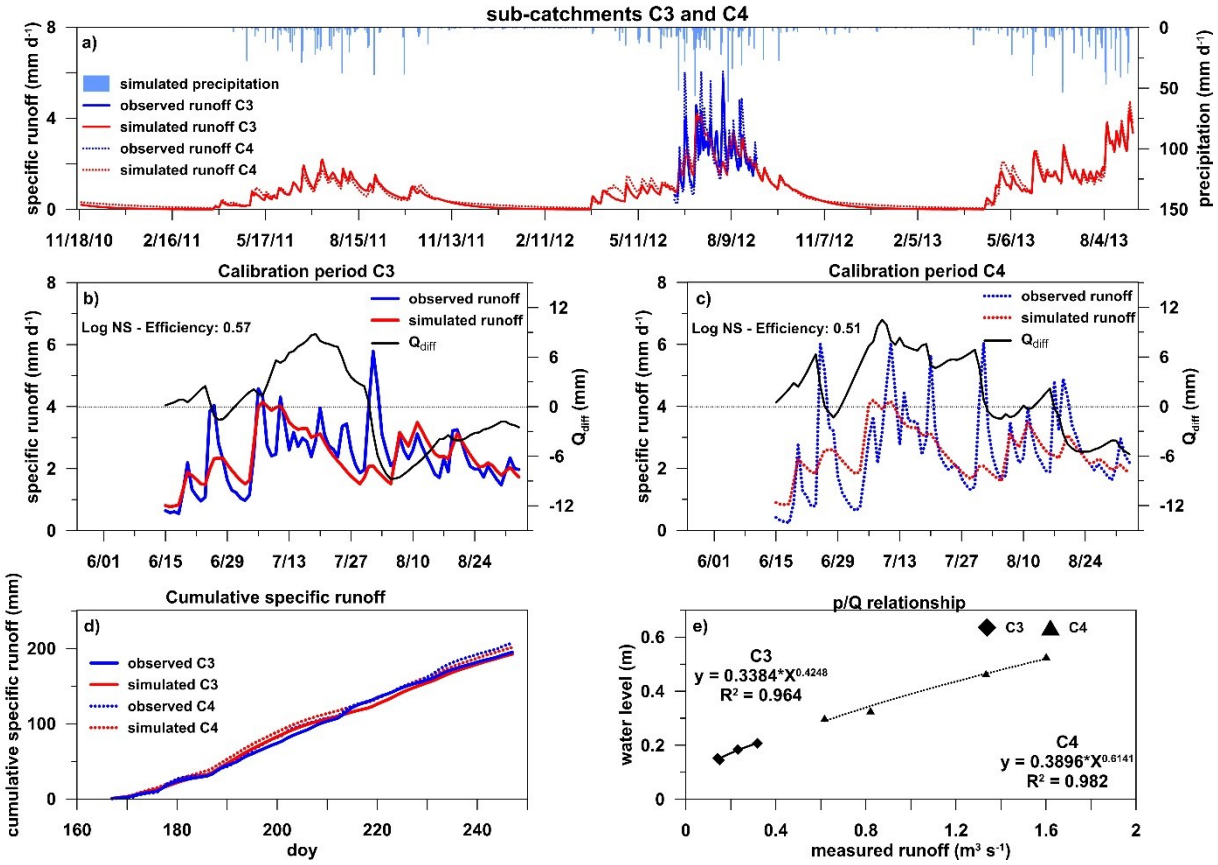

Figure 31: Overview of the model results applying the HBV-D model in the sub- catchments C3 and C4.

As the dynamic of stormflow events is reflected very poorly by the four models (Figure 29 to Figure 31), our study does not allow conclusions regarding land-cover change related alterations of single stormflow discharge dynamics. However, as the overall runoff level was simulated well, the models allow to derive statements about longer time periods, in particular monthly values (Figure 32, Figure 33).

This approach allows to study the inter-annual changes in mean monthly runoff between a relatively dry year (2011) and a relatively wet year (2012) (Figure 32). While the very dry and cold winter months (November - February) revealed no differences in runoff quantity between both years, runoff during the summer months (June - August) differed up to 60 %. Due to the high mean elevation, C1 and C4 were characterized by the highest specific runoff during the summer and the winter months. It becomes evident, that the mean specific runoff from December to March of the severely burned C3 sub-catchment is between 2.0 times and 4.1 times lower compared to the sub-catchments C1, C2 and C4 in both years.

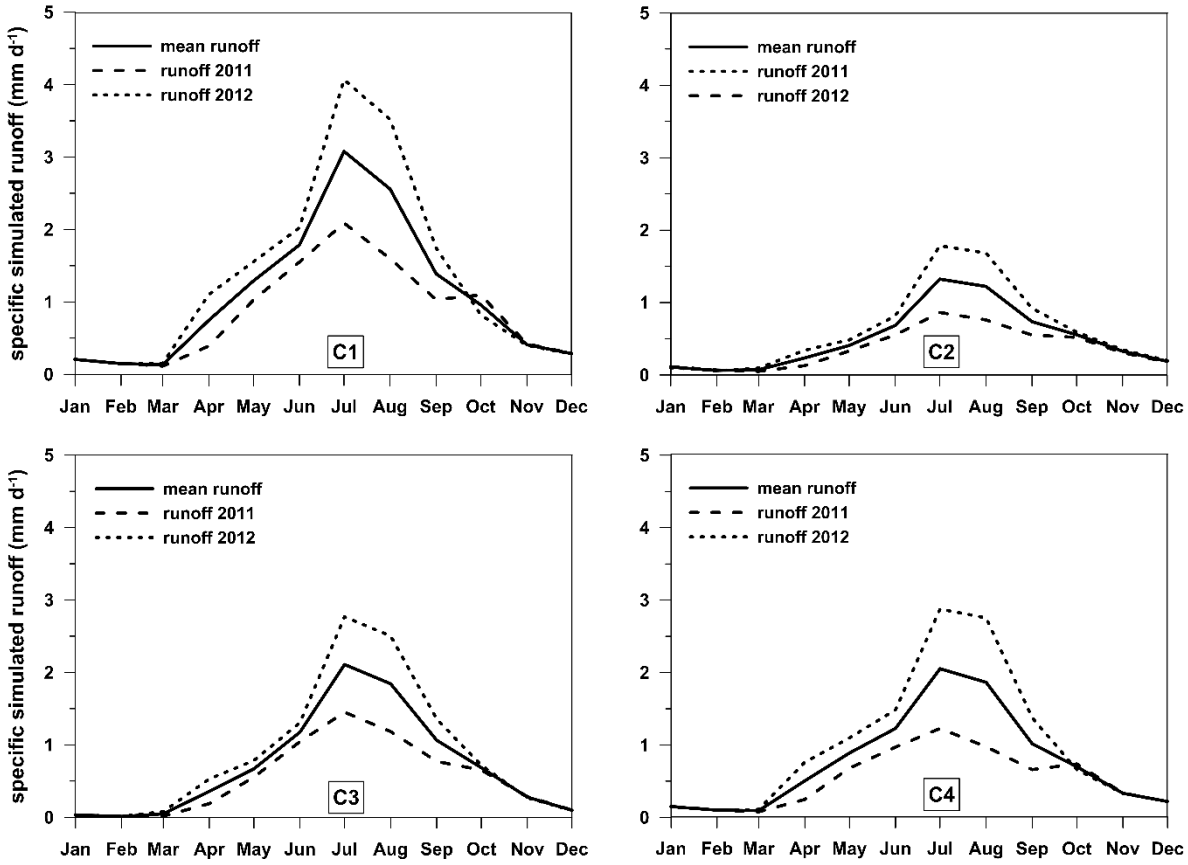

Figure 32: Monthly mean simulated runoff of the dry year 2011 and the wet year 2012 of the four sub catchments.

6.4.2.2. Land-Cover Change Scenarios

The results of the land-cover classification served as basis for the modeling of the land-cover change scenarios. In Scenario 1 all forest covered areas were classified as pristine forest (Table 14). Hence it represents the land-cover conditions of 1990. The same areas were classified as burned forest in Scenario 2 (Table 15). The remaining land-cover classes remained unchanged. The model parameters were adjusted for each Scenario based on the results of the model calibration (Table 9) and by implementing the results of the identified relevant hydrological processes obtained during the field measurements in 2011 and 2012. Therefore, the relevant parameters of the soil moisture zone, the upper zone and the lower zone were adjusted to represent unburned (Table 14) and burned conditions (Table 15). Additionally, the evapotranspiration constant was reduced in Scenario 2 due to the loss of the organic surface layer and trees.

Both scenarios were driven with daily precipitation and temperature values recorded from November 2010 until August 2013. The observed mean monthly runoff in 2011 and 2012 (Figure 32) served as the comparison period, which allowed to distinguish between the mean monthly runoff changes as a consequence of Scenario 1 and Scenario 2.

Table 14: Vegetation cover and model parameterization in Scenario 1 (unburned).

Vegetation cover and parameterization – Scenario 1	**C1**	**C2**	**C3**	**C4**
Forest area (%)	61.4	86.6	94.5	88.7
Burned forest area (%)	0.0	0.0	0.0	0.0
Steppe area (%)	5.5	4.1	1.9	2.2
Shrub area (%)	4.5	6.8	2.3	4.3
Alpine scree area (%)	28.6	2.6	1.3	4.8
field capacity (mm)	68	85	80	75
BETA (non-linearity in soil water zone)	1.21	1.12	2.08	1.20
threshold quick runoff (mm)	26.0	40.0	40.0	38.0
Quick time constant – upper zone	0.083	0.084	0.084	0.084
Slow time constant – upper zone	0.066	0.067	0.066	0.058
Slow time constant – lower zone	0.008	0.011	0.010	0.009
Groundwater recharge ($mm*d^{-1}$)	0.35	0.50	0.45	0.40
ET constant ($mm*(deg*d)^{-1}$)	0.042	0.042	0.042	0.042
Q_{sim} ($mm*d^{-1}$)	1.08 ± 0.45	0.42 ± 0.20	0.47 ±0.28	0.72 ±0.36
Q_{sim} 2011 ($mm*d^{-1}$)	0.80	0.28	0.27	0.48
Q_{sim} 2012 ($mm*d^{-1}$)	1.35	0.55	0.66	0.95

Table 15: Vegetation cover and model parameterization in Scenario 2 (burned).

Vegetation cover and parameterization – Scenario 2	C1	C2	C3	C4
Forest area (%)	0.0	0.0	0.0	0.0
Burned forest area (%)	61.4	86.6	94.5	88.7
Steppe area (%)	5.5	4.1	1.9	2.2
Shrub area (%)	4.5	6.8	2.3	4.3
Alpine scree area (%)	28.6	2.6	1.3	4.8
field capacity (mm)	200	290	300	280
BETA (non-linearity in soil water zone)	1.21	1.12	2.08	1.20
threshold quick runoff (mm)	6.0	6.0	6.0	6.0
Quick time constant – upper zone	0.089	0.089	0.090	0.089
Slow time constant – upper zone	0.066	0.076	0.066	0.058
Slow time constant – lower zone	0.027	0.037	0.037	0.035
Groundwater recharge ($mm*d^{-1}$)	1.20	1.50	1.50	1.45
ET constant ($mm*(deg*d)^{-1}$)	0.039	0.039	0.039	0.039
Q_{sim} ($mm*d^{-1}$)	1.26 ± 0.41	0.65 ± 0.18	0.75 ±0.25	1.01 ±0.31
Q_{sim} 2011 ($mm*d^{-1}$)	1.00	0.53	0.57	0.81
Q_{sim} 2012 ($mm*d^{-1}$)	1.52	0.77	0.92	1.21

In Scenario 1, the mean annual specific runoff is decreasing at all four sub-catchments (Figure 33). The changes within the today severely burned sub-catchment C3 were most distinct. Here, the mean annual runoff decreased by -33 %, while changes were smaller in the other sub-catchments (C2: -15 %, C4: -6 %, C1: -1 %). On a monthly scale, the changes were even more pronounced (Table 16). The mean monthly specific runoff remained equal or increased at all sub-catchments during winter and spring (January to May) and declined or remained equal during summer and autumn (June to November). Again, the changes in C3 were most distinct, as the mean specific runoff increased up to 700 % in February and declined by almost -60 % in September.

Table 16: Relative change in yearly and monthly specific runoff of Scenario 1 (unburned) compared to the observed mean runoff in 2011 and 2012.

Scenario 1: Relative change in runoff (%)	C1	C2	C3	C4
Year	-0.7	-15.3	-33.0	-5.7
January	-20.1	17.5	294.1	9.5
February	-12.5	45.1	726.5	23.5
March	-3.1	42.9	96.1	32.2
April	18.9	33.0	20.2	25.0
May	14.4	9.7	-3.5	8.1
June	3.3	-24.8	-51.3	-10.7
July	-3.8	-21.2	-52.4	-12.1
August	-1.8	-11.5	-22.7	-5.3
September	-1.7	-34.9	-57.2	-17.9
October	-2.1	-28.4	-46.5	-9.7
November	-28.9	-25.6	-18.7	-15.0
December	-28.7	-8.2	70.5	-5.2

In Scenario 2, the mean annual specific runoff increased at all four sub-catchments compared to mean conditions in 2011 and 2012 (Figure 33). As expected, the changes in the severely burned C3 were smallest (Figure 27, Table 11). Here, the mean yearly runoff increased by 7 %. Also in C2, runoff increases were small (8 %), while changes were more distinct in C1 (17 %) and C4 (33 %). Again, the changes were more pronounced on a monthly scale (Table 17). The mean monthly specific runoff declined at all sub-catchments during winter and spring (December to March) and increased during summer and autumn (May to October).

Although the relative changes of the specific runoff were greater during the winter months for both scenarios, runoff changes were most pronounced during summer months when total runoff is highest (Figure 32, Figure 33). However, the very low specific runoff in spring is to a high degree decisive for water availability in down streaming areas during the dry season from November to March. The simulated effect of a wildfire (Scenario 2) resulted in a more pronounced low-flow period during these months, whereas the overall monthly runoff increases from May to November.

Table 17: Relative change in yearly and monthly specific runoff of Scenario 2 (burned) compared to the observed mean runoff in 2011 and 2012.

Scenario 1: Relative change in runoff (%)	C1	C2	C3	C4
Year	16.7	7.5	7.2	32.7
January	-55.9	-79.8	-17.3	-70.9
February	-73.0	-88.7	-24.8	-85.2
March	-54.9	-70.2	8.2	-38.1
April	1.9	-21.2	9.5	10.3
May	8.9	26.8	6.6	13.7
June	32.0	41.0	9.7	51.3
July	25.4	12.0	8.6	52.7
August	11.1	4.1	3.8	23.4
September	31.7	11.7	10.2	54.7
October	27.1	24.4	8.3	45.8
November	18.4	-11.4	1.4	16.3
December	-26.6	-50.8	-7.7	-40.4

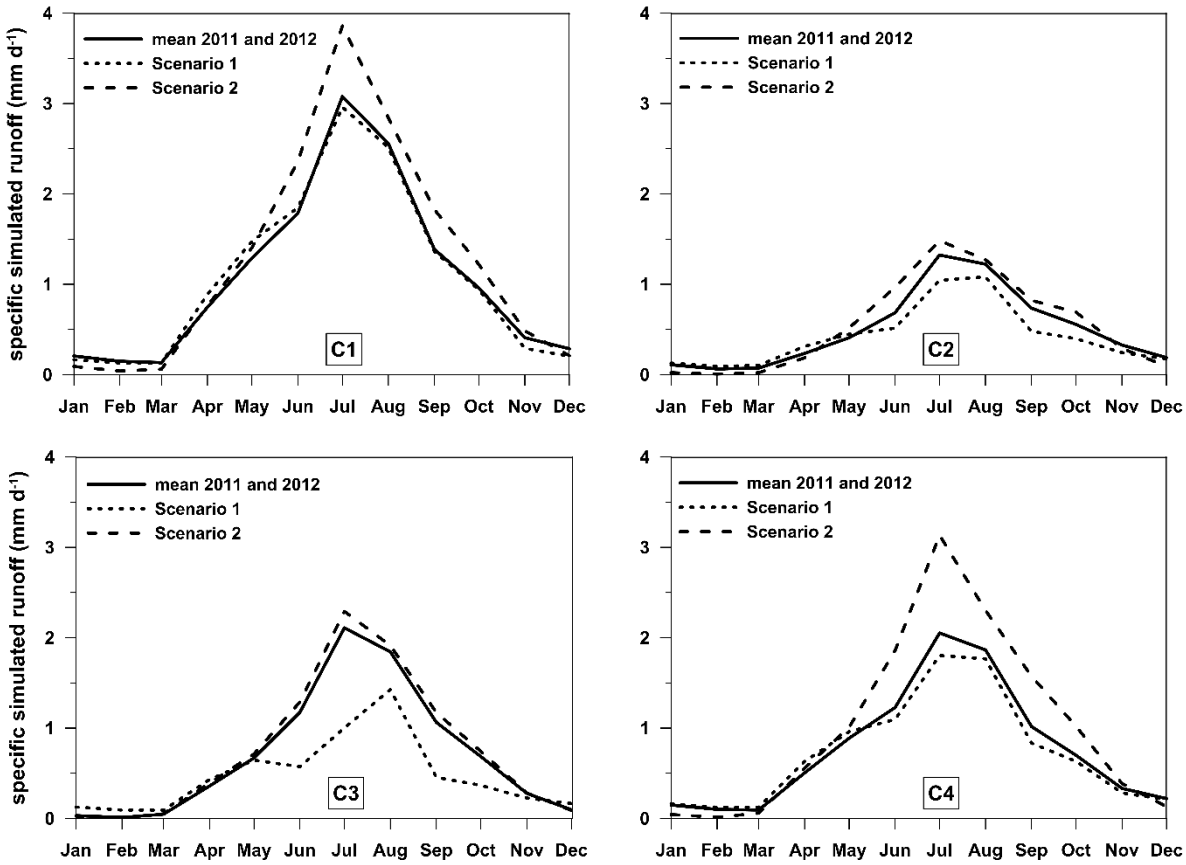

Figure 33: Mean monthly simulated runoff (2011 and 2012) in 2011 and 2012 compared to the mean monthly simulated runoff of Scenario 1 (unburned) and Scenario 2 (burned).

6.5. Discussion

6.5.1. Hydrological Regime

In many cold regions, especially in permafrost environments in Alaska, spring snowmelt has been shown to control both, timing and magnitude of the hydrograph (Hinzman and Kane, 1992; Carr, 2003). However, due to the dry conditions during winter months in the Khentii Mountains, the total snowpack water is relatively low. At an elevation of 1193 m a.s.l., a total snow water equivalent during the hydrological winter half year (November to April) of 18 mm, 57 mm and 47 mm has been measured. This amount corresponds to 6 %, 11 % and less than 10 % of the yearly precipitation in 2010/2011, 2011/2012 and 2012/2013, respectively (Figure 26). As Wimmer *et al*. (2009) modeled annual snow sublimation to account for approximately 80 % of total snowfall in northern Mongolia, it becomes obvious that snowmelt runoff during spring is of minor relevance regarding total yearly runoff amounts. However, snowmelt runoff is an important occasion in spring. The virtually dried out rivers are, for the first time of the year, supplied with freshet water after the very cold and dry winter months (Figure 29, Figure 30, Figure 31). Observations of snowmelt runoff are lacking at all sub-catchments due to their remote location. Furthermore, the presence of aufeis makes it virtually impossible to conduct manual runoff measurements during snowmelt.

Similar to the results of this study, particularly seasonal hydrographs in the two neighbored Kharaa River (Menzel *et al*., 2011) and Yeruu River (Pederson *et al*., 2013) were reported. The majority of flow was observed between May to October, with distinct stromflow events from June to August. In general, water availability is controlled by the differences between evapotranspiration and precipitation during summer months. Considering the fact that mean annual precipitation constitutes only 15 % of the mean annual potential evapotranspiration (Ma *et al*., 2003), it becomes obvious that runoff generation is controlled by the highly variable monthly and yearly precipitation amounts (Figure 26). Although precipitation in 2011 and 2012 differed by only 20 %, runoff in 2012 was 1.6 times the runoff in 2011 (Table 13, Figure 32). On a monthly basis, differences between the two years were even more pronounced as mean monthly runoff in April 2012 was 2.8 times and in August 2012 2.2 times the runoff in 2011, respectively. Distinct differences in runoff amounts have also been reported to occur on multi-decadal time spans (Pederson *et al*., 2013; Davi *et al*., 2013).

6.5.2. Land-Cover Change Scenarios

Depending on the applied land-cover scenario, the results of runoff simulations in the four sub-catchments C1, C2, C3 and C4 reveal distinct differences on a monthly scale. The low specific runoff in winter and spring results in the most distinct relative changes during these months in both scenarios. Relative changes of the specific discharge remained smaller during summer months, although the changes of the total runoff amounts are more pronounced.

In Scenario 1 (unburned), the simulated specific runoff from November to April of the three sub-catchments C1, C2 and C4 increased by 12 % (C4), 34 % (C2) and decreased by -12 % in C1 (Table 16), compared to the partly burned conditions in 2011 and 2012. This finding is a result of effective snow and water retention in the vegetation zone. Recession period is prolonged, resulting in higher low-flow conditions. In contrast, runoff amounts were simulated to remain equal (C1: 1 %) or to decrease (C4: -8 %, C2: -19 %) from May to October, which can be attributed to higher evapotranspiration losses (Heijmans *et al*., 2004; Lopez *et al*., 2008; Ohta *et al*., 2008).

In Scenario 2 (burned) yearly runoff increased by 8 % (C2), 17 % (C1) and 33 % (C4). However, the simulated specific runoff distinctly declined from December to March (C1: -53 %, C4: -59 %, C2: -72 %) and increased from May to October (C2: 20 %, C1: 23 %, C4: 40 %) (Table 17). Results agree with the mean simulated runoff of C3 during the comparison period of 2011 and 2012, as the catchment area is already burned by 82 % (Table 11, Figure 27). At C3, yearly simulated specific runoff was 8 % less than from the moderately burned C1, C2 and C4 sub-catchments. More specifically, runoff was 158 % lower during winter and spring, and increased by 14 % during the summer half year (Figure 28). The results are in accordance to Burke *et al*. (2005) who found runoff to increase significantly by 1.6 to 3.7 times following four subsequent years after a wildfire, compared to unburned sites. Similarly, Valeo *et al*. (2003) observed initial increases in runoff following wildfire in boreal forests in a variety of watersheds in Ontario, Canada, that decreased on the long term. Both observations could be related to the age distribution of the trees with subsequent impacts on water yields in both, the short and the long term.

Similar to the described more pronounced hydrograph magnitude on a monthly basis of all sub-catchments in Scenario 2 in this study, the results of our field studies indicate that the magnitude of stromflow runoff following wildfires is increasing on a shorter time scale. This is due to the high retardation capacity of the thick organic surface layer in pristine forests (Kopp

et al., 2016). Quinton *et al*. (2005) found hydraulic conductivities of the organic layer to decrease exponentially with depth. Both processes result in a dampened reaction of hillslope runoff following precipitation events. As a consequence, the recession period is prolonged. Wildfires have the capability to change this system drastically, depending on burn severity. As the organic surface cover is removed, stormflow runoff was observed to occur as overland flow above the exposed mineral horizon and as subsurface stormflow (SSF) on top of the degraded permafrost surface (Lange *et al*., 2015; Kopp *et al*., 2016). Both runoff processes occur at high velocities, resulting in increased peakflow, which in turn leads to lower low-flow conditions as the burned hillslope is drained more effectively.

6.5.3. Limitations of the HBV-D Model

Although permafrost was not a consideration when developing the HBV model, Bergström, (1976) stated frozen ground to be successfully represented with the free parameters of the model. Hinzman and Kane (1991) found the HBV model to adequately represent permafrost conditions by setting PERC equal to 0. Carr (2003) reported field capacity, groundwater recharge and the slow time constant of the lower soil zone to directly address the impact of permafrost in the HBV model. It can be assumed that a catchment features smaller values of field capacity, when a large fraction of the catchment is covered by permafrost. While C1 and C4 exhibit similarly low values for field capacity, groundwater recharge and slow time constant, the lower elevated C2 is characterized by medium values and the heavily burned C3 features the highest values of the parameters mentioned above (Table 9). Higher values reflect an increased thickness of the active layer due to wildfire.

Water fluxes in catchments are controlled by complex and heterogeneous physical processes. As field measurements can usually only be conducted at the point scale, they are hence of limited use for characterizing the relevant hydrological processes on a larger scale (Kirchner, 2009). In hydrological modeling of data scarce regions, conceptual models are generally considered to be an adequate way to simulate stream runoff at the basin outlet due to their low need of input data (Bergström, 1992). However, it has to be kept in mind that a high uncertainty exists regarding both, the calibrated parameters in the model as well as the quality of the input data (Carr, 2003).

Seibert (1997) argues that model fits usually average over the simulation period. The author concluded that in environments with changing conditions certain parameterizations fit, for

example, well during spring but less during autumn. It is therefore difficult to define a unique parameter set that represents the conditions of a single catchment. This is particularly true for the modeling of the four sub-catchments C1, C2, C3 and C4 as the calibration period only covered the summer months of 2012. In all sub-catchments the thickness of the active layer has been shown to increase in the course of summer (Kopp *et al.*, 2014). Hence, it is likely that certain parameters of the soil model need to be adjusted depending on the simulated time of the year. This may explain the obtained medium quality of the efficiency criteria of the calibrated HBV-D models for all four sub-catchments (Table 12). However, Hinzman and Kane (1991) observed that, although runoff differed from year to year in a permafrost affected watershed in Alaska, the HBV model adequately simulates the runoff for each year. Finally, it is evident that a longer calibration period covering several consecutive years would lead to a better fit of the simulation as a larger variety of runoff conditions are included in the calibration process.

When evaluating the results of the conceptual HBV-D model, it becomes obvious that the application of the model in such a heterogeneous environment as the transition zone between steppe and taiga is limited. The headwaters of the Sugnugr are characterized by enormous hydrological heterogeneities between steppe, taiga and burned taiga stands, further augmented by the presence of discontinuous permafrost, which prevails at taiga stands and higher elevated areas. Each land-cover type exhibits different soil moisture and soil temperature dynamics (Kopp *et al*., 2014) and individual runoff generating processes (Lange *et al*., 2015; Kopp *et al*., 2016). In the conceptual HBV-D model, the catchment is subdivided by elevation zones into classes, which are assumed to show a common hydrological response (hydrological response units / HRUs). By this conception, natural heterogeneity cannot be represented, as all spatially different processes are generalized to one common hydrological response unit. Thus, they are incorporated in the model in a very abstract way. Although the overall specific runoff was simulated very well, the limited model complexity of the HBV-D model does certainly contribute to the explanation of the poor simulation of the dynamic catchment response during stormflow events. To this end, it was not possible to derive statements about the hydrological alteration of single stormflow events as a result of land-cover changes on a daily or even hourly time scale. However, changes of the specific runoff of longer periods, as for example monthly values, have been shown to be met satisfactorily. For a detailed investigation of the effects of land-cover change effects on the response of single runoff events, a spatial modeling environment might be more suitable. This allows a grid based regionalization of the model,

which enables a better representation of heterogeneity in the catchment and hence a variety of spatially diverse processes (Lautenbach *et al*., 2006).

6.6. Conclusion

Upper reaches of the Kharaa River were identified to be water towers for the lower catchment area (Menzel *et al*., 2011). Today, water availability is the most important limiting factor for agricultural production in the Kharaa River catchment (Karthe *et al*., 2015). However, the Mongolian agricultural sector is currently expanding considerably (Pederson *et al*., 2013), leading to an increase in agricultural land between 50 % and 100 % (Priess *et al*., 2011). Irrigation is considered to fulfill the related growing water demands. Simultaneously, as a consequence of the flourishing economy, the mining and urban sectors are rapidly growing in the Kharaa River Basin, accompanied by enhanced water demands (Priess *et al*., 2011; Karthe *et al*., 2013; Hofmann *et al*., 2015).

The natural fire-return interval in Mongolia has been estimated to be at least 175 years (Johnson *et al*., 2009), while burned forests may take up to 200 years to regenerate (Goldammer, 2002; Harden *et al*., 2006). The recovery of the dominance of late successional conifers after fire can last 400 years (Schulze *et al*., 2005). However, the increased human presence in the headwater regions since the beginning of the 1990s (Priess *et al.*, 2011) has probably reduced the actual fire return interval (Hessl *et al*., 2012). Nyamjav *et al*. (2007) found the recent fire pattern to affect 14 percent of total forest land annually.

The simulation of runoff of a burned catchment shows a decrease of the specific runoff between -72 % and -53 % in the moderately burned C1, C2 and C4 sub-catchments from December to March. In contrast, specific runoff was simulated to increase in the summer half year between 20 % and 40 % in C1, C2 and C4. Although the overall runoff level was simulated satisfactorily, the quality of the simulation of single stormflow events in daily time-steps was poor. Thus, the results of the simulation of land-cover change effects are only suitable to derive statements on a longer time scale, e.g. on a monthly basis (Figure 33). Hence, the effects of wildfire on the dynamic of single stormflow events must be derived from results of a variety of field measurements (Chapter 2 to Chapter 4). While wildfires reduce retardation capacity and therefore runoff during low-flow conditions, the magnitude of runoff during stormflow is assumed to increase as event water is transferred quickly along an effective drainage network on top of a degraded permafrost layer towards the river (Lange *et al*., 2015; Kopp *et al*., 2016).

This is further enhanced by lower evaporation rates due to vegetation removal (Heijmans *et al*., 2004; Lopez *et al*., 2008; Ohta *et al*., 2008). It can be concluded that the water availability is not increasing following wildfire, despite the simulation of higher runoff during summer months (Figure 33).

The results of this study highlight the importance of preserving the taiga stands in the upper reaches of the Kharaa River Basin from deforestation and especially from forest-fire due to their regulating function on runoff generation. This area is representative of other semi-arid mountainous regions in northern Mongolia, serving as a scientific basis to derive guidelines on how to prepare for up-coming challenges in terms of urban, agricultural and mining water needs in the near future in terms of a sustainable water supply. To maintain their ecological service on both water quantity and quality, these regions must be exempted from mining, deforestation, overgrazing and overfishing.

CHAPTER 7

Conclusion

This dissertation has addressed the major runoff generating processes in a mountainous headwater in the transition zone between steppe and taiga in northern Mongolia. Although this region has been identified as water tower for lowland regions, knowledge about the governing factors on freshwater generation is still rare. The focus of this study was on the local and regional scale by conducting a variety of field measurements in the headwaters of the Khentii Mountains, supplemented by the hydrological simulation of land-cover change effects. The results suggest hydrological conditions to be governed by the dominant land-cover type. It has been shown that south-exposed steppe slopes only contribute to stream runoff via overland flow during intense rainfall events. The majority of runoff is generated by north-exposed, permafrost underlain taiga forests that exhibit a regulative function on discharge. Wildfires have been identified to significantly increase soil temperatures, which sustainably alter the hydrological system. As permafrost degraded, stormflow runoff increased and low-flow runoff decreased. This knowledge should be considered in the regional water resources management and is of special value for decision-makers and stakeholders in order to maintain the ecological service of this sensible region on water quantity. This is particularly important regarding the ongoing rapid economic growth with flourishing urban, mining and agricultural sectors, each characterized by enormous water demands.

The dissertation had five more specific aims, as stated in Chapter 1:

1. To examine soil moisture and soil temperature distribution and dynamics as well as physical soil variables at a steppe, pristine and burned taiga site.

This aim was addressed in Chapter 2. To study the effects of exposition, vegetation cover and wildfire, soil moisture sensors were installed across transects from a steppe slope towards the pristine and burned taiga. At each site, soil moisture was continuously recorded at the upper and lower slope in -5, -10 and -30 cm in triple replicates to account for heterogeneities. Additionally, soil surface infiltration rates were determined and soil temperatures were continuously recorded in -5, -10 and -30 cm at each site. A total of 24 soil samples were analyzed in the laboratory to derive site specific soil water retention curves. The results revealed

soil water contents to frequently reach the permanent wilting point at the steppe slopes, thus explaining the absence of conifers. On the contrary, soil moisture contents of the taiga stands remained high at -30 cm, while soil temperatures were low. These findings could be primarily attributed to the presence of a thick organic surface cover and the abundance of permafrost underneath the active layer. As wildfire removed the insulating organic surface cover, soil temperatures increased significantly ($p < 2.0 \times 10^{-16}$), while permafrost subsided to deeper depth. As a consequence, precipitation water infiltrated deeper along preferential pathways, resulting in an effective network of sub-surface drainage. However, soil moisture contents remained high and soil drying rates were found to be low 4 and 5 years after the wildfire. Results from studies in a similar setting in Alaska observed soil drying on the long-term (e.g. Yoshikawa *et al*., 2003). As a result, however speculative, water stress is increasing which prevents future regrowth of the taiga stands and promotes steppe vegetation.

2. To examine dominant freshwater generating processes at a steppe and pristine taiga site.

This aim was addressed in Chapter 3 and 4. Dominant seasonal runoff generating processes were investigated by isotopic and hydrometric data at the hillslope and catchment scale in the headwater of the Sugnugr River, northern Mongolia.

At the catchment scale, the regulative function of active layer depth became evident. Hydrograph analysis indicated short recession periods in early summer when precipitation water is quickly transferred on top of a shallow active layer towards the river. While active layer thickness increased in the course of summer, the storage capacity increased and slowflow became dominant as indicating by delaying flow fractions.

At the hillslope scale, the results of the north facing taiga vegetated slopes agree with other process studies on slopes underlain by permafrost (e.g. Quinton and Marsh, 1999, Carey and Woo, 2000; 2001a; 2001b). Dye tracer experiments showed precipitation water to infiltrate rapidly into a moist soil horizon, resulting in quick sub-surface stormflow (SSF) on top of the permafrost table. A regulative function of the taiga forest on stormflow generation, due to the water retardation capacity of the organic surface layer, could be derived. Only after a threshold of a relative increase in volumetric soil moisture content (VWC*i*) of 0.05 m^3 m^{-3} was reached during stormflow, hillslope runoff was observed. Thus, stormflow runoff is dampened while low-flow runoff is enhanced through persistent drainage of the soils. By applying tracer techniques, steppe slopes have been proven to solely contribute to river runoff during intense

rainfall events. Two component hydrograph analysis revealed an event water fraction of 70 % at the onset of a stormflow event in early summer. This finding was attributed to overland flow as a result of low infiltration rates at the steppe slopes and was verified by field observations. The results are in accordance with Minderlein and Menzel (2015) who found total actual evapotranspiration at a mountainous steppe site to exceed precipitation during the summer months.

3. To examine changes of dominant freshwater generating processes as a result of wildfires.

This aim was addressed in Chapter 3 and 4. A wildfire, four and five years prior to this study, combusted the organic surface layer to a high degree while trees were burned. Soil temperatures increased significantly and permafrost subsided to deeper depths, resulting in an effective drainage network on top of the permafrost surface. This sub-surface stormflow (SSF) system has also been observed during field stays, with water temperature measurements proving the role of the frost table as a base for SSF. It has been found that wildfires reduce the VWC_i to 0.01 m^3 m^{-3}, and thus water retardation capacity. As a consequence, the transfer of precipitation water towards the stream along preferential flow paths above the frost table is enhanced. The results indicate a substantial change of post-fire stormflow dynamics: while peakflow is increasing, low-flow runoff is decreasing.

4. To simulate the natural runoff from a variety of headwater watersheds.

While introducing the conceptual model HBV-D in Chapter 5, this aim was addressed in Chapter 6. Runoff from four headwater catchments during the two consecutive summers of 2011 and 2012 was simulated. Although the overall runoff level was simulated satisfactorily on a monthly basis, single stormflow events were simulated poorly on a daily time step. Nevertheless, the results give insight into the hydrological regime of the headwaters. The hydrographs were found to be characterized by enormous differences with runoff during the relatively wet summer months June to August 2012 (+20 % of precipitation) being up to 2.2 times the runoff of the dry summer 2011. No distinct differences were observed during the cold and dry winter months. In general, the hydrographs are particularly seasonal, with the majority of runoff occurring between May to October. Snowmelt was simulated to be comparatively

low. However, as the cold winter months are characterized by low-flow conditions, this occasion provides the virtually dried out rivers for the first time of the year with water.

5. To simulate the hydrological response under land-cover change scenarios in a variety of headwater watersheds.

This aim was addressed in Chapter 6. Two different land-cover scenarios were simulated. To this end, the calibrated models were adjusted to represent unburned and burned conditions. It has been shown that the governing parameters of the two land-cover scenarios of the HBV-D models were field capacity, groundwater recharge and the slow time constant for the lower soil zone. This is in accordance to Carr (2003), who found these parameters to directly address the impact of permafrost in the HBV model. The burned scenario resulted in a yearly runoff increase between 7 % and 33 % in the four catchments. However, on a monthly scale, wildfires were simulated to result in a drastic runoff decline from December to March between -72 % and -53 %, while summer runoff increased by 20 % to 40 %. This can be primarily attributed to the loss of the vegetation, and thus lower evapotranspiration rates (e.g. Ohta *et al*., 2001; Heijmans *et al*., 2004; Lopez *et al*., 2008; Ohta *et al*., 2008; Bond-Lamberty *et al.*, 2009). Nevertheless, it has to be taken in account when interpreting the results that runoff dynamics on a daily time scale were simulated poorly. In Chapter 3 and 4, it has been shown that stormflow runoff is increasing while low-flow is decreasing as a consequence of wildfires. Thus, the simulated increase in summer runoff must be caused by more intense flood events, while low-flow periods are propagating. As a result, water availability in down streaming areas is reduced.

References

Barrett, K., McGuire, A. D., Hoy, E. E., and Kasischke, E. S., 2011: Potential shifts in dominant forest cover in interior Alaska driven by variations in fire severity. *Ecological Applications*, 21: 2380-2396, DOI: 10.1890/10-0896.1

Batima, P., Natsagdorj, L., Gombluudev, P., and Erdenetsetseg, B., 2005: Observed climate change in Mongolia. *Assessments Impacts Adaptions Climate Change Working Papers*, 12: 1-26.

Beck P. S., Goetz, S. J., Mack, M.c., Alexander H. D., Jin, Y., Randerson, J. T., and Loranty, M. M., 2011: The impacts and implications of an intensifying fire regime on Alaskan boreal forest composition and albedo. *Global Change Biology*, 17: 2853-2866, DOI: 10.1111/j.1365-2486.2011.02412.x

Bergström, S., 1976: Development and Application of a Conceptual runoff Model for Scandinavian Catchments. *Bulletin Series A No. 52*, Lund University, 134 pp.

Bergström, S., 1992: The HBV model – its structure and applications. *SMHI RH no. 4,* Norrköping, Sweden.

Bergström, S., 1995: The HBV model. In: V.P. Singh (Hrsg.), Computer Models of Watershed Hydrology, *Water Resources Publications*, Littleton, Colorado, 443 - 476.

Bogner, C., Wolf, B., Schlather, W., and Huwe, B., 2008. Analysing flow patterns from dye tracer experiments in a forest soil using extreme value statistics. *European Journal of Soil Science*, 59: 103–113, DOI: 10.1111/j.1365-2389.2007.00974.x

Bond-Lamberty, B., Peckham, S. D., Gower, S. T., and Ewers, B. E., 2009: Effects of fire on regional evapotranspiration in the Central Canadian boreal forest. *Global Change Biology*, 15: 1242-1254, DOI: 10.1111/j.1365-2486.2008.01776.x

Boucher, J. L., and Carey, S. K., 2010: Exploring runoff processes using chemical, isotopic and hydrometric data in a discontinuous permafrost catchment. *Hydrology Research*, 41: 508-519, DOI: 10.2166/nh.2010.146

Brouchkov, A., Fukuda, M., Iwahana, G., Kobayashi, Y., and Konstantinov, P., 2005: Thermal Conductivity of Soils in the Active Layer of Eastern Siberia. *Permafrost and Periglacial Processes,* 16: 217-222, DOI: 10.1002/ppp.502

Brown R. J. E., 1983: Effects of fire on permafrost ground thermal regime, in *The role of fire in the Northern Circumpolar Ecosystems*, edited by Wein R.W. and MacLean D.A., pp. 97-110, John Wiley, New York.

Burke, J. M., Prepas, E. E., and Pinder, S., 2005: Runoff and phosphorous export patterns in large forested watersheds on the western Canadian Boreal Plain before and 4 years after wildfire. *Journal of Environmental Engineering and Science*, 4 (5): 319-325, DOI: 10.1139/s04-072

Burn, C. R., 1998. The Response (1958–1997) of Permafrost and Near-Surface Ground Temperatures to Forest Fire, Takhini River Valley, Southern Yukon Territory, *Canadian Journal of Earth Sciences*, 35: 184–199.

Carey, S. K., and Woo, M. K., 2000: The role of soil pipes as a slope runoff mechanism, Subarctic Yukon, Canada. *Journal of Hydrology,* 233: 206-222, DOI: 10.1016/S0022-1694(00)00234-1

Carey, S. K., and Woo, M. K., 2001a: Spatial variability of hillslope water balance, wolf creek basin, subarctic Yukon. *Hydrological Processes*, 15: 3113-3132, DOI: 10.1002/hyp.319

Carey, S. K., and Woo, M. K., 2001b: Slope runoff processes and flow generation in a subarctic, subalpine catchment. *Journal of Hydrology,* 253: 110-129, DOI: 10.1016/S0022-1694(01)00478-4

Carey, S. K., and Quinton, W. L., 2005: Evaluating runoff generation during summer using hydrometric, stable isotope and hydrochemical methods in a discontinuous permafrost alpine catchment. *Hydrological Processes*, 19: 95-114, DOI: 10.1002/hyp.5764

Carr, A. T., 2003: Hydrological comparisons and model simulations of subarctic watersheds containing continuous and discontinuous permafrost, Seward Peninsula, Alaska. University of Fairbanks, M. S. thesis, 112 p.

Davi, N., Jacoby, G., Fang, K., Li, J., D'Arrigo, R., Baatarbileg, N., and Robinson, D., 2010: Reconstructed drought across Mongolia based on a large-scale network of tree ring records 1693-1993. *Journal of Geophysical Research,* 15: D22103, DOI: 10.1029/2010JD013907

Davi, N. K., Pederson, N., Leland, C., Nachin, B., Suran, B., and Jacoby, G. C., 2013: Is eastern Mongolia drying? A long-term perspective of a multidecadal trend. *Water Resources Research*, 49: 151-158, DOI: 10.1029/2012WR011834

DeBano, L. F., 2000: The role of fire and soil heating on water repellency in wildland environments: a review. *Journal of Hydrology*, 231-232: 195-206, DOI: 10.1016/S0022-1694(00)00194-3

Dobinski, W., 2011: Permafrost. *Earth Science Reviews*, 108 (3-4): 158-169, DOI: 10.1016/j.earscirev.2011.06.007

Dulamsuren C., Hauck M., and Mühlenberg, M., 2005: Ground vegetation in the Mongolian taiga forest-steppe ecotone does not offer evidence for the human origin of grasslands. *Applied Vegetation Science*, 8: 149-154, DOI: 10.1111/j.1654-109X.2005.tb00640.x

Dulamsuren, C., and Hauck, M., 2008: Spatial and seasonal variation of climate on steppe slopes of the northern Mongolian Taiga. *Japanese Society of Grassland Science*, 54: 217-230, DOI: 10.1111/j.1744-697X.2008.00128.x

Dulamsuren, C., Hauck, M., and Mühlenberg, M., 2008: Insect and small mammal herbivores limit tree establishment in northern Mongolian steppe. *Plant Ecology*, 195: 143-156, DOI: 10.1007/s11258-007-9311-z

Dulamsuren, C., Hauck, M., and Leuschner, C., 2010a: Recent drought stress leads to growth reductions in *Larix sibirica* in the western Khentey, Mongolia. *Global Change Biology*, 16: 3024-3035, DOI: 10.1111/j.1365-2486.2009.02147.x

Dulamsuren, C., Hauck, M., Khishigjargal, M., Leuschner, H. H., and Leuschner, C., 2010b: Diverging climate trends in Mongolian taiga forests influence growth and regeneration of Larix sibirica. *Oecologia*, 163: 1091-1102, DOI: 10.1007/s00442-010-1689-y

Etzelmüller, B., Flo Heggem, E. S., Sharkuu, N., Frauenfelder, R., Kääb, A., and Goulden, C., 2006: Mountain Permafrost Distribution Modelling using a Multi-criteria Approach in the Hövsgöl Area, Northern Mongolia. *Permafrost and Periglacial Processes*, 17: 91-104, DOI: 10.1002/ppp.554

Flannigan, M., and Van Wagner, C., 1991: Climate change and wildfire in Canada. *Canadian Journal of Forest Research*, 21: 66-72, DOI: 10.1139/x91-010

Flannigan, M., Stocks, B., Turetsky, M., and Wotton, M., 2009: Impacts of climate change on fire activity and fire management in the circumboreal forest. *Global Change Biology*, 15: 549-560, DOI: 10.1111/j.1365-2486.2008.01660.x

Flury, M., and Flühler, H., 1994: Brilliant blue FCF as a dye tracer for solute transport studies, a toxicological overview. *Journal of Environmental Quality*, 23: 1108–1112.

Flury, M., Flühler, H., Jury, W. A., and Leuenberger, J., 1994: Susceptibility of soils to preferential flow of water: a field study. *Water Resources Research*, 30: 1945–1954, DOI: 10.1029/94WR00871

Genereux, D., 1998: Quantifying uncertainty in tracer-based hydrograph separations. *Water Resources Research*, 34: 915-919.

Goldammer, J. G., 2002: Fire Situation in Mongolia. *International Forest Fire News,* 26: 75-83.

Gunin, P. D., Vostokova, E. A., Dorofeyuk, N. I., Tarasov, P. E., and Black, C. C., 1999: Vegetation dynamics of Mongolia. *Geobotany*, 26: Kluwer Academic Publishers, Dordrecht.

Harden, J. W., Manies, K. L., Turetsky, M. R., and Neff, J. C., 2006: Effects of wildfire and permafrost on soil organic matter and soil climate in interior Alaska. *Global Change Biology*, 12: 2391-2404, DOI: 10.1111/j.1365-2486.2006.01255.x

Heggem, E. S. F., Etzelmüller, B., Anarmaa, S., Sharkuu, N., Goulden, C. E., and Nandinsetseg, B., 2006: Spatial distribution of ground surface temperatures and active layer depths in the Hövsgöl area, northern Mongolia. *Permafrost and Periglacial Processes*, 17: 357-369, DOI: 10.1002/ppp.568

Heijmans, M. M. P. D., Arp, W. J., and Chapin Ill, F. S., 2004: Controls on moss evaporation in a boreal black spruce forest. *Global Biochemical Cycles*, 18: GB2004, DOI: 10.1029/2003GB002128

Hessl, A. E., Ariya, U., Brown, P., Byambasuren, O., Green, T., Jacoby, G., Kennedy Sutherland, E., Nachin, B., Stockton Maxwell, R., Pederson, N., De Grandpré, L., Saladyga, T., and Tardif, J. C., 2012: Reconstructing fire history in central Mongolia from tree-rings. *International Journal of Wildland Fire*, *21*: 86-92, DOI: 10.1071/WF10108

Hinzman, L. D., and Kane, D. L., 1991: Snow hydrology of a headwater Arctic basin: 2. Conceptual analysis and computer modeling. *Water Resources Research*, 27: 1111-1121, DOI: 10.1029/91WR00261

Hinzman, L. D., Kane, D. L., Gieck, R. E., and Everett, K. R., 1991: Hydrologic and thermal properties of the active layer in the Alaskan Arctic. *Cold Regions Science and Technology*, 19: 95-110, DOI: 10.1016/0165-232X(91)90001-W

Hinzman, L. D., and Kane, D. L., 1992: Potential Response of an Arctic watershed during a period of Global Warming. *Journal of Geophysical Research,* 97 (D3): 2811-2820.

Hinzman, L. D., Fukuda, M., Sandberg, D.V., Chapin, III F. S., and Dash, D., 2003: FROSTFIRE: An experimental approach to predicting the climate feedbacks from the changing boreal fire regime. *Journal of Geophysical Research*, 108 (D1): 8153, DOI: 10.1029/2001JD000415

Hofmann, J., Watson, V., and Scharaw, B., 2014: Groundwater quality under stress: contaminants in the Kharaa River basin (Mongolia). *Environmental Earth Science*, 73: 629-648, DOI: 10.1007/s12665-014-3148-2

Hofmann, J., Karthe, D., Ibisch, R., Schäffer, M., Kaus, A., Avlyush, S., and Heldt, S., 2015: Initial Characterization and Water Quality Assessment of Stream Landscapes in Northern Mongolia and its Integration into a River Basin Management Plan. *Water*, 7: 3166-3205, DOI:10.3390/w7073166

Hülsmann, L., Geyer, T., Schweitzer, C., Priess, J., and Karthe, D., 2015: The Effect of Subarctic Conditions on Water Resources: Initial Results and Limitations of the SWAT Model applied to the Kharaa River Catchment in Northern Mongolia. *Environmental Earth Science*, 73 (2): 581-592, DOI:10.1007/s12665-014-3173-1

IPCC, 2007: The Physical Science Basis. Contribution of Workinbg Group 1 to the Fourth Assessment Report of the Intergovernmental Panel on Climate Change. Solomon, S., Qin, D., Manning, M., Chen, Z., Marquis, M., Averyt, K. B., Tignor, M., and Miller, H. L. (eds.). Cambridge University Press, Cambridge, UK, 996 pp.

IPCC, 2012: Managing the Risks of Extreme Events and Disasters to Advance Climate Change Adaptation. A Special Report of Working Groups I and II of the Intergovernmental Panel on Climate Change. Field, C. B., Barros, V., Stocker, T. F., Qin, D., Dokken, D. J., Ebi, K. L., Mastrandrea, M. D., Mach, K. J., Plattner, G. -K., Allen, S. K., Tignor, M., and Midgley, P. M. (eds.). Cambridge University Press, Cambridge, UK, and New York, NY, USA, 582 pp.

Ishikawa, M., Sharkhuu, N., Zhang, Y., Kadota, T., and Ohata, T., 2005: Ground Thermal and Moisture Conditions at the Southern Boundary of Discontinuous Permafrost, Mongolia. *Permafrost and Periglacial Processes*, 16: 209-216, DOI: 10.1002/ppp.483

Iwahana, G., Machimura, T., Kobayashi, Y., Fedorov, A. N., Konstantinov, P. Y., and Fukuda, M., 2005: Influence of forest clear-cutting on the thermal and hydrological regime of the active layer near Yakutsk, eastern Siberia. *Journal of Geophysical Research*, 110: G02004, DOI: 10.1029/2005JG000039

Iwata, H., Harazono, Y., and Ueyama, M., 2012: The role of permafrost in water exchange of a black spruce forest in Interior Alaska. *Agricultural and Forest Meteorology*, 161: 107–115, DOI:10.1016/j.agrformet.2012.03.017

Jensen, J. R., 2005: Introductory Digital Image Processing, 3rd edn. Pearson Prentice Hall: Upper Saddle River, NJ.

Johnson, D., Oyunsanaa, B., Myers, R. L., and Babler, M., 2009: Fire management assessment of the eastern steppe, Mongolia. GFI technical report. The Nature Conservancy, Arlington.

Johnstone, F. F., and Chapin, F.S., 2006: Fire interval effects on successional trajectory in boreal forests of northwest Canada. *Ecosystems*, 9: 268-277.

Karthe, D., Malsy, M., Kopp, B. J., Minderlein, S., and Hülsmann, L., 2013: Assessing water availability and its drivers in the context of an Integrated Water Resources Management (IWRM): A case study from the Kharaa River Basin, Mongolia. *Geoöko,* 34: 5-26.

Karthe, D., Heldt, S., Houdret, A., and Borchardt, D., 2014: IWRM in a country under rapid transition: lessons learnt from the Kharaa River basin, Mongolia. *Environmental Earth Science*, 73: 681-695, DOI: 10.1007/s12665-014-3435-y

Karthe, D., Hofmann, J., Ibisch, R., Heldt, S., Westphal, K., Menzel, L., Avlyush, S., and Malsy, M., 2015: Science-Based IWRM Implementation in a Data-Scarce Central Asian Region: Experiences from a Research and Development Project in the Kharaa River Basin, Mongolia. *Water,* 7: 3486-3514, DOI: 10.3390/w7073486

Kirchner, W. J., 2009: Catchments as simple dynamical systems: Catchment characterization, rainfall-runoff modelling, and doing hydrology backward. *Water Resources Research*, 45 (2): W02429, DOI: 10.1029/2008WR006912

Knudson, J. A., and Hinzman, L. D., 2000: Prediction of Streamflow in an Alaskan Watershed Underlain by Permafrost. *American Water Resources Association Technical Publication Series* TPS 00-1: 309-313.

Kopp, B. J., Minderlein, S., and Menzel, L., 2014: Effect of exposition, vegetation and wildfire on soil moisture distribution in a mountainous headwater area in the discontinuous permafrost zone of northern Mongolia. *Arctic Antarctic and Alpine Research*, 46: 459-470 , DOI: 10.1657/1938-4246-46.2.459

Kopp, B. J., Lange, J., and Menzel, L., 2016: Effects of wildfire on runoff generating processes in northern Mongolia. *Regional Environmental Change*, in revision.

Krause, P., Boyle, D. P., and Bäse, F., 2005: Comparison of different efficiency criteria for hydrological model assessment. *Advances in Geosciences*, 5: 89-97, DOI: 10.5194/adgeo-5-89-2005

Krysanova, V., Bronstert, A., and Müller-Wohlfeil, D.-I., 1999: Modelling river discharge for large drainage basins: from lumped to distributed approach. *Hydrological Sciences,* 44: 313-331.

Lange, J., Leibundgut, C., Grodek, T., Lekach, J., and Schick, A. P., 1998: Using artificial tracers to study water losses of ephemeral floods in small arid streams. *IAHS*-Publications, 247: 31 – 40.

Lange. J., and Haensler, A., 2012: Runoff generation following a prolonged dry period. *Journal of Hydrology*, 464-465: 157-164, DOI: 10.1016/j.jhydrol.2012.07.010

Lange, J., Kopp, B. J., Bents, M., and Menzel, L., 2015: Tracer-hydrological process investigations on two opposite slopes in a mountainous, semi-arid, permafrost environment, northeastern Mongolia. *Hydrological Processes*, 29: 1046-1055, DOI: 10.1002/hyp.v29.6

Lautenbach, S., Voinov, A., and Seppelt, R., 2006: Localization effects of land use change on hydrological models. In: Voinov, A., Jakeman, A., and Rizzoli, A., (eds.). iEMSs Third Biennial Meeting "Summit on Environmental Modelling an Software", Burlington, 9-13 July 2006.

Leibundgut, C., Maloszewski. P., and Külls, C., 2009: Tracers in Hydrology. Wiley.

Li, S. G., Asanuma, J., Kotani, A., Davaa, G., and Oyunbaatar, D., 2007a: Evapotranspiration from a Mongolian steppe under grazing conditions and its environmental constraints. *Journal of Hydrology,* 333: 133-143, DOI: 10.1016/j.jhydrol.2006.07.021

Li, S. G., Romero-Saltos, H., Tsujimura M., Sugimoto A., Sasaki L., Davaa G., and Oyunbaatar D., 2007b: Plant water sources in the cold semiarid ecosystem of the upper Kherlen River catchment in Mongolia: A stable isotope approach. *Journal of Hydrology*, 333: 109-117, DOI: 10.1016/j.jhydrol.2006.07.020

Liancourt, P., Sharkhuu, A., Ariuntsetseg, L., Boldgiv, B., Helliker, B. R., Plante, A. F., Petraitis, P. S., and Casper, B. B., 2012: Temporal and spatial variation in how vegetation alters the soil moisture response to climate manipulation. *Plant Soil*, 351: 249-261, DOI: 10.1007/s11104-011-0956-y

Lindström, G., Johansson, B., Persson, M., Gardelin, M., and Bergström, S., 1997: Development and test of the distributed HBV-96 hydrological model. *Journal of Hydrology* 201: 272-288, DOI: 10.1016/S0022-1694(97)00041-3

Liu, H., Williams, A. P., Allen, C. D., Guo, D., Wu, X., Anenkhonov, O. A., Liang, E., Sandanov, D. V., Yin, Y., Qi, Z., Badmaeva, N. K., 2013: Rapid warming accelerates tree growth decline in semi-arid forests of Inner Asia. *Global Change Biology*, 19: 2500-2510, DOI: 10.111/gcb.12217

Lopez, M. L., Gerasimov, E., Machimura, T., Takakai, F., Iwahana, G., Fedorov, A. N., and Fukuda, M., 2008: Comparison of carbon and water vapor exchange of forest and grassland in permafrost regions, Central Yakutia, Russia. *Agricultural and Forest Meteorology*, 148: 1968-1977, DOI: 10.1016/j.agrformet.2008.09.013

Lopez, M. L., Hatano, R., Guggenberger, G., Ohta, T., Gerasimov, E., and Fedorov, A. N., 2012: Forest Fires Effects on Carbon Stocks and Soil Chemistry in Central Yakutia, Eastern Siberia. *Eurasian Journal of Forest Research*, 15: 9-17.

Ma, X., Yasunari, T., Ohata, T., Natsagdorj, L., Davaa, G., and Oyunbaatar, D., 2003: Hydrological regime analysis of the Selenge River basin, Mongolia. *Hydrological Processes*, 17: 2929-2945, DOI: 10.1002/hyp.1442

Maillet, E., 1905: Essais d'hydraulique souterraine et fluvial. A. Hermann, Paris.

MARCC, 2009: Mongolia: Assessment Report on Climate Change 2009. Dagvadorj, D., Natsagdorj, L., Dorjpurev, J., Namkhainyam, B., Gomboluudev, P., Batimaa, P., Jugder, D., Mijiddorj, R., Davaa, G., Erdenetsetseg, B., and Khaulenbek. Ministry of Environment, Nature and Tourism, Mongolia, 228 pp.

McNamara, J. P., Kane, D. L., and Hinzman, L. D., 1998: An analysis of streamflow hydrology in the Kuparuk River basin, Arctic Alaska: A nested watershed approach. *Journal of Hydrology*, 206: 39-57, DOI: 10.1016/S0022-1694(98)00083-3

Menzel, L., and Bürger, G., 2002: Climate change scenarios and runoff response in the Mulde catchment (Southern Elbe, Germany). *Journal of Hydrology,* 267: 53-64, DOI: 10.1016/S0022-1694(02)00139-7

Menzel, L., Thieken, A. H., Schwandt, D., and Bürger, G., 2006: Impact of climate change on the Regional Hydrology – Scenario-based modelling studies in the German Rhine catchment. *Natural Hazards*, 38: 45-61, DOI: 10.1007/s11069-005-8599-z

Menzel, L., Hofmann, J., and Ibisch, R., 2011: Studies of water and mass fluxes to provide a basis for an Integrated Water Resources Management (IWRM) in the catchment of the River Kharaa in Mongolia. *Hydrologie und Wasserbewirtschaftung,* 55 (2): 88-103.

Minderlein. S., and Menzel, L., 2015: Evapotranspiration and energy balance dynamics of a semi-arid mountainous steppe and shrubland site in northern Mongolia. *Environmental Earth Science,* 73 (2): 593-609, DOI: 10.1007/s12665-014-3335-1

Namkhaijanstan, G., 2006: Climate and climate change of the Hövsgöl region. In: Goulden, C. E., Sitnikova, T., Gelhaus, J., Boldgiv, B., (eds). The Geology, Biodiversity and Ecology of Lake Hövsgöl (Mongolia). Backhuys Publisher, Leiden.

Nandintsetseg, B., Greene, J. S., and Goulden, C. E., 2007: Trends in extreme daily precipitation and temperature near Lake Hövsgöl, Mongolia. *International Journal of Climatology*, 27: 341-347, DOI: 10.1002/joc.1404

Ohta, T., Hiyama, T., Tanaka, H., Kuwada, T., Maximov, T. C., Ohata, T., and Fukushima, Y., 2001: Seasonal variation in the energy and water exchanges above and below a larch

forest in eastern Siberia. *Hydrological Processes*, 15: 1459-1476, DOI: 10.1002/hyp.219

Ohta, T., Maximov, T. C., Dolman, A. J., Nakai, T., van der Molen, M. K., Kononov, A. V., Maximov, A. P., Hiyama, T., Iijima, Y., Moors, E. J., Tanaka, H., Toba, T., and Yabuki, H., 2008: Interannual variation of water balance and summer evapotranspiration in an eastern Siberian larch forest over a 7-year period (1998-2006). *Agricultural and Forest Meteorology*, 148: 1941-1953, DOI: 10.1016/j.agrformet.2008.04.012

Onodera, S. I., and van Stan, J. T., 2011: Effect of forest fires on hydrology and biogeochemistry of watersheds. In: Levia, D. F., Carlyle-Moses, D., and Tanakas, T., eds. *Forest Hydrology and Biogeochemistry*. Springer, Dordrecht, pp 599-621

Osterkamp, T. E., 2007: Characteristics of the recent warming of permafrost in Alaska. *Journal of Geophysical Research*, 112: F02S02, DOI: 10.1029/2006JF000578

Otoda, T., Doi, T., Sakamoto, K., Hirobe, M., Nachin, B., and Yoshikawa, K., 2012: Frequent fires may alter the composition of the boreal forest in northern Mongolia. *Journal of Forest Research*, 18: 246-255, DOI: 10.1007/s10310-012-0345-2

Pederson, N., Leland, C., Nachin, B., Hessl, A. E., Bell, A. R., Martin-Benito, D., Saladyga, T., Suran, B., Brown, P. M., and Davi, N. K., 2013: Three centuries of shifting hydrolimatic regimes across the Mongolian Breadbasket. *Agricultural and Forest Meteorology*, 178-179: 10-20, DOI: 10.1016/j.agrformet.2012.07.003

Petrone, K. C., Hinzman, L. D., Shibata, H., Jones, J. B., and Boone, R.D., 2007: The influence of fire and permafrost on sub-arctic stream chemistry during storms. *Hydrological Processes*, 21: 423-434, DOI: 10.1002/hyp.6247

Priess, J. A., Schweitzer, C., Wimmer, F., Batkhishig, O., and Mimler, M., 2011: The consequences of land-use change and water demands in Central Mongolia. *Land Use Policy*, 28: 4-10, DOI: 10.1016/j.landusepol.2010.03.002

Quinton, W. L., and Marsh, P., 1999: A conceptual framework for runoff generation in a permafrost environment. *Hydrological Processes*, 13: 2563-2581, DOI: 10.1002/(SICI)1099-1085(199911)13:16<2563::AID-HYP942>3.0.CO;2-D

Quinton, W. L., Shirazi, T., Carey, S. K., and Pomeroy, J. W. 2005: Soil Water Storage and Active-layer Development in a Sub-alpine Tundra Hillslope, Southern Yukon Territory, Canada. *Permafrost and Periglacial Processes,* 16: 369-382, DOI: 10.1002/ppp.543

Rowe, J., and Scotter, G., 1973: Fire in the boreal forest. *Quaternary Research*, 3: 444-464, DOI: 10.1016/0033-5894(73)90008-2

Sælthun, N. R., 1999: The "Nordic" HBV Model. Description and documentation of the model version developed for the project Climate Change and Energy Production. *NVE Publication7*, Norwegian Water Resources and Energy Administration, Oslo. 26p. ISBN 82-410-0273-4

Saladyga, T., Hessl, A., Nachin, B., and Pederson, N., 2013. Privatization, Drought, and Fire Exclusion in the Tuul River Watershed, Mongolia. *Ecosystems*, 16: 1139-1151, DOI: 10.1007/s10021-013-9673-0

Sato, T., Kimura, F., and Kitoh, A., 2007: Projection of global warming onto regional precipitation over Mongolia using a regional climate model. *Journal of Hydrology,* 333: 144-154, DOI: 10.1016/j.jhydrol.2006.07.023

Schrödter, H., 1985: Verdunstung. Anwendungsorientierte Meßverfahren und Bestimmungsmethoden. Springer-Verlag, Berlin.

Schulze, E.-D., Wirth, C., Mollicone, D., and Ziegler, W., 2005: Succession after stand replacing disturbances by fire, wind throw, and insects in the dark taiga of central Siberia. *Oecologia*, 146: 77-88, DOI: 10.1007/s00442-005-0173-6

Schwandt, D., 2003: Abflussentwicklung in Teileinzugsgebieten des Rheins. Simulationen für den Ist-Zustand und für Klimaszenarien. PhD-Dissertation, *PIK Report*, 88: 19-38.

Seibert, J., 1997: Estimation of parameter uncertainty in the HBV model. *Nordic Hydrology*, 28 (4/5): 247-262.

Shur, Y.L., and Jorgenson, M.T. 2007: Patterns of Permafrost and Degradation in Relation to Climate and Ecosystems. *Permafrost and Periglacial Processes*, 18: 7-19, DOI: 10.1002/ppp.582

Sklash, M. G., and Farvolden, R. N., 1979: The role of groundwater in storm runoff. *Journal of Hydrology*, 43: 45-66, DOI: 10.1016/0022-1694(79)90164-1

Steinmann, A., 2010: Runoff generation in Mediterranean areas. PhD-thesis, University of Freiburg, Freiburg, Germany.

Sugimoto, A., Yanagisawa, N., Naito, D., Fujita, N., and Maximov. T. C., 2002: Importance of permafrost as a source of water plants in east Siberian taiga. *Ecological Research*, 54: 493-503, DOI: 10.1046/j.1440-1703.2002.00506.x

Sugimoto, A., Naito, D., Yanagisawa, N., Ichiyanagi, K., Kurita, N., Kubota, J., Kotake, T., Ohata, T., Maximov, T. C., and Federov, A. N., 2003: Characteristics of soil moisture in permafrost observed in East Siberian taiga with stable isotopes of water. *Hydrological Processes*, 17: 1073-1092, DOI: 10.1002/hyp.1180

Swanson, D. K., 1996: Susceptibility of Permafrost Soils to Deep Thaw after Forest Fires in Interior Alaska, U.S.A. and Some Ecological Implications. *Arctic, Antarctic and Alpine Research*, 28: 217–227.

Takata, K., 2002: Sensitivity of land surface processes to frozen soil permeability and surface water storage. *Hydrological Processes*, 16: 2155-2172, DOI: 10.1002/hyp.1148

Tchebakova, N. M., Parfenova, E., and Soja, A. J., 2009: The effects of climate, permafrost and fire on vegetation change in Siberia in a changing climate. *Environmental Research Letters*, 4: 045013 (9pp), DOI: 10.1088/1748-9326/4/4/045013

Törnros, T., and Menzel, L., 2010: Heading for knowledge in a data scarce river basin: Kharaa, Mongolia. In: Herrmann, A., and Schumann, S. (eds.): Status and Perspectives of hydrology in small basins. *IAHS Publications*, 336: 270-275.

Törnqvist, R., Jarsjö, J., Pietroń, J., Bring, A., Rogberg, P., Asokan, S. M., Destouni, G., 2014: Evolution of the hydro-climate system in the Lake Baikal basin. *Journal of Hydrology*, 519: 1953-1962, DOI:10.1016/j.jhydrol.2014.09.074

Tsujimura, M., Abe. Y., Tanaka, T., Shimada, J., Higuchi, S., Yamanaka, T., Davaa, G., and Oyunbaatar, D., 2007: Stable isotopic and geochemical characteristics of groundwater in Kherlen River basin, a semi-arid region in eastern Mongolia. *Journal of Hydrology*, 333: 47-57, DOI: 10.1016/j.jhydrol.2006.07.026

Valeo, C., Beaty, K., and Hesslein, R., 2003: Influence of forest fires on climate change studies in the central boreal forest of Canada. *Journal of Hydrology*, 280: 91-104, DOI: 10.1016/S0022-1694(03)00185-9

van Genuchten M. T. 1980: A Closed-form Equation for Predicting the Hydraulic Conductivity of Unsaturated Soils. *Soil Science Society of America Journal*, 44 (5): 892-898, DOI: 10.2136/sssaj1980.03615995004400050002x

Viviroli, D., Dürr, H. H., Messerli, B., Meybeck, M., and Weingartner, R., 2007: Mountains of the world, water towers for humanity: Typology, mapping, and global significance. *Water Resources Research*, 43: W07447, DOI:10.1029/2006WR005653

Weiler, M., and Naef, F., 2003: An experimental tracer study of the role of macropores in infiltration in grassland soils. *Hydrological Processes*, 17: 477–493, DOI: 10.1002/hyp.1136

Wernli, H. R., 2011: Einführung in die Tracerhydrologie, Geographisches Institut Univ. Bern, Bern, Switzerland.

Wimmer, F., Schlaffer, S., aus der Beek, T., and Menzel, L., 2009: Distributed modelling of climate change impacts on snow sublimation in Northern Mongolia. *Advances in Geosciences*, 21: 117-124.

Woo, M. K., Kane, D.L., Carey, S. K., and Yang, D., 2008: Progress in permafrost hydrology in the new millennium. *Permafrost and Periglacial Processes*, 19: 237–254, DOI: 10.1002/ppp.613

Wright, N., Hayashi, M., and Quinton, W. L., 2009: Spatial and temporal variations in active layer thawing and their implication on runoff generation in peat-covered permafrost terrain. *Water Resources Research*, 45: W05414, DOI: 10.1029/2008WR006880

Wu, T., Wang, Q., Zhao, L., Batkhishig, O., and Watanabe, M., 2011: Observed trends in surface freezing/thawing index over the period 1987–2005 in Mongolia. *Cold Regions Science and Technology*, 69: 105–111, DOI:10.1016/j.coldregions.2011.07.003

Yamazaki, Y., Kubota, J., Ohata, T., Vuglinsky, T., and Mizuyama, T., 2006: Seasonal changes in runoff characteristics on a permafrost watershed in the southern mountainous region of eastern Siberia. *Hydrological Processes,* 20: 453–467, DOI: 10.1002/hyp.5914

Yoshikawa, K., Bolton, W. R, Romanovsky, V. E., Fukuda, M., and Hinzman, L. D., 2003: Impacts of wildfire on the permafrost in the boreal forests of Interior Alaska. *Journal of Geophysical Research,* 108: NO. D1, 8148, DOI: 10.1029/2001JD000438

Zhang, R., 1997: Determination of soil sorptivity and hydraulic conductivity from the disk infiltrometer. *Soil Science Society of America Journal*, 61: 1024-1030, DOI: 10.2136/sssaj1997.03615995006100040005x

Zhang, N., Yasunari, T., and Ohta, T., 2011: Dynamics of the larch taiga-permafrost coupled system in Siberia under climate change. *Environmental Research Letters*, 6: 024003 (6pp), DOI: 10.1088/1748-9326/6/2/024003

Zhao, L., Wu, Q., Marchenko, S. S., and Sharkhuu, N., 2010: Thermal state of permafrost and active layer in central Asia during the international polar year. *Permafrost and Periglacial Processes*, 21: 198-207, DOI:10.1002/ppp.688

Erklärung

Eidesstattliche Versicherung gemäß § 8 der Promotionsordnung der Naturwissenschaftlich-Mathematischen Gesamtfakultät der Universität Heidelberg

1. Bei der eingereichten Dissertation zu dem Thema

RUNOFF GENERATING PROCESSES IN A MOUNTAINOUS HEADWATER IN THE TRANSITION ZONE BETWEEN STEPPE AND TAIGA IN NORTHERN MONGOLIA

handelt es sich um meine eigenständig erbrachte Leistung.

2. Ich habe nur die angegebenen Quellen und Hilfsmittel benutzt und mich keiner unzulässigen Hilfe Dritter bedient. Insbesondere habe ich wörtlich oder sinngemäß aus anderen Werken übernommene Inhalte als solche kenntlich gemacht.

3. Die Arbeit oder Teile davon habe ich bislang nicht an einer Hochschule des In- oder Auslands als Bestandteil einer Prüfungs- oder Qualifikationsleistung vorgelegt.

4. Die Richtigkeit der vorstehenden Erklärungen bestätige ich.

5. Die Bedeutung der eidesstattlichen Versicherung und die strafrechtlichen Folgen einer unrichtigen oder unvollständigen eidesstattlichen Versicherung sind mir bekannt.

Ich versichere an Eides statt, dass ich nach bestem Wissen die reine Wahrheit erklärt und nichts verschwiegen habe.

Hof, 07.02.2016
Ort und Datum

Benjamin Kopp